Tuning the selectivity of bimetallic NiBi catalysts for glycerol electrooxidation into value-added chemicals

by

Asma Shubair

A thesis submitted in conformity with the requirements for the degree of

Masters of Applied Science

Department of Chemical and Biological Engineering

University of Ottawa

Supervised by: Dr. Elena Baranova

Statement of Contributions of Co-Authors

I hereby declare that I am the sole writer of this thesis and the work presented is of my own effort. I have performed the experiments and analyses under scientific supervision of Dr. Elena A. Baranova. I have acknowledged the assistance in experimentation by co-authors where applicable.

In Chapter 3, Mohamed Houache and my thesis supervisor Dr. Elena A. Baranova are the co-authors. Mohamed provided assistance with physical characterization section of the chapter and provided graphical abstract.

In chapter 4, there are two other co-authors other than the thesis supervisor, Pratik Parawani and Dr. Mohamed Houache. MEng student Pratik Parawani assisted with running electrocatalyst synthesis, electrochemical and HPLC tests. In addition, he helped with the discussion of the results in which I further refined for the publication. Mohamed Houache provided the graphical diagrams to be submitted for the publication.

ABSTRACT

In the process of biodiesel production, glycerol is produced as a byproduct in bulk amounts. The amount of glycerol supplied is larger than its demand thus stockpiling and acting as waste. As a solution, glycerol which is a highly functionalized molecule must be converted to value-added products. Several catalytic routes were thoroughly investigated including, hydrogenolysis, dehydration, pyrolysis, transesterification, etherification, carboxylation and electro-oxidation. All of these routes produce products of high economic interests. However, electro-oxidation seems to be the most promising as it runs under milder conditions and the selectivity may be easily tuned by varying the applied potential and the catalyst type. In addition, the electrical energy required may be provided by renewable energy sources. Some of the value-added products that may be produced by electrooxidation listed from highest economic value to lowest are glyceraldehyde, dihydroxyacetone, lactate, glycerate, tartronate (C_3 products) > mesooxalate, glycolate, oxalate (C_2 products) > and formate (C_1 products).

Noble metals (Pt, Pd and Au) are considered to be the best for alcohol electrooxidation reactions as they present high electrocatalytic activity and selectivity. To date, research is focused on enhancing the activity and selectivity of noble metals by changing the nanoparticles morphology and adding adatoms/promoters/supports. On the other hand, these metals are non-abundant and expensive which limits their actual use in the industry. For this reason, non-noble metals (Ni and Co) have gained interest as potential alternatives. Particularly, nickel has proved to have significant activity, high durability and anti-poisoning capability for GEOR. A few studies presented enhancement in catalytic performance by varying the nanoparticles structure and adjusting the surface with a bimetallic promoter. However, there is still so much space for further research to enhance the catalytic performance and selectivity of Ni-based materials.

In this thesis, carbon supported bimetallic Ni_xBi_{100-x} [x= 100, 95, 90, 80, and 50 at.%] and $Ni_{95}Bi_5$/C mixed with small amounts of metal oxides (CeO_2, SnO_2 and Sb_2O_3:SnO_2) were studied for GEOR application. All catalysts were synthesized by facile sodium borohydride reduction method which can be easily scaled up. Transmission

electron microscopy (TEM) and electron dispersive x-ray spectroscopy (EDS) techniques were implemented to gather physical characterizations of the as-synthesized bimetallic NiBi/C catalyst. Different electrochemical tests such as; cyclic voltammetry, linear sweep voltammetry and chronoamperometry were conducted using a conventional three electrode electrochemical cell and a potentiostat to get insight on the electrochemical performance of all catalysts. Finally, quantitative product analysis was generated by running continuous glycerol electrolysis experiments in a 25 cm^2 cell accompanied by HPLC analysis.

The nanoparticles size of $Ni_{95}Bi_5/C$ was ≥6nm as determined by TEM images. Results indicated that tuning the nanoparticles size has an impact on both activity and selectivity of bimetallic carbon supported NiBi catalyst. For instance, the NiBi/C (≥6nm NP size) synthesized herein had 40% higher selectivity to C_3 products compared to NiBi/C (≤3nm NP size) reported in literature. Additionally, the selectivity of Ni-based catalysts to C_3 products were largely enhanced by developing bimetallic carbon supported NiBi catalysts of different Ni:Bi atomic ratios and adding metal oxides (CeO_2, SnO_2 and $Sb_2O_3.SnO_2$) to NiBi/C catalysts. Results indicate that addition of metal oxides greatly enhanced selectivity to C_3 products in the following order; $Ni_{95}Bi_5/C$-ATO (100%)> Ni/C-ATO (99.17%)> $Ni_{95}Bi_5/C$-ceria (98.05%)> Ni/C-ceria (78.29%)> $Ni_{95}Bi_5/C$ (41.43%)> Ni/C (34.57%). However, the activity of $Ni_{95}Bi_5/C$-X [X=CeO_2, SnO_2, and Sb_2O_3:SnO_2] was lower than that of $Ni_{95}Bi_5/C$ and Ni/C which was explained by the strong metal support interactions between metal oxides and nickel.

ACKNOWLEDGMENTS

To begin with I would like to express my sincere gratitude and appreciation to my thesis supervisor Dr. Elena A. Baranova. Thank you, Dr. Baranova, for giving me this opportunity of being part of your wonderful LEE team and guiding me till the end of my journey. I will be forever grateful to you.

I would like to extend my appreciation to the technical officers in the department of Chemical and Biological Engineering: Gerard Nina, Franco Ziroldo and James Macdermid for their prompt assistance and cooperation especially during difficulties with the lab equipment and experimental setup.

I wish to thank my colleagues from the LEE team for their good company, great advice and for making my research journey more enjoyable. Special thanks to PhD graduate Mohamed Houache for providing me with in-depth training on all experimental procedures, it has been great pleasure working directly with you.

I would like to express my gratefulness to the friends (Shaaima Al Akwaa, Najmeh Ahladel, Niloofar Aligholizadeh, Mohamed Houache, Waed Abu Watfa, and Ranwa Al-Saadi) who gave me the strength to proceed through difficult times during my masters.

Mostly, thanks to my husband Hilal Al-Salih for being a great supporter and always encouraging me to work harder.

Last and foremost, thanks to my wonderful parents for all their love and support. Mom and dad thank you for being wonderful role models, I always look up to be as successful as you are.

TABLE OF CONTENTS

LIST OF FIGURES

LIST OF TABLES

Chapter 1: Introduction

1.1 Background and Problem statement

Burning fossil fuels for energy is one of the biggest contributors to the emissions of greenhouse gases, particularly CO_2, leading to global warming. In addition, fossil fuel reserves are depleting. For these reasons, alternative energy sources such as; biodiesel, nuclear power, hydroelectric dams, geothermal, wind, and solar energies are required to replace the depleting fossil fuel sources. Up to date, fossil fuel combustion remains to be the biggest source of energy in the world. At present, approximately 80 percent of the energy produced in the world is by means of fossil fuels followed by combustible biomass and waste (10.2%), nuclear energy (5.8%), hydroelectric dams (2.3%) and less than 1% by wind, solar and geothermal energy.[1] In particular, the transportation sector has the highest reliance on fossil fuels. It is well known that biofuels are the most promising alternatives to petroleum-derived fuels as they are highly compatible with current energy systems.[2] Biodiesel, a biodegradable and non-toxic fuel is of main interest as it is produced from food waste or vegetable oils. Compared to diesel oil, applying biodiesel may reduce hydrocarbons, CO_2 and particulate matter emissions by 70, 78 and 50% respectively, according to data obtained by the United States Environmental protection Agency (US EPA).[3] Currently, biodiesel is mainly produced by the transesterification of animal fats or vegetable oils which yields to 10% of crude glycerol as a byproduct.[4] With the ongoing increase in production of biodiesel there is a consequent increase in supply of crude glycerol. The production of glycerol in 2020 is approximately 4.2 million tons annually, while the demand is predicted to be less than 3.5 million tons.[5] Consequently, there is an accumulation of glycerol from the biofuel industry which must be disposed or stored, resulting in either environmental concerns or extra storage expenses. Thus, it is of high importance to explore alternative approaches for the catalytic transformation of glycerol into value-added chemicals.

The use of glycerol in electrochemical systems for the production of value-added chemicals with the consequent generation of electrical energy (fuel cell mode) or H_2 (electrolysis cell mode), has gained attention in the past two decades. However, there are still limited number of studies due to the complexity of the reaction pathways. Initially,

glycerol may be oxidized to glyceraldehyde (primary hydroxyl group) or dihydroxyacetone (secondary hydroxyl group). Then further metal-catalyzed oxidation reactions take place to form various valuable compounds (Glycerate, Tartronate, Hydroxypyruvate, Mesooxalate, Glycolate, Oxalate, and Formate), all of which have economic/industrial interest such as; tartronic acid which is an expensive reagent (US $ 1,564/ gram) used in the pharmaceutical industry to treat obesity.[6] Some of these valuable products are presently being produced by slow fermentation process that result in products with low yield [7] or by a non-environmental friendly and costly stoichiometric oxidation process.[8] The reaction pathway is mainly dependent on the nature of the catalyst, reaction medium and the applied potential. The main challenge is to develop a catalyst that has high catalytic activity, stability and selectivity to valuable C_3 products [DHA, GLYAC, GLYALD, HYPAC, TARAC and MESAC].

Up to date, research is focused on tuning and improving the activity and selectivity of platinum, palladium and gold catalysts.[3] However, these noble metals are expensive which may impact their actual practicality in industry. Thus, research interests moved to studying comparably less expensive catalysts such as; nickel, cobalt and copper. Nickel (Ni) proved to have high electrochemical redox activity, large specific capacitance and high stability in alkaline medium.[9] It was also shown that the incorporation of a secondary metal (Co, Fe, Cu, Pd, Bi) into Ni catalyst, negatively shifts the onset potential and higher activity is achieved.[10–12] Moreover, the incorporation of an electrically conducting support with high S.A such as carbon, improves the activity of the catalyst. However, carbon at severe alkaline or acidic conditions may corrode resulting in weak metal-support interactions.[13] Alternatively, metal-oxide supports exhibit high stability and conductivity.[14] There is still more space for improvement of catalytic performance (i.e. activity and durability) and selectivity of nickel-based catalysts.

1.2 Scope of work

The main objective of this thesis is to develop active/durable bimetallic Ni-rich NiBi catalysts and tune their selectivity to C_3 value-added chemicals by hindering the cleavage of glycerol C-C bonds. In order to fulfill this overall objective of this thesis, the following approach was taken:

- Develop carbon supported Ni_xBi_{100-x} catalysts with different Ni:Bi atomic ratios [x=100, 95, 90, 80 and 50 at.%] to determine the effect of composition of nanoparticles on GEOR electrochemical performance in alkaline medium by running various electrochemical tests [cyclic voltammetry (CV), linear sweep voltammetry (LSV) and chronoamperometry (CA)].
- Study the product selectivity of $Ni_{95}Bi_5$/C and Ni/C by means of continuous electrolysis accompanied by HPLC analysis, to study effect of bismuth on product distributions for GEOR.
- Determine the effect of experimental conditions (applied potential, temperature and residence time) on product selectivity of NiBi/C.
- Fabricate NiBi/C-X (X=CeO_2, SnO_2 and ATO) nanocatalysts to determine effect of metal oxides on GEOR electrochemical performance and selectivity to C_3 products.

1.3 Thesis structure

This thesis contains 5 main chapters and appendices. Chapters 3 and 4 present articles to be submitted to publication.

Chapter 1: Brief overall introduction to the thesis presenting the main problem statements along with thesis objectives.

Chapter 2: A literature review on the glycerol electrooxidation into value added products

Chapter 3: Shows detailed investigation of electrochemical performance and product selectivity of carbon supported NiBi catalysts with different atomic ratios of Ni:Bi for GEOR in alkaline medium. In addition, effect of experimental conditions on product distributions is extensively discussed.

Chapter 4: describes the role of metal oxides (CeO_2, SnO_2 and ATO) on the electrochemical performance and product selectivity of carbon supported Ni and NiBi catalysts.

Chapter 5: shows an overall conclusion of the thesis along with summary of chapter results and comparison with platinum and non-platinum group metals reported in literature for GEOR. In addition, a few suggested future recommendations are given for this work.

Appendices: presents work done as second author during the period of my study. I have contributed to the synthesis and electrochemical testing of all catalysts.

1.4 References

[1] M. Hook, X. Tang, *Energy Policy* **2013**, *52*, 797.

[2] J. Lee, J. Kim, Y. Sik, E. E. Kwon, *Bioresour. Technol.* **2017**, *239*, 17.

[3] M. S. E. Houache, K. Hughes, E. A. Baranova, *Sustain. Energy Fuels* **2019**, *3*, 1892.

[4] F. Yang, M. A. Hanna, R. Sun, *Biotechnol. Biofuels* **2012**, *5*, 1.

[5] Z. Li, J. Yan, J. Sun, P. Xu, C. Ma, C. Gao, *Commun. Chem.* **2018**, *1*, 1.

[6] J. Sankar, E. N. Onyeozili, E. E. Kalu, *ChemEngineering* **2017**, *1*, 1.

[7] R. Bauer, D. Hekmat, *Biotechnol. Prog.* **2006**, *22*, 278.

[8] S. Carrettin, P. Mcmorn, P. Johnston, K. Griffin, J. Kiely, G. J. Hutchings, *Phys. Chem. Chem. Phys.* **2003**, *5*, 1329.

[9] V. L. Oliveira, C. Morais, K. Servat, T. W. Napporn, P. Olivi, K. B. Kokoh, G. Tremiliosi-Filho, *Electrocatalysis* **2015**, *6*, 447.

[10] V. L. Oliveira, C. Morais, K. Servat, T. W. Napporn, G. Tremiliosi-Filho, K. B. Kokoh, *J. Electroanal. Chem.* **2013**, *703*, 56.

[11] M. S. E. Houache, K. Hughes, A. Ahmed, R. Safari, H. Liu, G. A. Botton, E. A. Baranova, *ACS Sustain. Chem. Eng.* **2019**, *7*, 14425.

[12] M. S. E. Houache, K. Hughes, R. Safari, G. A. Botton, E. A. Baranova, *ACS Appl. Mater. Interfaces* **2020**, *12*, 15095.

[13] C. Zhou, F. Peng, H. Wang, H. Yu, C. Peng, J. Yang, *Electrochem. commun.* **2010**, *12*, 1210.

[14] S. Takenaka, H. Matsumori, K. Nakagawa, H. Matsune, E. Tanabe, M. Kishida, **2007**, 15133.

Chapter 2: Literature Review

2.1 History of glycerol; Discovery, market and applications

In 1783, glycerol ($C_3H_8O_3$) was discovered by a chemist Carl Wilhelm Scheele while purifying oils with alkali metals forming a sweet liquid which he called "Scheele's sweet".[1] He published an article titled "Discovery of a special sweet and volatile constituent of pressed oils and animal fats" in year 1784.[2] Glycerol did not have any practical use until year 1866, it was used to produce dynamite which is an explosive material used in construction.[1] At the end of the 19th century, the production of glycerol largely and continuously increased by the processing of natural oils and fats.[1] Today, crude glycerol is produced as a byproduct from fats and oils in oleochemical or biodiesel plants. The three main routes are saponification (Y=ONa), hydrolysis (Y=OH) and transesterification ($Y=OCH_3$) reactions with the schemes shown in Figure 2.1.[3] Crude glycerol produced as a byproduct of biodiesel (fatty acid methyl esters) is usually a mixture of glycerol, water, organic and inorganic salts, soap, alcohol, traces of glycerides and vegetable colors which requires treatment to get pure glycerol.[4]

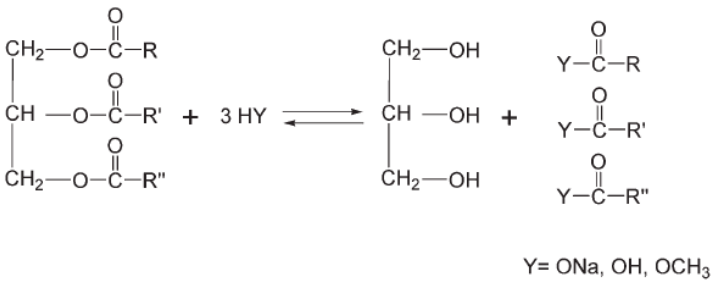

Figure 2.1: Three main routes of glycerol formation. [1]

The automotive industry in Europe and U.S increased its use of biodiesel, a renewable oil, affecting the glycerol market. As the demand for biodiesel increased, the additional glycerol formed as a byproduct saturated the market.[5] The amount of glycerol produced increased by approximately 3 times from year 1970 to 2005 and was predicted to increase further in the subsequent years.[1] Consequently, the price of glycerol dropped by half from year 2003-2006.[1] Although, glycerol is used in wide applications; pharmaceuticals, cosmetics, and food industry.[3] The production of glycerol largely exceeds its demand causing an oversupply which threatens both the environment and the

economic feasibility of biofuels. For this reason, different applications of crude glycerol are required.

Glycerol is a highly functionalized polyol compound that can be converted to a wide range of value-added chemicals through chemically selective catalysis routes. These routes include; oxidation, hydrogenolysis, dehydration, pyrolysis and gasification, transesterification and esterification, etherification and carboxylation. A summary of different routes with products formed are shown in Table 2.1.[6] Unfortunately, the use of crude glycerol is not a favorable option in catalytic processes as it contains salts and ashes that may poison the catalysts and affect their stability.[6] Thus, purification of glycerol is a requirement.

Table 2.1: Processes of catalytic conversions of glycerol

CATALYTIC PROCESS	PRODUCTS
ELECTRO-OXIDATION	DHA, GLYAC, GLYALD, HYPAC, MESAC, TARAC, OXAC, GLYCOAC, LA, FA
HYDROGENOLYSIS	1,2-PD, 1,3-PD, EG, ROH (R=C_1-C_3)
DEHYDRATION	Acetol, ACR, PGs
PYROLYSIS/GASIFICATION	C_nH_{2n+2}, C_nH_{2n}, ROH, CO/H_2, C/H_2
TRANSESTERIFICATION	MG, DG, TG
ETHERIFICATION	Mono-, di-, and tri-ethers
CARBOXYLATION	Glycerol carbonate, glycidol

Abbreviations: ACR: acrolein, DG: diglyceride, DHA: dihydroxyacetone, EG: ethylene glycol, FA: formic acid, GLYAC: glyceric acid, GLYALD: glyceraldehyde, GLYCOAC: glycolic acid, HYPAC: hydroxypyruvic acid, LA: lactic acid, MESAC: mesooxalic acid, MG: monoglyceride, OXAC: oxalic acid, PD: propanediol, PG: propylene glycol, TARAC: tartronic acid, TG: triglyceride

All of these catalytic routes produce products that are useful in various industries. For instance, DHA is used in the cosmetics industry to produce tanning skincare products. 1,2- PD is used for polyester resins, liquid detergents, pharmaceuticals and cosmetics. ACR is used as an intermediate for various chemical processes such as; acrylic acid esters, super absorbent polymers and detergents productions. TG and DG used as useful petrol additives to improve viscosity and other properties. Finally, inexpensive glycerol carbonates can be utilized for new sources of polymeric materials.[5] Detailed description and applications of products formed by GEOR are shown in Table 2.2.[7]

Table 2.2: GEOR products and applications [7]

Product	Description	Application
Glyceraldehyde 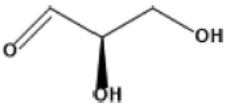	Glyceraldehyde ($C_3H_6O_3$), also known as glyceral, is a triose monosaccharide, which is the simplest of all common aldoses. It is a colorless and sweet crystalline solid, which could be obtained as an intermediate species during glycerol oxidation	Anti-aging agent, production of advanced glycation end-products (AGEs), fundamental metabolite, modification and cross-linking of proteins
Dihydroxyacetone 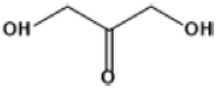	Dihydroxyacetone ($C_3H_6O_3$) (DHA), also called glycerone, is a simple saccharide (a triose). It is a ketotriose comprising acetone with hydroxy substituents at 1 and 3 positions. It is the parent of the class of glycerones and the simplest member of the class of ketoses	Antifungal agent, raw material for D,L-serine production, monomer for polymeric biomaterials, metabolite for human, *Escherichia coli*, and *Saccharomyces cerevisiae* metabolite, tanning agent in cosmetics, synthon in organic chemistry
Glyceric acid 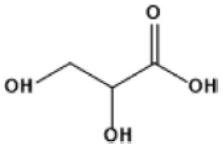	Glyceric acid ($C_3H_6O_4$) is a conjugate acid of glycerate, and a natural three-carbon sugar acid, product of glycerol oxidation. It is a trionic acid, comprising propionic acid substituted at the second and third positions by hydroxy groups	Treatment of skin disorder, intermediate in amino acid synthesis, metabolite in glycolysis cycle, medicine
Tartronic acid 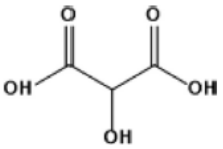	Tartronic acid ($C_3H_4O_5$), also called 2-hydroxymalonic acid, is a conjugate acid of tartronate and a dicarboxylic acid. It is a malonic acid substituted by a hydroxy group at the second position and its derivative, 2-methyltartronic acid, is an isomalic acid. Tartronic acid is a conjugate acid of a hydroxymalonate and a hydroxymalonate(1-)	Treatment of obesity and osteoporosis, oxygen scavenger
Mexoxalic acid 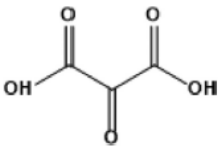	Mesoxalic acid ($C_3H_2O_5$), also known as ketomalonic acid or oxomalonic acid, is a conjugate acid of mesoxalate. Mesoxalic acid is both a ketonic acid and a dicarboxylic acid, which voluntarily loses two protons to produce mesoxalate, a divalent anion $C_3O_5^{2-}$	Anti-HIV agent, raw material for organic synthesis, complexing agent
Lactic acid 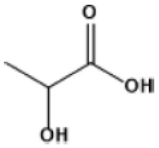	Lactic acid ($C_3H_6O_3$) is the conjugate acid of lactate, and an α-hydroxy acid (AHA) because of the existence of a carboxyl group which is adjacent to the OH group. Lactic acid is synthesized conventionally by chemical synthesis or by fermentation of carbohydrates like glucose, lactose, or sucrose	Synthetic intermediate in many organic synthesis industries and in various biochemical industries, food preservative, flavoring agent, and curing agent, decontaminant in meat processing, moisturizer in cosmetics, dyeing agent in textile industry, for making yogurt and cheese production in dairy industry, tanning leather, raw material in pharmaceutical industry, production of inks and lacquers

Glycolic acid 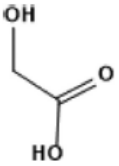	Glycolic acid ($C_2H_4O_3$), also known as hydroxyacetic acid or hydroacetic acid, is a conjugate acid of glycolate and the smallest α-hydroxy acid (AHA). It is an odorless, hygroscopic, and colorless crystalline solid, which is extremely water-soluble. Glycolic acid is found in some sugar crops	Skin care products, leather tanning agent, decreasing agent, textile dyeing, rust removal, chemical peels performed in dermatology
Oxalic acid 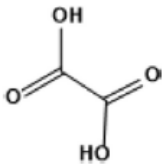	Oxalic acid ($C_2H_2O_4$) is a conjugate of oxalate and the simplest dicarboxylic acid. It forms a colorless solution in water since it is a colorless crystalline solid. It is a stronger acid than acetic acid and occurs in various vegetables and plants, and produced in human body by metabolism of ascorbic acid or glyoxylic acid	Cleaning agent, including sterilizing of household articles, rust removal, cleaning of kitchen sinks, bathtubs and counters, detergent and bleach additive, mineral processing mechanisms, bleaching agent in textile industry, purification and dilution of certain chemicals
Formic acid 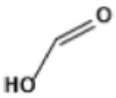	Formic acid (HCOOH), also called methanoic acid, is a conjugate of formate ion, a strong electrolyte, a liquid fuel at room temperature, and the simplest form of carboxylic acid. It is an important intermediate in chemical synthesis and could occur naturally, particularly in some ants	Fuel in fuel cells, reducing agent, environmentally benign runway anti-icing (formic acid salts), important intermediate in the synthesis of some organic compounds, finishing, grass silage in Europe, food additive, leather tanning in Asia

Some of the catalytic approaches have drawbacks such as low selectivity, high production costs [e.g., high temperatures and pressures] and/or long reaction time.[8] Developing electrochemical technologies is a much more efficient and sustainable technique than other catalysis approaches as it may be conducted at room temperature and does not require the use of pressurized oxygen.[9] The electrochemical method is favorable as it can be integrated in totally renewable systems; use of renewable energy sources for the oxidation of glycerol at the anode with the consequent production of electric energy (fuel cell mode) or H_2 (electrolysis cell mode) at the cathode compartment. The conversion rates and selectivity of the catalytic reactions may be controlled by developing different structures/compositions of the catalysts and optimizing reaction conditions such as; applied potential in the case of electro-oxidation of glycerol.[9]

2.2 Glycerol Electrooxidation Reaction (GEOR)

The use of alcohols as fuels to generate electricity is one of the many advances in the science and technology of fuel cells. These electrochemical devices are known as direct alcohol fuel cells (DAFC's). The working principles of DAFC's is similar to that of a hydrogen fuel cell, the alcohol is electro-oxidized at the anode and an oxidizing agent

(usually O_2 from air) is electro-reduced at the cathode with ions migrating through an ionic exchange membrane from the anode to the cathode. The magnitude of power produced is equivalent to the number of electrons generated by the oxidation of the alcohol.[10] In this case, it is favorable for the reaction to go to completion which may be facilitated by means of a catalyst. On the other hand, alcohols were also proposed to be used in electrolyzers for the purpose of electrosynthesis.[10] Electrolyzers, opposite to fuel cells, use electrical current to drive a non-spontaneous reaction to produce value-added chemicals.

As previously mentioned, glycerol is a highly functionalized molecule with three hydrated molecules which makes it an interesting alcohol for both applications; DAFC's and electrolyzers. The use of glycerol in fuel cells has several advantages over hydrogen; it is cheap, non-toxic and low volatile liquid which require less severe storage conditions compared to hydrogen gas.[11] In addition, the price of glycerol is 6 times cheaper than that of hydrogen.[10] As for its application in electrolyzers, glycerol may be electrooxidized into other intermediate products that are of economic and industrial interest. Notably, replacing O_2 evolution reaction by glycerol oxidation significantly decreases cell voltage requirement for H_2 production.[12]

The working principle of glycerol fuels cells and electrolyzers in acidic or alkaline medium are shown below in Figure 2.2.[13]

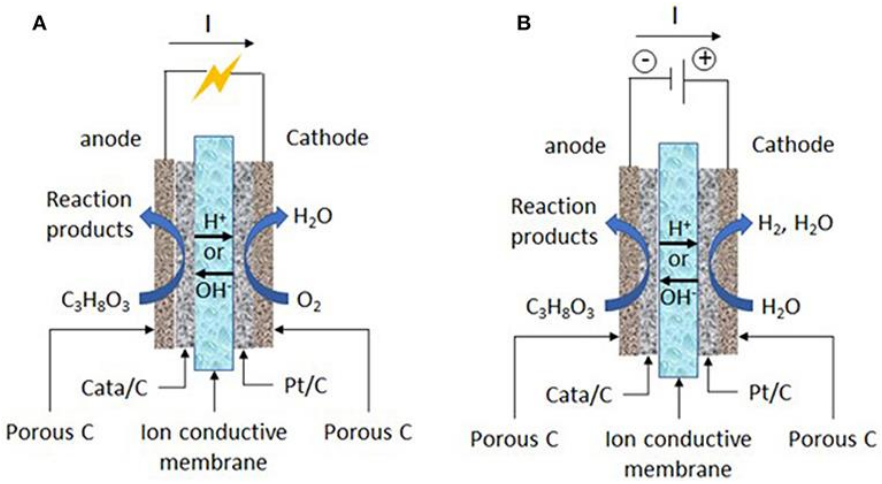

Figure 2.2: Application of glycerol in a) fuel cells and b) electrolysis cell.[13]

In the electrolysis cell mode, glycerol is fed at the anode compartment and is completely oxidized to CO_2 and protons (reaction 1).

$$C_3H_8O_3 + 3H_2O \rightarrow 3CO_2 + 14H^+ + 14e^- \quad \text{[rxn 1]}$$

Reaction 1 occurring at the anode of an electrolysis cell is thermodynamically unfavorable as the calculated reaction enthalpy ($\Delta G°$) is 3.9 kJ/mol which is greater than zero, this indicates that an external energy source is required for the reaction to take place.[14]

Presently, there still lies some challenges that make the use of glycerol in fuel cells and electrolyzers impractical. The main complexity is that GEOR occurs in several reaction pathways which lead to the partial oxidation of glycerol into various products. For DAFC's, it is difficult to completely break the C-C-C bond to form CO_2 with the release of 14 electrons. As for electrolyzers, the challenge lies in tuning the selectivity to higher value C_3 products such as; tartronate which is an expensive compound (US $ 1,564/gram) used in pharmaceutical formulations.[15] The different reaction pathways are shown in Figure 2.3.[16]

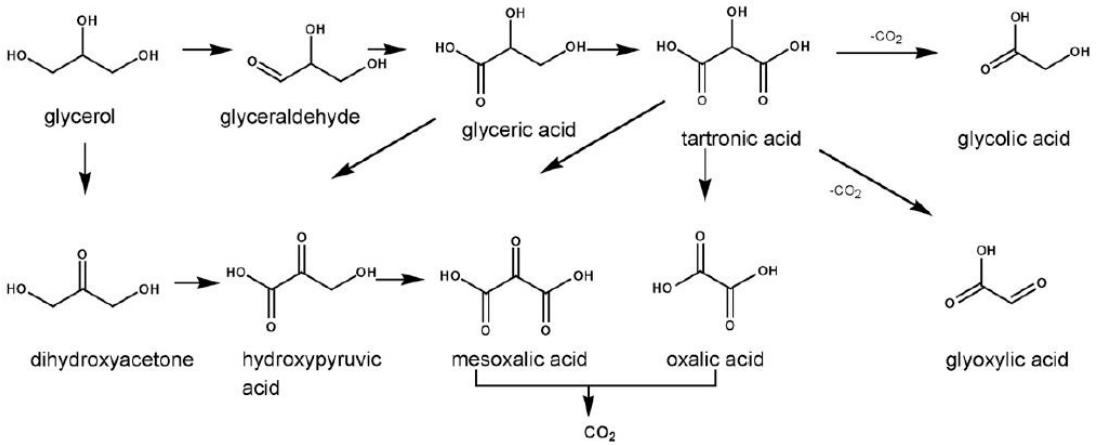

Figure 2.3: glycerol oxidation reaction pathways. [22]

Generally, for alcohol electro-oxidation reactions the process goes through several phases: adsorption of the alcohol, breakage of inter-atomic bonds, electron charge transfer, reactions between oxygenated species and fragments of the alcohol, and desorption of reaction products.[16] Glycerol undergoes oxidation by interacting with OH^- ions in alkaline medium which are regenerated by reaction of electrons in an oxygen atmosphere.[7] By means of theoretical and experimental methods, the fundamentals of glycerol oxidation mechanism were intensively explored for various catalysts at different applied potentials. For instance, the most spontaneous pathway for GEOR on Au (111) catalyst was determined via computational DFT study.[13] It was shown that at higher

potentials greater than 0.5V vs RHE the Au active sites are blocked by CO. Additionally, spectroscopic and chromatographic experimental techniques are commonly applied such as; ion chromatography (IC) and nuclear magnetic resonance (NMR) spectroscopy[17], in-situ electro-modulated infrared reflectance spectroscopy (EMIRS)[18], Fourier transform infrared spectroscopy (FTIR)[19], in-situ FTIR[20,21], differential electrochemical mass spectroscopy (DEMS) [22] and high performance liquid chromatography (HPLC)[23] which aid in proposing the different reaction mechanisms.

It has been determined that the efficiency and selectivity to valuable C_3 products of the GEOR varies with some aspects, including the applied potential, reaction medium and mostly the surface reactions occurring at the interface between the electrode and the solution. The surface reactions are highly dependent on the nature and size of the catalyst deposited on the surface. The catalyst varies the reaction pathway by altering the rate of parallel and consecutive reactions that usually occur during the conversion of any reactant.[10] The properties of supported catalysts may be tuned by (i) control the size and shape of the active metal particles, (ii) form a bimetallic phase, and/or (iii) use of metal support interactions (MSI) as shown in Figure 2.4.

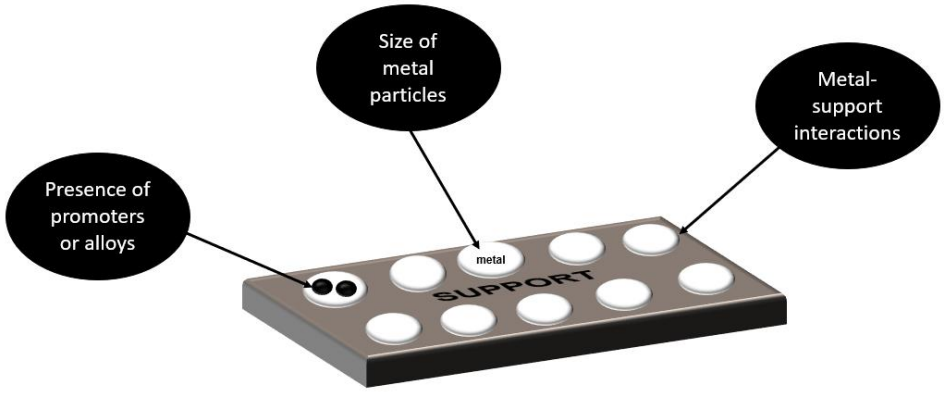

Figure 2.4: Fine tuning of active metal catalysts

2.3 Development of Electro-catalysts for GEOR

In the process of evaluating the performance of anodic electro-catalysts, it is desired that they possess high selectivity towards C_3 value-added products and achieve high catalytic activity at a lower onset potential to reduce electrical energy consumption. In order to achieve high performing catalysts for GEOR, the number and activity of the active sites must be increased. As previously mentioned, the catalytic performance and selectivity may be affected by modifying the surface of the anode with co-catalysts/promoters, different morphologies and supports.

2.3.1 Noble metals Pt, Pd and Au in acidic and alkaline medium

Platinum, palladium and gold are the most widely studied catalysts for glycerol electrooxidation reaction.[24–30] These catalysts show different catalytic activity and selectivity depending on the reaction medium. Platinum and platinum- based catalysts are among the few materials that show excellent activity and high stability in acidic medium.[31] However, during the reaction platinum active sites are blocked by carbonaceous species adsorbed on the surface which inhibits its activity.[32] Thus, effective oxidation of alcohols on platinum catalysts may only be achieved at higher potentials where the poisonous species can also be oxidized.[33] This drove researchers to explore alternative Pt-free materials such as palladium and gold-rich catalysts.[34–43] Although previous research indicated that gold is an inactive catalyst in acidic medium, a recent study by Valter et al. (2018) proposed that gold is an electroactive catalyst for GEOR in acidic medium.[44,45] This contradiction was explained by the nature of the supporting electrolyte used by those researchers. In 0.1 M $HClO_4$ compared to 0.5 M H_2SO_4, gold shows activity for alcohol oxidation. It appears that the sulfates highly adsorb on the gold surface compared to perchlorate ions, blocking the active sites or competing with glycerol adsorption.[46] In alkaline medium, the activity and stability of all noble metal catalysts including platinum is higher.[47] The first glycerol deprotonation step in alkaline medium does not depend on the catalytic ability of the surface and is base catalyzed which is the reason for activity enhancement in alkaline medium.[48]

Unmodified polycrystalline platinum and gold electrodes were studied for the glycerol electrooxidation reaction (GEOR) in alkaline medium. By means of cyclic

voltammograms, gold had approximately 10x higher current density than the platinum electrode, only at higher potentials.[44] While the onset potential of platinum was 0.4V lower than that of gold.[44] Zhang et al. compared the catalytic performance of platinum, palladium and gold electrodes for GEOR.[49] Similarly, gold had a remarkable peak current density of 55.4 mA/cm^2 (1.232V) compared to 8.5 mA/cm^2 (0.87V) on platinum electrode. On the other hand, palladium electrode had a comparable peak current density and potential of 6.3 mA/cm^2 (0.895V) to platinum electrode. [49]

On both platinum and gold electrodes, the main product detected was glyceric acid however, glyceric acid is easily oxidized to glycolic and formic acid on gold electrodes due to the larger potential required to activate the gold electrode.[44] A schematic diagram in Figure 2.5 describes the reaction mechanism of platinum and gold electrodes.

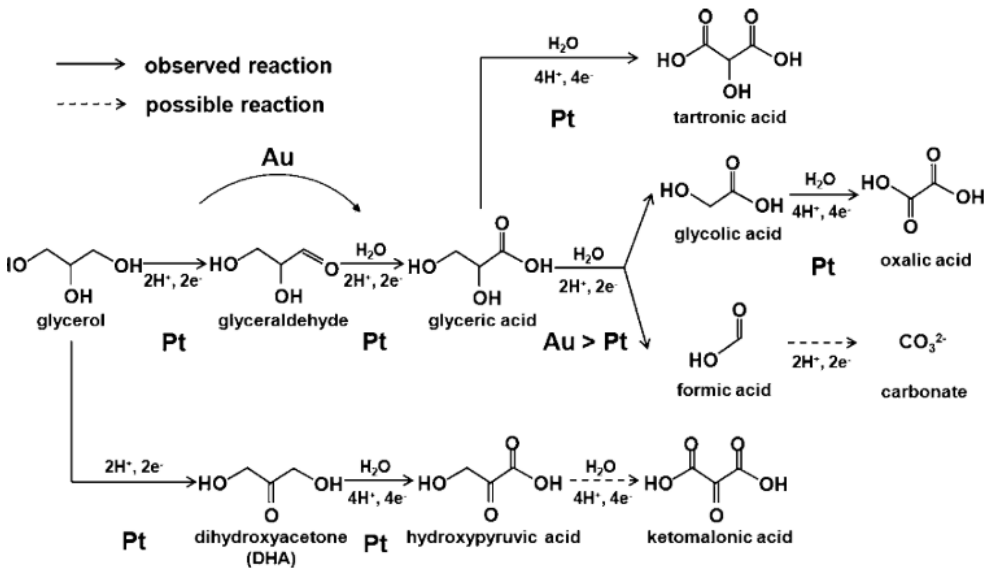

Figure 2.5: Reaction mechanism of Au and Pt in alkaline medium. [44]

Up to date, plenty of platinum, palladium and gold- based materials with improved stability and electrochemical performance have been developed e.g. PtNi [30,50], PtAg [51], PtBi [52], PdAg [53], PdNi [54], PdRu [55], PdPb [56], AuPt [57], AuPd [58], AuNi [59] and AuAg [42]. This improvement may be dedicated to bifunctional, synergistic and/or electronic effects. These effects are observed when two foreign metals from different functional groups or different electronic configurations are alloyed forming a

catalyst with new reactivity and/or selectivity for the reaction. When Pt- rich catalyst is alloyed with Ni, the peak current density of the catalyst Pt_2Ni_1/C was 1.5 folds higher compared to pure Pt/C.[50] Different surface compositions of Pt:Ni were studied, catalytic activity from highest to lowest are Pt_2Ni_1 > Pt_3Ni_1 > Pt_1Ni_1 >Pt owing to the higher electrochemical active surface area of Pt_2Ni_1.[50] In addition to higher EASA, the bifunctional effect also known as third body effect was observed, nickel enhanced the number of OH adsorbed species on the Pt surface which aided the removal of the adsorbed intermediate carbonaceous species (CO) via Langmuir-Hinshelwood mechanism (CO_{ads} + $OH_{ads} \rightarrow CO_2 + H^+ + e^-$).[9,30] Recent studies showed that modifying platinum electrodes with bismuth (Bi) or antimony (Sb), which are p-group metal promoters, led to a promotion in activity due to the third body effect.[60] In addition, modifying Pt surface with bismuth adatoms enhanced selectivity to C_3 valuable products such as; glyceric acid, dihydroxyacetone and glyceraldehyde while, on bare Pt surface main products were glycolic and formic acid.[61] Results by Kwon et al. also showed that the Pt surface modified with Bi favored the oxidation of the secondary hydroxyl group leading to dihydroxyacetone which was not observed in the absence of promoter Bi, as shown in Figure 2.6.[61]

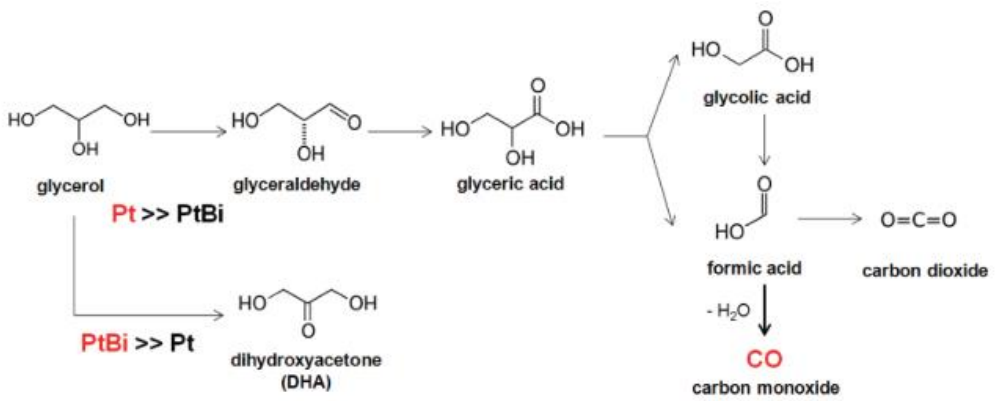

Figure 2.6: Reaction mechanism on Pt compared to PtBi. [61]

It is worthy to note that metal oxides promoters (CeO_2, Co_3O_4, Mn_3O_4, and NiO) enhanced the catalytic performance of Pd/C and Pt/C for ethanol electrooxidation.[62] Similarly, the addition of CeO_2 to Pt/C increased the activity and stability of the Pt catalyst for glycerol, methanol, ethanol and ethylene glycol electrooxidation reactions.[63] Specifically for GEOR, the peak current density and peak potential of Pt/C and Pt-CeO_2/C were 21.0

mA/cm^2 (-0.07V) and 36.0 mA/cm^2 (-0.09V), respectively.[63] The addition of ceria to Pt/C improved the activity although, the electrochemical active surface areas of both Pt/C and Pt-CeO_2/C were similar. Ceria has the ability to adsorb oxygen-containing species which reacts with the poisoning species (e.g CO), leaving the active sites for glycerol oxidation.[63] Thus, ceria increased the poisoning tolerance of Pt/C.

In addition to alloys and promoters, different structures of Pt, Pd and Au were intensively studied. The surface structure highly influences both the activity and selectivity of the catalyst. By varying the synthesis method, various structures of Pt were constructed such as; cuboctahedral, tetrahedral and colloidal NP's.[64] Cuboctrahedral Pt-based NP's showed higher catalytic activity compared to tetrahedral. However, the selectivity remained unchanged. On the other hand, colloidal Pt-based NP's enhanced the selectivity to glyceraldehyde which is a C_3 valuable product.[64] Though, the activity of the colloidal catalyst declined faster. In addition, Pt catalysts with larger nanoparticle size had higher reaction kinetics.[64] Moreover, Pd nanocubes compared to nanospheres exhibited higher catalytic performance. The catalytic performance of Pd nanocubes were further increased by modifying with Bismuth adatoms.[65]

2.3.2 Nickel-based catalysts

Although, precious metals (Pt, Pd and Au) are considered the top electrocatalysts for GEOR in terms of catalytic performance, their high cost and limited availability, as well as poor anti-poisoning capability to carbonaceous species (e.g. CO) are drawbacks to large scale commercial applications. On the other hand, nickel (Ni) is a cheap metal that is abundantly available. In addition, Ni has anti-poisoning capability and long-term stability in alkaline media, making them an attractive alternative for glycerol electrooxidation in alkaline medium.[66] It is well known that Ni has noticeable activity for Alcohol electrooxidation in alkaline medium.[67] Since a coating of nickel hydroxides covers the Ni surface as soon as it is placed in alkaline medium [68], the surface transformation can be written as:

$$Ni + 2OH^- \rightarrow Ni(OH)_2 + 2e^- \quad \text{[rxn 2]}$$

$$Ni(OH)_2 + OH^- \rightarrow NiOOH + H_2O + e^- \quad \text{[rxn 3]}$$

The nickel bode scheme (shown in Figure 2.7) is a widely accepted mechanism that demonstrates the charging/discharging process of nickel hydroxides. The hydrated α-$Ni(OH)_2$ phase is converted to the less hydrated, more crystalline β-$Ni(OH)_2$ phase via electrochemical aging.

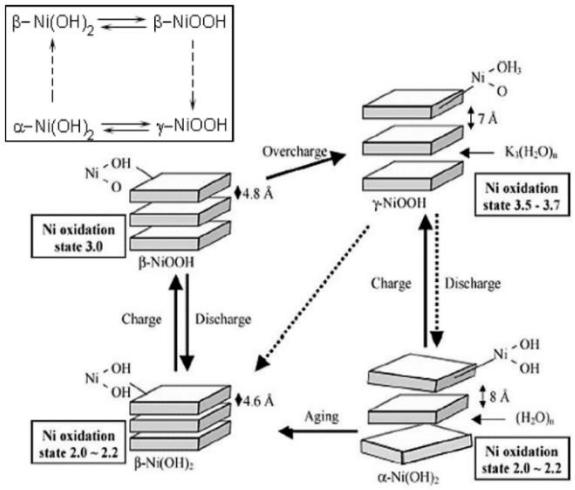

Figure 2.7: Nickel hydroxides Bode scheme. [69]

By electrochemical cycling, the β-$Ni(OH)_2$ is reversibly converted to β-NiOOH under oxidation/reduction conditions. Overcharging of β-NiOOH leads to γ-NiOOH which is reversibly converted to α-$Ni(OH)_2$. This mechanism is shown above in Figure 2.7.[69]

Overcharging β-NiOOH to γ-NiOOH is undesirable, as it consequently leads to a large volumetric change causing weak electric interaction between the current collector and the catalyst.[66] According to the "indirect" mechanism proposed by Fleishmann et al. (reaction 4), β-NiOOH is the required nickel-hydroxide phase that activates GEOR.[68] In this mechanism, glycerol is electrooxidized to form intermediate products and NiOOH is reduced to $Ni(OH)_2$.

$$\beta\text{-NiOOH} + C_3H_8O_3 \rightarrow \beta\text{-Ni(OH)}_2 + \text{products} \quad [\text{rxn } 4]$$

Another mode of reaction was proposed which is known as the "direct" electron transfer mechanism.[70] In this reaction, glycerol adsorbs to the $Ni(OH)_2$ phase and is oxidized by OH^- ions without depleting the NiOOH phase, which is represented in reaction 5.

$$Ni(OH)_2 + C_3H_8O_3 \rightarrow Ni(OH)_2(C_3H_8O_3)ads \rightarrow NiOOH + products + H^+ + e^- \quad [5]$$

Typically, the mode of reaction "indirect" or "direct" is governed by the concentration of glycerol. At lower glycerol concentration (<100mM) the "direct" mechanism is reported and "indirect" electron transfer mechanism at higher glycerol concentration (>100mM).[71]

For Ni-based catalysts, the transition from $Ni(OH)_2$ to NiOOH occurs at higher potentials (~1.3V vs RHE).[67] Therefore, according to the indirect mechanism the GEOR reaction may only occur at higher potentials than 1.3V vs. RHE. However, several studies on Ni-based materials reported glycerol oxidation at potentials lower than 1.3V vs RHE.[72,73] It appears that the early steps of the transition of Ni^{2+} to Ni^{3+} were crucial for the oxidation of glycerol.

To characterize the electrode surface electrochemically, cyclic voltammetry (CV) in the absence of glycerol may be conducted. A typical cyclic voltagramm (potential-current profile) of pure Ni nanoparticles in the absence of glycerol is shown in Figure 2.8 (black line).[67] The peak in the forward scan at 1.4V is associated with the oxidation of β-$Ni(OH)_2$ to β-NiOOH and the vice versa in the reverse scan. Since the β-phase is the most thermodynamically stable phase thus, the α/γ- phases are not usually observed.

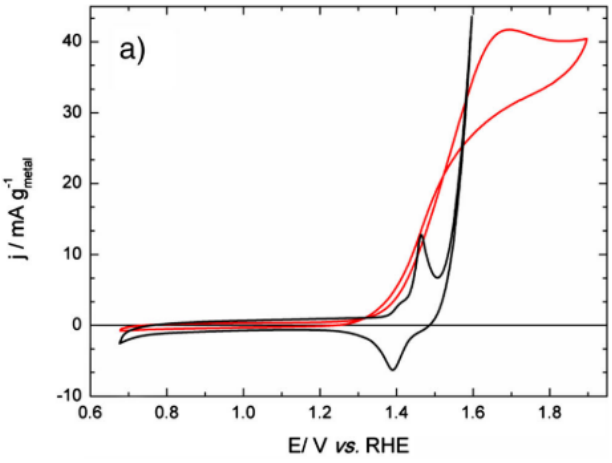

Figure 2.8: CV of pure Ni/C in 0.1 mol/L NaOH at scan rate 5 mV.s^{-1} in the absence of glycerol (black line) and in the presence of 0.1 M glycerol (red line). [67]

Running CV's in the presence of glycerol provide an understanding of the catalytic performance in terms of activity (peak current density) and energy required (onset potential). As shown in Figure 2.8 (red line), the cathodic peak completely disappeared indicating an indirect mechanism took place as the NiOOH is depleting from the surface.

To develop nickel-based catalysts with enhanced performance, characterization of the nickel surface is essential as it provides an understanding of the nature of the active sites and their influence on GEOR product distributions. The typical reaction mechanism on nickel-based catalysts is shown in Figure 2.9.[71]

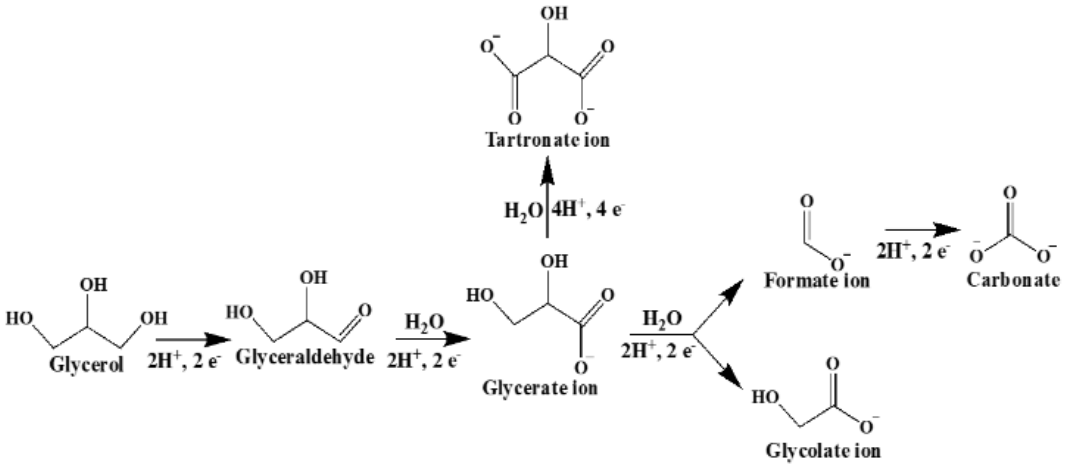

Figure 2.9: proposed reaction mechanism of Ni rich catalyst Ni_xPd_{1-x} in alkaline medium for GEOR. [71]

GEOR on Ni electrocatalysts in alkaline medium has been explored in several studies.[71,72,74–78] Different structures of Nickel such as; hexagonal close-packed nickel nanocrystals [73], $Ni(OH)_2$ modified with poly[Ni(salen)] [79], Ni surface treated with electrochemical sinusoidal-waves [74], and indium tin oxide (ITO) electrode implanted/modified by nickel ions [80], all of which showed higher performance than the conventional Ni electrode. The study by Houache et. al. on pretreatment of Ni surface with electrochemical sinusoidal-waves in ascorbic acid, showed that before the treatment the surface comprised of Ni metal, $Ni(OH)_2$, NiOOH and NiO.[74] After the treatment, the surface was 97% covered by $Ni(OH)_x$ significantly reducing the metallic surface. This treatment led to a significant increase (9 folds) in current density.

However, the performance is still too low for large scale commercial applications. Thus, modifying the electrodes with a bimetallic promoter/adatom such as; Co, Fe, Pd, Cu, Bi and TiO_2 has been considered. The addition of Co had a positive effect on the catalytic performance of Ni.[23,75,81–85] This observation is attributed to NiOOH formation at lower onset potential. Additionally, a DFT study shows that the addition of Co to Ni may enhance the surface coverage by redox species while, weakening the adsorption of CO.[86] Moreover, the presence of TiO_2 on Ni (TiO_2-Ni/C) alters chemical state of Ni: enhancing $Ni(OH)_2$ and reducing NiO on the surface.[85] This led to 2.4 times higher GEOR activity than Ni/C. Moreover, adding (Pd, Au and Bi) to Ni in small amounts (≤20 wt&) resulted in an enhancement in catalytic performance by lowering the onset potential and increasing the current density.[87] In terms of selectivity, generally on nickel-based catalysts the C-C bonds tend to break leading to higher selectivity towards C_2 and C_1 products (mainly formate, glycolate and other carboxylates).[13] For NiCo electrocatalyst, the addition of Co enhanced the C-C bond cleavage to lower value products.[72] Adding (Pd, Au and Bi) in small amounts did not alter the selectivity of Ni/C leading to 100% selectivity to formic acid as detected by in-situ FTIR and HPLC.[87]

2.4 Metal-support interaction effect on GEOR

As discussed earlier, the catalytic activity and selectivity of metal catalysts may be tuned by NP morphology (size and shape), composition, and support. The role of nanoparticles support must not be disregarded as it is a critical parameter. Utilizing support-induced phenomena may allow the design of catalysts with advanced catalytic activity and selectivity.[88] The degree of metal-support interactions is affected by the type [89–91], structure [92,93] and composition [94–96] of support material.

The use of catalyst supports is essential as they provide better dispersion of nanoparticles and reduce agglomerations of the active metal species. Most of the catalysts are supported on carbon, specifically Vulcan XC72, as it exhibits large surface area (~250 m^2/g for Vulcan XC72), low cost, high electrical conductivity and may be easily tuned.[97] When carbon black is used alone as a support in fuel cells, the catalyst suffers from loss of activity and stability under highly acidic or alkaline medium at higher temperatures over time.[98] Reason is due to the corrosion of the carbon support and consequently

detachment of the metal nanoparticles. This is an example of weak metal-support interactions which results in quick degradation of catalytic performance.

To combat these problems, several studies concentrated on developing alternate supports to carbon. Metal-oxides seemed to be the best and most widespread alternative as they are resistant to corrosion and display strong metal-support interactions (SMSI). In addition, oxide supports have the ability to improve the stability and conductivity of the catalyst, it may also act as a co-catalyst influencing the activity.[99] However, one must note that the surface area of these oxides (~20-80 $m^2.g^{-1}$) are much lower than carbon which might prevent uniform distribution of the metals and less area for active sites.

Most commonly used oxides are TiO_2 nanotubes and nanofibers [100,101], β-MnO_2 nanotubes [102], Al_2O_3 [103], CeO_2 [104,105] and SnO_2 [106,107].

2.4.1 Applications and electrochemical properties of CeO_2

Ceria (CeO_2) was first discovered by scientists in Sweden and Germany in the year 1803.[108] It is light rare-earth metal, mainly found in minerals Bastnasite, Monazite and loparite.[108] It has a calcium fluoride (fluorite) chemical structure with Fm3m space groups over a wide temperature range.[109] Due to its rare properties, it has been widely used in various industrial applications such as; capturing free oxygen and sulfur from iron casting melts and a polishing agent in glass/screen manufacturing processes.[108] In addition, ceria-rich materials were explored as electrolytes in solid oxide fuel cells owing to their high ionic conductivity.[110] Ceria was also used as an oxygen storage material in automotive three-way catalytic converters (TWC's) which is known to be the most successful industrial application of ceria since the 1980's.[108] It was reported that ceria is highly stable at higher temperatures and its redox cycle Ce^{3+} to Ce^{4+} is easily reversible which are the main reasons for its success in TWC's.[111] It is important to note that CeO_2 compared to other metal oxides such as; Al_2O_3, SnO_2, Co_3O_4, MnO_2, Fe_2O_3 and TiO_2 has higher oxygen storage (release) capacity (OSC) due to its facile redox process. [112]

CeO_2 on its own has insufficient activity to perform oxidation thus, it must be either doped with metal in its lattice or loading metals on its surface.[113] Depending on the concentration of ceria, it may act as a support for active materials or the active metal may

be incorporated in the fluorite lattice of ceria forming solid solutions.[108] Usually, at lower concentrations of ceria the latter occurs. Incorporating metals in the lattice of ceria may alter the activity and physical properties depending on the type of metal doped.[88] Also, loading metal on the ceria surface can form novel interface active sites.[113] The activity of metal-ceria catalysts depends on metal particle size, support morphology, metal-support interactions (MSI), and oxygen storage capacity (OSC).[113]

2.4.2 Applications and electrochemical properties of SnO_2

Pure stannic oxide (SnO_2) has a tetragonal rutile chemical structure with D_{4h}^{14} space groups.[114] SnO_2 in its undoped form is an n-type semiconductor with a wide bandgap.[114] They are widely applied as conducting transparent materials in photovoltaics and optoelectronics. [115] For instance, SnO_2 films are used to produce transparent heating elements and transistors. Recently, tin oxides have also been viewed as potential alternative support material in the field of electrochemistry.[106] The main advantages of using these oxides are their relatively high conductivity and good stability.[116,117] Tin-based oxides have proved to enhance the catalytic activity and stability of catalysts due to strong-metal-support interactions (SMSI).[115]

The most commonly used tin-based conductive oxides in electrochemical cells are antimony tin oxide (ATO), indium tin oxide (ITO) and fluorine tin oxide (FTO). Extensive research using these materials were studied, a few of the studies will be mentioned here. ATO is used as a cathode support material in proton exchange membrane (PEM) fuel cells and for catalyzing the oxygen evolution reaction (OER) in PEM electrolysis cell making it a promising material in regenerative fuel cells.[118–120] ITO is studied as a support material to platinum to oxidize methanol and formaldehyde and enhance oxygen reduction reaction in fuel cells.[121–123] FTO is mainly used in solar cells and other electrochemical applications.[124,125] A study by Hyung-Suk Oh et al. shows that ATO has an electrical conductivity of 0.295 $S.cm^{-1}$ which is higher than 0.0017 $S.cm^{-1}$ for undoped SnO_2, 0.102 $S.cm^{-1}$ for FTO and 0.223 $S.cm^{-1}$ for ITO.[116] One can conclude that doping tin oxides results in higher electrical conductivity.

2.5 References

[1] A. Behr, J. Eilting, K. Irawadi, J. Leschinski, F. Lindner, Cutting-edge research for a greener sustainable future Improved utilisation of renewable resources : New important derivatives of glycerol, Green Chem. 10 (2008) 13–30. https://doi.org/10.1039/b710561d.

[2] A. Lennartson, The Chemical Works of Carl Wilhelm Scheele, Springer nature, 2017. https://doi.org/DOI 10.1007/978-3-319-58181-1.

[3] H.W. Tan, A.R.A. Aziz, M.K. Aroua, Glycerol production and its applications as a raw material : A review, Renew. Sustain. Energy Rev. 27 (2013) 118–127. https://doi.org/10.1016/j.rser.2013.06.035.

[4] M. Hájek, F. Skopal, Bioresource Technology Treatment of glycerol phase formed by biodiesel production, Bioresour. Technol. 101 (2010) 3242–3245. https://doi.org/10.1016/j.biortech.2009.12.094.

[5] C.A.G. Quispe, C.J.R. Coronado, J.A. Carvalho, Glycerol : Production , consumption , prices , characterization and new trends in combustion Glycerol : Production , consumption , prices , characterization and new trends in combustion, Renew. Sustain. Energy Rev. 27 (2013) 475–493. https://doi.org/10.1016/j.rser.2013.06.017.

[6] N.P. and S.C. Jan C.J. Bart, Valorisation of the glycerol by-product from biodiesel production, in: Biodiesel Sci. Technol. from Soil to Oil, 2010: pp. 571–615. https://doi.org/10.1533/9781845697761.571.

[7] P.A. Alaba, C.S. Lee, F. Abnisa, M.K. Aroua, A review of recent progress on electrocatalysts toward efficient glycerol electrooxidation, Rev Chem Eng. (2020).

[8] P. Gallezot, Selective oxidation with air on metal catalysts, Catal. Today. 37 (1997) 405–418.

[9] C. Coutanceau, S. Baranton, R.S.B. Kouamé, Selective Electrooxidation of Glycerol Into Value-Added Chemicals : A Short Overview, Front. Chem. 7 (2019) 1–15. https://doi.org/10.3389/fchem.2019.00100.

[10] C.A. Martins, P.S. Fernandez, G.A. Camara, Alternative Uses for Biodiesel Byproduct: Glycerol as Source of Energy and High Valuable Chemicals, in: Increased Biodiesel Effic., 2018: pp. 159–186. https://doi.org/10.1007/978-3-319-73552-8.

[11] K. Kakaei, M.D. Esrafili, A. Ehsani, Alcohol Oxidation and Hydrogen Evolution, in: Graphene Surfaces Part. Catal., 2019: pp. 253–301. https://doi.org/10.1016/B978-0-12-814523-4.00007-1.

[12] A.T. Marshall, R.G. Haverkamp, Production of hydrogen by the electrochemical reforming of glycerol-water solutions in a PEM electrolysis cell, Int. J. Hydrogen Energy. 33 (2008) 4649–4654. https://doi.org/10.1016/j.ijhydene.2008.05.029.

[13] C. Coutanceau, S. Baranton, R.S.B. Kouamé, Selective electrooxidation of glycerol into value-added chemicals: A short overview, Front. Chem. 7 (2019) 1–15. https://doi.org/10.3389/fchem.2019.00100.

[14] M.S.E. Houache, K. Hughes, E.A. Baranova, Study on catalyst selection for electrochemical valorization of glycerol, Sustain. Energy Fuels. 3 (2019) 1892–1915. https://doi.org/10.1039/c9se00108e.

[15] X. Tian, Z. Wang, P. Yang, R. Hao, S. Jia, N. Li, RSC Advances Green oxidation of bio-lactic acid with H 2 O 2 into tartronic acid under UV irradiation †, (2016) 41007–41010. https://doi.org/10.1039/C6RA05028J.

[16] S. Demirel, K. Lehnert, M. Lucas, P. Claus, Use of renewables for the production of chemicals : Glycerol oxidation over carbon supported gold catalysts, Appl. Catal. B, Environ. 70 (2007) 637–643. https://doi.org/10.1016/j.apcatb.2005.11.036.

[17] L. Huang, J.Y. Sun, S.H. Cao, M. Zhan, Z.R. Ni, H.J. Sun, Z. Chen, Z.Y. Zhou, E.G. Sorte, Y.Y.J. Tong, S.G. Sun, Combined EC-NMR and in Situ FTIR Spectroscopic Studies of Glycerol Electrooxidation on Pt/C, PtRu/C, and PtRh/C, ACS Catal. 6 (2016) 7686–7695. https://doi.org/10.1021/acscatal.6b02097.

[18] S.G. Sun, J. Clavilier, A. Bewick, The mechanism of electrocatalytic oxidation of formic acid on Pt (100) and Pt (111) in sulphuric acid solution: an emirs study, J. Electroanal. Chem. 240 (1988) 147–159. https://doi.org/10.1016/0022-0728(88)80319-X.

[19] J.F. Gomes, G. Tremiliosi-Filho, Spectroscopic Studies of the Glycerol Electro-Oxidation on Polycrystalline Au and Pt Surfaces in Acidic and Alkaline Media, Electrocatalysis. 2 (2011) 96–105. https://doi.org/10.1007/s12678-011-0039-0.

[20] J.L. Bott-Neto, A.C. Garcia, V.L. Oliveira, N.E. De Souza, G. Tremiliosi-Filho, Au/C catalysts prepared by a green method towards C3 alcohol electrooxidation: A cyclic voltammetry and in situ FTIR spectroscopy study, J. Electroanal. Chem. 735 (2014) 57–62. https://doi.org/10.1016/j.jelechem.2014.10.010.

[21] V. Del Colle, L.M.S. Nunes, C.A. Angelucci, J.M. Feliu, G. Tremiliosi-Filho, The influence of stepped Pt[n(111)×(110)] electrodes towards glycerol electrooxidation: Electrochemical and FTIR studies, Electrochim. Acta. 346 (2020) 136187. https://doi.org/10.1016/j.electacta.2020.136187.

[22] J. Schnaidt, M. Heinen, D. Denot, Z. Jusys, R. Jürgen Behm, Electrooxidation of glycerol studied by combined in situ IR spectroscopy and online mass spectrometry under continuous flow conditions, J. Electroanal. Chem. 661 (2011) 250–264. https://doi.org/10.1016/j.jelechem.2011.08.011.

[23] M.S.E. Houache, K. Hughes, R. Safari, G.A. Botton, E.A. Baranova, Modification of Nickel Surfaces by Bismuth: Effect on Electrochemical Activity and Selectivity Towards Glycerol Modification of Nickel Surfaces by Bismuth : Effect on Electrochemical Activity and Selectivity Towards Glycerol, ACS Appl. Mater. Interfaces. 12 (2020) 15095–15107. https://doi.org/10.1021/acsami.9b22378.

[24] P.K. Shen, C. Bianchini, Palladium-based electrocatalysts for alcohol oxidation in half cell and in direct alcohol fuel cells, Chem. Rev. 109 (2009) 4183.

[25] M. Simões, S. Baranton, C. Coutanceau, Electro-oxidation of glycerol at Pd based nano-catalysts for an application in alkaline fuel cells for chemicals and energy cogeneration, Appl. Catal. B Environ. 93 (2010) 354–362. https://doi.org/10.1016/j.apcatb.2009.10.008.

[26] J.H. Zhang, Y.J. Liang, N. Li, Z.Y. Li, C.W. Xu, S.P. Jiang, A remarkable activity of glycerol electrooxidation on gold in alkaline medium, Electrochim. Acta. 59 (2012) 156–159. https://doi.org/10.1016/j.electacta.2011.10.048.

[27] P. Johnston, K. Griffin, P. McMorn, G.J. Hutchings, S. Carrettin, Selective oxidation of glycerol to glyceric acid using a gold catalyst in aqueous sodium hydroxide, Chem. Commun. (2002) 696–697. https://doi.org/10.1039/b201112n.

[28] J.H. Zhang, T. Zhu, N. Li, C.W. Xu, Glycerol Electrooxidation on Au Supported on Carbon Spheres by Stober Method in Alkaline Medium, Int. J. Electrochem. Sci. 8 (2013) 9508–9517.

[29] E. Habibi, H. Razmi, Glycerol electrooxidation on Pd, Pt and Au nanoparticles supported on carbon ceramic electrode in alkaline media, Int. J. Hydrogen Energy. 37 (2012) 16800–16809. https://doi.org/10.1016/j.ijhydene.2012.08.127.

[30] Y. Zhou, Y. Shen, J. Piao, Sustainable Conversion of Glycerol into Value-Added Chemicals by Selective Electro-Oxidation on Pt-Based Catalysts, ChemElectroChem. 5 (2018) 1636–1643. https://doi.org/10.1002/celc.201800309.

[31] Y. Kim, H.W. Kim, S. Lee, J. Han, D. Lee, J.R. Kim, T.W. Kim, C.U. Kim, S.Y. Jeong, H.J. Chae, B.S. Kim, H. Chang, W.B. Kim, S.M. Choi, H.J. Kim, The Role of Ruthenium on Carbon-Supported PtRu Catalysts for Electrocatalytic Glycerol Oxidation under Acidic Conditions, ChemCatChem. 9 (2017) 1683–1690. https://doi.org/10.1002/cctc.201601325.

[32] C. Lamy, A. Lima, V. LeRhun, F. Delime, C. Coutanceau, J.M. Léger, Recent advances in the development of direct alcohol fuel cells (DAFC), J. Power Sources. 105 (2002) 283–296. https://doi.org/10.1016/S0378-7753(01)00954-5.

[33] F. Kadirgan, S. Beyhan, T. Atilan, Preparation and characterization of nano-sized Pt-Pd/C catalysts and comparison of their electro-activity toward methanol and ethanol oxidation, Int. J. Hydrogen Energy. 34 (2009) 4312–4320. https://doi.org/10.1016/j.ijhydene.2009.03.024.

[34] Y. Zhou, Y. Shen, J. Xi, Seed-mediated synthesis of Pt x Au y @ Ag electrocatalysts for the selective oxidation of glycerol, Appl. Catal. B Environ. 245 (2019) 604–612. https://doi.org/10.1016/j.apcatb.2019.01.009.

[35] Y. Zhou, Y. Shen, Selective electro-oxidation of glycerol over Pd and Pt@Pd nanocubes, Electrochem. Commun. 90 (2018) 106–110. https://doi.org/10.1016/j.elecom.2018.04.012.

[36] C. Coutanceau, A. Zalineeva, S. Baranton, M. Simoes, Modification of palladium surfaces by bismuth adatoms or clusters: Effect on electrochemical activity and selectivity towards polyol electrooxidation, Int. J. Hydrogen Energy. 39 (2014) 15877–15886. https://doi.org/10.1016/j.ijhydene.2014.03.076.

[37] P. Atanassov, T. Asset, I. Matanovic, M. Padilla, A. Serov, M. Chatenet, A.J. Roy, F. Maillard, Design of Pd-Pb Catalysts for Glycerol and Ethylene Glycol Electrooxidation in Alkaline Medium, Electrocatalysis. 9 (2018) 480–485. https://doi.org/10.1007/s12678-017-0449-8.

[38] N. Pittayaporn, A. Therdthianwong, S. Therdthianwong, Au/C catalysts promoted with Ni

for glycerol electrooxidation in alkaline media, J. Appl. Electrochem. 48 (2018) 251–262. https://doi.org/10.1007/s10800-018-1155-9.

[39] A. Zalineeva, S. Baranton, C. Coutanceau, G. Jerkiewicz, Electrochemical behavior of unsupported shaped palladium nanoparticles, Langmuir. 31 (2015) 1605–1609. https://doi.org/10.1021/la5025229.

[40] C. Wang, P. Song, F. Gao, T. Song, Y. Zhang, C. Chen, L. Li, L. Jin, Y. Du, Precise synthesis of monodisperse PdAg nanoparticles for size-dependent electrocatalytic oxidation reactions, J. Colloid Interface Sci. 544 (2019) 284–292. https://doi.org/10.1016/j.jcis.2019.02.066.

[41] C. Bianchini, P.K. Shen, Palladium-based electrocatalysts for alcohol oxidation in half cells and in direct alcohol fuel cells, Chem. Rev. 109 (2009) 4183–4206. https://doi.org/10.1021/cr9000995.

[42] A.C. Garcia, J. Caliman, E.B. Ferreira, G. Tremiliosi-Filho, J.J. Linares, Promotional Effect of Ag on the Catalytic Activity of Au for Glycerol Electrooxidation in Alkaline Medium, ChemElectroChem. 2 (2015) 1036–1041. https://doi.org/10.1002/celc.201500022.

[43] S.S. Chen, Z.Z. Yang, A.J. Wang, K.M. Fang, J.J. Feng, Facile synthesis of bimetallic gold-palladium nanocrystals as effective and durable advanced catalysts for improved electrocatalytic performances of ethylene glycol and glycerol oxidation, J. Colloid Interface Sci. 509 (2018) 10–17. https://doi.org/10.1016/j.jcis.2017.08.063.

[44] Y. Kwon, K.J.P. Schouten, M.T.M. Koper, Mechanism of the Catalytic Oxidation of Glycerol on Polycrystalline Gold and Platinum Electrodes, ChemCatChem. 3 (2011) 1176–1185. https://doi.org/10.1002/cctc.201100023.

[45] M. Valter, M. Busch, B. Wickman, H. Grönbeck, J. Baltrusaitis, A. Hellman, Electrooxidation of Glycerol on Gold in Acidic Medium: A Combined Experimental and DFT Study, J. Phys. Chem. C. 122 (2018) 10489–10494. https://doi.org/10.1021/acs.jpcc.8b02685.

[46] H. Angerstein-Kozlowska, B.E. Conway, A. Hamelin, L. Stoicoviciu, Elementary steps of electrochemical oxidation of single-crystal planes of Au-I. Chemical basis of processes involving geometry of anions and the electrode surfaces, Electrochim. Acta. 31 (1986) 1051–1061. https://doi.org/10.1016/0013-4686(86)80020-2.

[47] Y. Wang, L. Li, L. Hu, L. Zhuang, J. Lu, B. Xu, A feasibility analysis for alkaline membrane direct methanol fuel cell: Thermodynamic disadvantages versus kinetic advantages, Electrochem. Commun. 5 (2003) 662–666. https://doi.org/10.1016/S1388-2481(03)00148-6.

[48] Y. Kwon, S.C.S. Lai, P. Rodriguez, M.T.M. Koper, Electrocatalytic oxidation of alcohols on gold in alkaline media: Base or gold catalysis?, J. Am. Chem. Soc. 133 (2011) 6914–6917. https://doi.org/10.1021/ja200976j.

[49] J. Zhang, Y. Liang, N. Li, Z. Li, C. Xu, S. Ping, A remarkable activity of glycerol electrooxidation on gold in alkaline medium, Electrochim. Acta. 59 (2012) 156–159. https://doi.org/10.1016/j.electacta.2011.10.048.

[50] S. Lee, H. Ju, S. Mook, M. Ho, W. Bae, Applied Catalysis A : General The promotional

effect of Ni on bimetallic PtNi / C catalysts for glycerol electrooxidation, "Applied Catal. A, Gen. 429–430 (2012) 39–47. https://doi.org/10.1016/j.apcata.2012.04.002.

[51] Y. Zhou, Y. Shen, J. Xi, X. Luo, Selective Electro-Oxidation of Glycerol to Dihydroxyacetone by PtAg Skeletons, ACS Appl. Mater. Interfaces. 11 (2019) 28953–28959. https://doi.org/10.1021/acsami.9b09431.

[52] X. Ning, Y. Li, H. Yu, F. Peng, H. Wang, Y. Yang, Promoting role of bismuth and antimony on Pt catalysts for the selective oxidation of glycerol to dihydroxyacetone, J. Catal. 335 (2016) 95–104. https://doi.org/10.1016/j.jcat.2015.12.020.

[53] C. Wang, P. Song, F. Gao, T. Song, Y. Zhang, C. Chen, L. Li, L. Jin, Y. Du, Precise synthesis of monodisperse PdAg nanoparticles for size- dependent electrocatalytic oxidation reactions, J. Colloid Interface Sci. 544 (2019) 284–292. https://doi.org/10.1016/j.jcis.2019.02.066.

[54] L.L. Carvalho, F. Colmati, A.A. Tanaka, Nickel-palladium electrocatalysts for methanol , ethanol , and glycerol oxidation reactions, Int. J. Hydrogen Energy. 42 (2017) 16118–16126. https://doi.org/10.1016/j.ijhydene.2017.05.124.

[55] B. Ran, S. Liu, J. Zhao, T. Tan, B. Liang, W. Wang, An adenine-originated N-doped carbon supporting Pd 3 Ru nanoparticle with high performance for glycerol electrooxidation, J. Mater. Sci. 54 (2019) 4579–4588. https://doi.org/10.1007/s10853-018-3180-9.

[56] H. Xu, P. Song, C. Fernandez, J. Wang, M. Zhu, Y. Shiraishi, Y. Du, Sophisticated Construction of Binary PdPb Alloy Nanocubes as Robust Electrocatalysts toward Ethylene Glycol and Glycerol Oxidation, ACS Appl. Mater. Interfaces. 10 (2018) 12659–12665. https://doi.org/10.1021/acsami.8b00532.

[57] P. Lertthahan, S. Yongprapat, A. Therdthianwong, S. Therdthianwong, Pt-modified Au/C catalysts for direct glycerol electro-oxidation in an alkaline medium, Int. J. Hydrogen Energy. 42 (2017) 9202–9209. https://doi.org/10.1016/j.ijhydene.2016.05.120.

[58] S. Chen, Z. Yang, A. Wang, K. Fang, J. Feng, Facile synthesis of bimetallic gold-palladium nanocrystals as effective and durable advanced catalysts for improved electrocatalytic performances of ethylene glycol and glycerol oxidation CH 2 OH CH 2 OH GOR CH 2 OH CHOH, J. Colloid Interface Sci. 509 (2018) 10–17. https://doi.org/10.1016/j.jcis.2017.08.063.

[59] N.P.A.T.S. Therdthianwong, Au / C catalysts promoted with Ni for glycerol electrooxidation in alkaline media, J. Appl. Electrochem. 48 (2018) 251–262. https://doi.org/10.1007/s10800-018-1155-9.

[60] A.C. Garcia, Y.Y. Birdja, G. Tremiliosi-filho, M.T.M. Koper, Glycerol electro-oxidation on bismuth-modified platinum single crystals, J. Catal. 346 (2017) 117–124. https://doi.org/10.1016/j.jcat.2016.12.013.

[61] Y. Kwon, Y. Birdja, I. Spanos, P. Rodriguez, M.T.M. Koper, Highly selective Electro-oxidation of Glycerol to Dihydroxyacetone on Platinum in the Presence of Bismuth, ACS Catal. 2 (2012) 759–764. https://doi.org/10.1021/cs200599g.

[62] C. Xu, Z. Tian, P. Shen, S.P. Jiang, Oxide (CeO2, NiO, Co3O4 and Mn3O4)-promoted Pd/C electrocatalysts for alcohol electrooxidation in alkaline media, Electrochim. Acta. 53

(2008) 2610–2618. https://doi.org/10.1016/j.electacta.2007.10.036.

[63] C. Xu, K.S. Pei, Novel Pt/CeO2/C catalysts for electrooxidation of alcohols in alkaline media, Chem. Commun. (2004) 2238–2239. https://doi.org/10.1039/b408589b.

[64] Y. Li, F. Zaera, Sensitivity of the glycerol oxidation reaction to the size and shape of the platinum nanoparticles in Pt / SiO 2 catalysts, J. Catal. 326 (2015) 116–126. https://doi.org/10.1016/j.jcat.2015.04.009.

[65] A. Zalineeva, S. Baranton, C. Coutanceau, Bi-modified palladium nanocubes for glycerol electrooxidation, Electrochem. Commun. 34 (2013) 335–338. https://doi.org/10.1016/j.elecom.2013.07.022.

[66] E. Antolini, Glycerol electro-oxidation in alkaline media and Alkaline direct glycerol fuel cells, Catalysts. 9 (2019) 980. https://doi.org/10.3390/catal9120980.

[67] V.L. Oliveira, C. Morais, K. Servat, T.W. Napporn, P. Olivi, K.B. Kokoh, G. Tremiliosi-Filho, Kinetic Investigations of Glycerol Oxidation Reaction on Ni/C, Electrocatalysis. 6 (2015) 447–454. https://doi.org/10.1007/s12678-015-0261-2.

[68] M. Fleischmann, K. Korinek, D. Pletcher, The oxidation of organic compounds at a nickel anode in alkaline solution, J. Electroanal. Chem. 31 (1971) 39–49. https://doi.org/10.1016/S0022-0728(71)80040-2.

[69] M.E.G. Lyons, R.L. Doyle, I. Godwin, M.O. Brien, L. Russell, Hydrous Nickel Oxide : Redox Switching and the Oxygen Evolution Reaction in Aqueous Alkaline Solution, Electrochem. Soc. 159 (2012) 932–944. https://doi.org/10.1149/2.078212jes.

[70] A.A. El-Shafei, Electrocatalytic oxidation of methanol at a nickel hydroxide /glassy carbon modified electrode in alkaline medium, J. Electroanal. Chem. 471 (1999) 89–95.

[71] M. Houache, K. Hughes, Electrochemical Valorization of Glycerol on Ni-rich Bimetallic NiPd Nanoparticles: Insight into product selectivity using in-situ PM-IRRAS, ACS Sustain. Chem. Eng. 17 (2019) 14425–14434. https://doi.org/10.1021/acssuschemeng.9b01070.

[72] V.L. Oliveira, C. Morais, K. Servat, T.W. Napporn, G. Tremiliosi-Filho, K.B. Kokoh, Studies of the reaction products resulted from glycerol electrooxidation on Ni-based materials in alkaline medium, Electrochim. Acta. 117 (2014) 255–262. https://doi.org/10.1016/j.electacta.2013.11.127.

[73] R.M.A. Tehrani, S. Ab, Electrocatalysis of free glycerol at a nanonickel modified graphite electrode and its determination in biodiesel, Electrochim. Acta. 70 (2012) 153–157. https://doi.org/10.1016/j.electacta.2012.03.044.

[74] M.S.E. Houache, E. Cossar, S. Ntais, E.A. Baranova, Electrochemical modification of nickel surfaces for efficient glycerol electrooxidation, J. Power Sources. 375 (2018) 310–319. https://doi.org/10.1016/j.jpowsour.2017.08.089.

[75] B. Habibi, N. Delnavaz, Electrooxidation of glycerol on nickel and nickel alloy (Ni-Cu and Ni-Co) nanoparticles in alkaline media, RSC Adv. 6 (2016) 31797–31806. https://doi.org/10.1039/c5ra26006j.

[76] V.L. Oliveira, C. Morais, K. Servat, T.W. Napporn, G. Tremiliosi-Filho, K.B. Kokoh, Glycerol

oxidation on nickel based nanocatalysts in alkaline medium - Identification of the reaction products, J. Electroanal. Chem. 703 (2013) 56–62. https://doi.org/10.1016/j.jelechem.2013.05.021.

[77] B. Habibi, N. Delnavaz, Electrooxidation of glycerol on nickel and nickel alloy (Ni-Cu and Ni-Co) nanoparticles in alkaline media, RSC Adv. 6 (2016) 31797–31806. https://doi.org/10.1039/c5ra26006j.

[78] D. Coviello, I.G. Casella, Electrochemical Performance of Binary Ni-Co Particles Deposited on Graphene Oxide/Polyvinyl alcohol Substrate in Alkaline Medium, Electrochim. Acta. 261 (2018) 104–112. https://doi.org/10.1016/j.electacta.2017.12.082.

[79] A.S. Machado, E.A. Ticianelli, J.L. Bott-neto, T.S. Martins, P.O. Box, Electrocatalytic Oxidation of Methanol , Ethanol , and Glycerol on Ni (OH)2 Nanoparticles Encapsulated with Poly [Ni(salen)] Film, ACS Appl. Mater. Interfaces. 11 (2019) 30810–30818. https://doi.org/10.1021/acsami.9b08441.

[80] Q. Lin, Y. Wei, W. Liu, Y. Yu, J. Hu, Electrocatalytic oxidation of ethylene glycol and glycerol on nickel ion implanted-modified indium tin oxide electrode, Int. J. Hydrogen Energy. 42 (2016) 1403–1411. https://doi.org/10.1016/j.ijhydene.2016.10.011.

[81] M. Alsabet, M. Grdeń, G. Jerkiewicz, Electrochemical Growth of Surface Oxides on Nickel. Part 3: Formation of β-NiOOH in Relation to the Polarization Potential, Polarization Time, and Temperature, Electrocatalysis. 6 (2014) 60–71. https://doi.org/10.1007/s12678-014-0214-1.

[82] F. Muench, M. Oezaslan, M. Rauber, S. Kaserer, A. Fuchs, E. Mankel, J. Brötz, P. Strasser, C. Roth, W. Ensinger, Electroless synthesis of nanostructured nickel and nickeleboron tubes and their performance as unsupported ethanol electrooxidation catalysts, J. Power Sources. 222 (2013) 243–252. https://doi.org/10.1016/j.jpowsour.2012.08.067.

[83] B.N. Zope, D.D. Hibbitts, M. Neurock, R.J. Davis, Reactivity of the Gold / Water Interface During Selective Oxidation Catalysis Linked references are available on JSTOR for this article : Reactivity of the Gold / Water Interface, 330 (2019) 74–78.

[84] A. Ashok, J.E. Soc, A. Ashok, A. Kumar, F. Tarlochan, Single Step Synthesis of Porous NiCoO 2 for Effective Electrooxidation of Glycerol in Alkaline Medium, J. Electrochem. Soc. 165 (2018) J3301–J3309. https://doi.org/10.1149/2.0401815jes.

[85] J. Han, Y. Kim, H.W. Kim, D.H.K. Jackson, D. Lee, H. Chang, H. Chae, K. Lee, H.J. Kim, Effect of atomic-layer-deposited TiO2 on carbon-supported Ni catalysts for electrocatalytic glycerol oxidation in alkaline medium, Electrochem. Commun. 83 (2017) 46–50. https://doi.org/10.1016/j.elecom.2017.08.023.

[86] X. Cui, W. Guo, M. Zhou, Y. Yang, Y. Li, P. Xiao, Y. Zhang, X. Zhang, Promoting Effect of Co in NimCon (m + n = 4) Bimetallic Electrocatalysts for Methanol Oxidation Reaction, ACS Appl. Mater. Interfaces. 7 (2014) 493–503.

[87] M.S.E. Houache, R. Safari, U.O. Nwabara, T. Rafa, G.A. Botton, C. Coutanceau, E.A. Baranova, P.J.A. Kenis, Selective Electrooxidation of Glycerol to Formic Acid over Carbon Supported Ni1−xMx (M = Bi , Pd , and Au) Nanocatalysts and Coelectrolysis of CO2, ACS Appl. Energy Mater. 3 (2020) 8725–8738. https://doi.org/10.1021/acsaem.0c01282.

[88] M. Ahmadi, H. Mistry, B. Roldan Cuenya, Tailoring the Catalytic Properties of Metal Nanoparticles via Support Interactions, J. Phys. Chem. Lett. 7 (2016) 3519–3533. https://doi.org/10.1021/acs.jpclett.6b01198.

[89] M. Comotti, W.C. Li, B. Spliethoff, F. Schüth, Support effect in high activity gold catalysts for CO oxidation, J. Am. Chem. Soc. 128 (2006) 917–924. https://doi.org/10.1021/ja0561441.

[90] B. Olthof, A. Khodakov, A.T. Bell, E. Iglesia, Effects of Support Composition and Pretreatment Conditions on the Structure of Vanadia Dispersed on SiO2, Al2O3, TiO2, ZrO2, and HfO2, J. Phys. Chem. B. 104 (2000) 1516–1528. https://doi.org/10.1021/jp9921248.

[91] J. Barbero, M.A. Peña, J.M. Campos-Martin, J.L.G. Fierro, P.L. Arias, Support effect in supported Ni catalysts on their performance for methane partial oxidation, Catal. Letters. 87 (2003) 211–218. https://doi.org/10.1023/A:1023407609626.

[92] C. Wen, Y. Zhu, Y. Ye, S. Zhang, F. Cheng, Y. Liu, P. Wang, F. Tao, Water Gas Shift Reaction on Metal Nanoclusters Encapsulated in Mesoporous Ceria Studied with, ACS Nano. 6 (2012) 9305–9313.

[93] T. Yang, X.D. Wen, D.B. Cao, Y.W. Li, J.G. Wang, C.F. Huo, Structures and energetics of H2O adsorption on the Fe3O4 (111) surface, Ranliao Huaxue Xuebao/Journal Fuel Chem. Technol. 37 (2009) 506–512. https://doi.org/10.1016/s1872-5813(10)60006-0.

[94] M.D. Salazar-Villalpando, B. Reyes, Hydrogen production over Ni/ceria-supported catalysts by partial oxidation of methane, Int. J. Hydrogen Energy. 34 (2009) 9723–9729. https://doi.org/10.1016/j.ijhydene.2009.10.019.

[95] T.E. James, S.L. Hemmingson, T. Ito, C.T. Campbell, Energetics of Cu Adsorption and Adhesion onto Reduced CeO2(111) Surfaces by Calorimetry, J. Phys. Chem. C. 119 (2015) 17209–17217. https://doi.org/10.1021/acs.jpcc.5b04621.

[96] C. Bozo, N. Guilhaume, J.M. Herrmann, Role of the ceria-zirconia support in the reactivity of platinum and palladium catalysts for methane total oxidation under lean conditions, J. Catal. 203 (2001) 393–406. https://doi.org/10.1006/jcat.2001.3320.

[97] J. Thepkaew, S. Therdthianwong, A. Therdthianwong, Effect of pre-treatment approach of a carbon support on activity of PtSn/C electrocatalysts for direct ethanol fuel cells, J. Appl. Electrochem. 41 (2011) 435–444. https://doi.org/10.1007/s10800-010-0253-0.

[98] C. Zhou, F. Peng, H. Wang, H. Yu, C. Peng, J. Yang, Development of stable PtRu catalyst coated with manganese dioxide for electrocatalytic oxidation of methanol, Electrochem. Commun. 12 (2010) 1210–1213. https://doi.org/10.1016/j.elecom.2010.06.021.

[99] S. Guerin, B.E. Hayden, D. Pletcher, M.E. Rendall, J. Suchsland, L.J. Williams, Combinatorial Approach to the Study of Particle Size Effects in Electrocatalysis : Synthesis of Supported Gold Nanoparticles, J. Comb. Chem. 8 (2006) 791–798.

[100] L. Su, W. Jia, A. Schempf, Y. Lei, Palladium/titanium dioxide nanofibers for glycerol electrooxidation in alkaline medium, Electrochem. Commun. 11 (2009) 2199–2202. https://doi.org/10.1016/j.elecom.2009.09.030.

[101] L. Xing, J. Jia, Y. Wang, B. Zhang, S. Dong, Pt modified TiO2 nanotubes electrode: Preparation and electrocatalytic application for methanol oxidation, Int. J. Hydrogen Energy. 35 (2010) 12169–12173. https://doi.org/10.1016/j.ijhydene.2010.07.162.

[102] M.W. Xu, G.Y. Gao, W.J. Zhou, K.F. Zhang, H.L. Li, Novel Pd/β-MnO2 nanotubes composites as catalysts for methanol oxidation in alkaline solution, J. Power Sources. 175 (2008) 217–220. https://doi.org/10.1016/j.jpowsour.2007.09.069.

[103] E. Skrzyńska, S. Zaid, A. Addad, J.S. Girardon, M. Capron, F. Dumeignil, Performance of Ag/Al2O3 catalysts in the liquid phase oxidation of glycerol-effect of preparation method and reaction conditions, Catal. Sci. Technol. 6 (2016) 3182–3196. https://doi.org/10.1039/c5cy01581b.

[104] Q. Tan, C. Du, Y. Sun, L. Du, G. Yin, Y. Gao, A palladium-doped ceria@carbon core-sheath nanowire network: a promising catalyst support for alcohol electrooxidation reactions, Nanoscale. 7 (2015) 13656–13662. https://doi.org/10.1039/c5nr03023d.

[105] J. Zhao, W. Chen, Y. Zheng, Effect of ceria on carbon supported platinum catalysts for methanol electrooxidation, Mater. Chem. Phys. 113 (2009) 591–595. https://doi.org/10.1016/j.matchemphys.2008.07.107.

[106] L.A. Soares, C. Morais, T.W. Napporn, K.B. Kokoh, P. Olivi, Beneficial effects of rhodium and tin oxide on carbon supported platinum catalysts for ethanol electrooxidation, J. Power Sources. 315 (2016) 47–55. https://doi.org/10.1016/j.jpowsour.2016.03.013.

[107] L. Jiang, L. Colmenares, Z. Jusys, G.Q. Sun, R.J. Behm, Ethanol electrooxidation on novel carbon supported Pt/SnOx/C catalysts with varied Pt:Sn ratio, Electrochim. Acta. 53 (2007) 377–389. https://doi.org/10.1016/j.electacta.2007.01.047.

[108] J. Beckers, G. Rothenberg, Sustainable selective oxidations using ceria-based materials, Green Chem. 12 (2010) 939–94. https://doi.org/10.1039/c000191k.

[109] C. Sun, H. Li, L. Chen, Nanostructured ceria-based materials: Synthesis, properties, and applications, Energy Environ. Sci. 5 (2012) 8475–8505. https://doi.org/10.1039/c2ee22310d.

[110] B. Zhu, M.D. Mat, Studies on dual phase ceria-based composites in electrochemistry, Int. J. Electrochem. Sci. 1 (2006) 383–402.

[111] R. Di Monte, J. Kašpar, On the role of oxygen storage in three-way catalysis, in: Top. Catal., 2004: pp. 47–58. https://doi.org/10.1023/b:toca.0000024333.08447.f7.

[112] X. Yuan, X. Wu, Y. Wu, T. van Ree, Metal oxides for emission control, in: Met. Oxides Energy Technol., Elsevier Inc., 2018: pp. 391–414. https://doi.org/10.1016/b978-0-12-811167-3.00015-8.

[113] H.J. Kim, M.G. Jang, D. Shin, J.W. Han, Design of Ceria Catalysts for Low-Temperature CO Oxidation, ChemCatChem. 12 (2020) 11–26. https://doi.org/10.1002/cctc.201901787.

[114] M.J.P. Jarzebski Z.M., Physical Properties of SnO Materials, J. Electrochem. Soc. Rev. (1976) 199–205.

[115] S. Geiger, O. Kasian, A.M. Mingers, K.J.J. Mayrhofer, S. Cherevko, Stability limits of tin-

based electrocatalyst supports, Sci. Rep. 7 (2017) 3–9. https://doi.org/10.1038/s41598-017-04079-9.

[116] H.S. Oh, H.N. Nong, P. Strasser, Preparation of mesoporous Sb-, F-, and in-doped SnO2 bulk powder with high surface area for use as catalyst supports in electrolytic cells, Adv. Funct. Mater. 25 (2015) 1074–1081. https://doi.org/10.1002/adfm.201401919.

[117] G. Cognard, G. Ozouf, C. Beauger, G. Berthomé, D. Riassetto, L. Dubau, R. Chattot, M. Chatenet, F. Maillard, Benefits and limitations of Pt nanoparticles supported on highly porous antimony-doped tin dioxide aerogel as alternative cathode material for proton-exchange membrane fuel cells, Appl. Catal. B Environ. 201 (2017) 381–390. https://doi.org/10.1016/j.apcatb.2016.08.010.

[118] E. Fabbri, A. Rabis, R. Kötz, T.J. Schmidt, Pt nanoparticles supported on Sb-doped SnO2 porous structures: Developments and issues, Phys. Chem. Chem. Phys. 16 (2014) 13672–13681. https://doi.org/10.1039/c4cp00238e.

[119] V.K. Puthiyapura, M. Mamlouk, S. Pasupathi, B.G. Pollet, K. Scott, Physical and electrochemical evaluation of ATO supported IrO2 catalyst for proton exchange membrane water electrolyser, J. Power Sources. 269 (2014) 451–460. https://doi.org/10.1016/j.jpowsour.2014.06.078.

[120] J.C. Cruz, S. Rivas, D. Beltran, Y. Meas, R. Ornelas, G. Osorio-Monreal, L. Ortiz-Frade, J. Ledesma-García, L.G. Arriaga, Synthesis and evaluation of ATO as a support for Pt-IrO2 in a unitized regenerative fuel cell, Int. J. Hydrogen Energy. 37 (2012) 13522–13528. https://doi.org/10.1016/j.ijhydene.2012.06.095.

[121] Y. Yu, T. Wang, Y. Fu, W. Su, J. Hu, Platinum nanoparticles ion-implanted-modified indium tin oxide electrode for electrocatalytic oxidation of formaldehyde, Int. J. Hydrogen Energy. 39 (2014) 17617–17621. https://doi.org/10.1016/j.ijhydene.2014.08.149.

[122] I.-S. Park, E. Lee, A. Manthiram, Electrocatalytic Properties of Indium Tin Oxide-Supported Pt Nanoparticles for Methanol Electro-oxidation, J. Electrochem. Soc. 157 (2010) B251–B255. https://doi.org/10.1149/1.3268126.

[123] F. Liang, H. Tian, M. Jia, J. Hu, Pt nanoparticles ion-implanted onto indium tin oxide electrodes and their electrocatalytic activity towards methanol, J. Power Sources. 225 (2013) 9–12. https://doi.org/10.1016/j.jpowsour.2012.09.093.

[124] C.K.T. Chew, C. Salcianu, P. Bishop, C.J. Carmalt, I.P. Parkin, Functional thin film coatings incorporating gold nanoparticles in a transparent conducting fluorine doped tin oxide matrix, J. Mater. Chem. C. 3 (2015) 1118–1125. https://doi.org/10.1039/c4tc02275k.

[125] H. Chen, Z. Sun, X. Liu, A. Han, P. Du, Cobalt-Salen Complexes as Catalyst Precursors for Electrocatalytic Water Oxidation at Low Overpotential, J. Phys. Chem. C. 119 (2015) 8998–9004. https://doi.org/10.1021/jp511584z.

Chapter 3: Tuning the Product Selectivity of Glycerol Electrooxidation on Carbon supported Ni_xBi_{100-x} (x= 100, 95, 90, 80, 50 at. %) Nanocatalyst

Asma Shubair,[a] Mohamed S. E. Houache,[a] and Elena A. Baranova[a*]

To be submitted to Journal of Chemical Technology and Biotechnology

[a]Department of Chemical and Biological Engineering, Centre for Catalysis Research and Innovation (CCRI), University of Ottawa, 161 Louis-Pasteur Ottawa ON, Canada, K1N 6N5

Abstract (250 words-MAX)

BACKGROUND: Glycerol, a byproduct in the process of biodiesel production, is produced in large quantities exceeding its demand. The saturation of glycerol resulted in a sharp reduction in its market value and the surplus waste may pose risk to the environment. By means of electrochemical technologies, glycerol may be oxidized into value-added products such as; glycerate, tartronate, lactate, etc. In the present work, nickel-bismuth bimetallic catalysts of larger particle size (≥6nm) are fabricated by sodium borohydride reduction method and utilized in a glycerol electrolysis cell.

RESULTS: The as-fabricated catalysts were characterized and analyzed by means of various physicochemical characterizations; including Transmission electron microscopy and Energy dispersive X-ray spectroscopy. Glycerol electrooxidation was conducted in the presence of NiBi/C catalyst with different Ni:Bi atomic ratios to assess their catalytic activity. Using a three-electrode electrochemical cell, $Ni_{95}Bi_5$/C showed the highest current density of 104 mA.cm^{-2} with an onset potential of 1.32 V vs. RHE. By means of continuous electrolysis accompanied by High performance liquid chromatography, $Ni_{95}Bi_5$/C (≥6nm) had higher selectivity to glycerate C_3 product compared to Ni/C. Additionally, the effect of experimental conditions (applied potential, residence time and temperature) are thoroughly studied. The role of bismuth and experimental conditions on selectivity are discussed in detail.

CONCLUSION: the above results indicate that the incorporation of bismuth to nickel improves the catalytic activity of the catalyst and tuned the selectivity to higher value-added products.

GRAPHICAL ABSTRACT

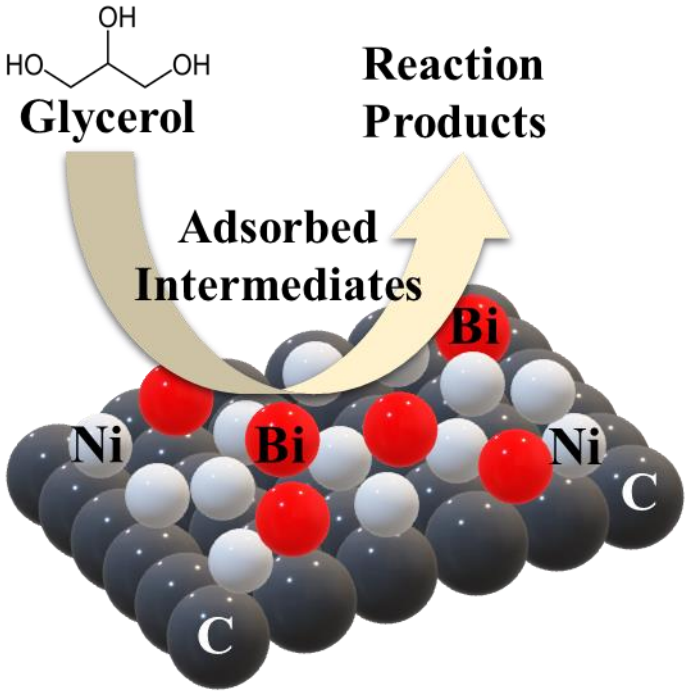

Keywords: Electrocatalysis, Glycerol Electrooxidation, Bimetallic catalysts, synergistic effect, Selectivity

3.1 Introduction

As countries are developing and populations are growing, there is an ever-increasing demand for energy. For many years, fossil fuels have been the main source of energy.[1] However, the alarming risks of global warming along with the depletion of fossil fuels calls for exploring alternative energy sources. Among various energy sources, biodiesel which is renewable and biodegradable is considered to be the best candidate as it has potential of reducing greenhouse gas (GHG) emissions by more than 80%.[2] By transesterification reaction of fatty acids with an alcohol and a catalyst, biodiesel is produced with 10wt% by-product glycerol.[3] Fortunately, glycerol has a wide demand in various commercial industries.[4] With the growth of the biodiesel industry, there is a consequent increase in stocks of glycerol which exceeds their demand.[5] The saturation of glycerol in the market is causing a gradual decrease in its price.[6] Thus, utilizing glycerol in electrolysis cells for the purpose of electrosynthesis is considered to be a promising technique as it runs at mild conditions.[7]

Nickel catalysts are among the inexpensive non-Pt group metals with promising characteristics such as; anti-corrosion capability, long-term stability and high electrocatalytic oxidation performance by forming active nickel oxyhydroxide species (β-NiOOH) in alkaline medium.[7,8] Unsupported nickel catalyst suffers from poor electrical conductivity and agglomeration of nanoparticles.[9] This is because unsupported particles grow rapidly compared to supported particles.[10] Supporting nickel on high surface area carbon can enhance the catalytic performance by faster electron transfer kinetics, more active sites and higher electrical conductivity.[11] In addition, adding a p-group metal promoter bismuth (Bi) proved to further enhance activity by having synergistic effects with Ni. [12]

Developing electrocatalysts that are active, stable and selective to value-added products remains to be a challenge in glycerol electrooxidation reaction (GEOR). Therefore, fine tuning by altering the NP morphology and chemical composition of the electrocatalyst are necessary.[13,14] The synthesis method is the ruling factor in the tuning process of electrocatalysts.[15–18] Several synthesis methods were developed for production of pure nickel and nickel alloys. Electrodeposition and co-deposition are the most common techniques to form thin films on glassy carbon, graphite, and polymers.[19–21] Another non-aqueous synthesis technique is thermal decomposition of nickel commercial precursors.[22] However, aqueous synthesis techniques are easier and more commonly implemented with nickel soluble precursor salts with the help of a reducing agent.[23–25] Different reducing agents such as NH_4OH and NaOH result in nickel catalysts with various physical characteristics.[26] In addition, different metal precursor salts $NiCl_2$, $NiSO_4$ and $NiNO_3$ proved to have an effect on the particles size which in return varies their electrochemical performance.[27] Limited number of studies cover how different factors in the synthesis affect the electrocatalyst morphology thus yielding different electrocatalytic behaviors for GEOR application.

Recently, Ni_xBi_{1-x} (x= 100, 98, 95, 90 at. %) nanostructured electrocatalysts have been reported for glycerol electrooxidation. [28,29] Carbon supported and unsupported NiBi electrocatalysts were both prepared by sodium borohydride reduction method. The unsupported bimetallic catalyst showed superior activity compared to Ni and selectivity to

C_3 products glycerate and tartronate were evidently enhanced in the presence of bismuth.[28] Whereas, the carbon supported NiBi catalyst was 100% selective to formate. [29]

It is well known that the synthesis procedure of nano-structured catalyst could significantly impact the morphology, shape, structure as well as the surface and bulk composition of the resulting nanomaterials and lead to modification of their catalytic activity and selectivity. Therefore, in this work we investigate the effect of the synthesis procedure and Ni:Bi ratio on glycerol electrooxidation and in particular the product selectivity. Nanoparticles were thoroughly evaluated in the three-electrode electrochemical cell and in the 5 cm^2 electrolysis cell that allowed to study NPs stability and product selectivity. We show that modification of the synthesis procedure of NiBi nanoparticles through varying the precursor salt type, mixing technique (sonication vs mechanical mixing) and drying technique (oven vs vacuum freeze dryer) has an effect on the catalytic performance and significantly altered the product selectivity. Herein, the effect of Ni_xBi_{100-x}/C nanoparticle size on electrochemical performance and product selectivity is studied. In addition, the effect of experimental conditions (applied potential, residence time and temperature) on product distributions is investigated.

3.2 Experimental Procedures

3.2.1 Synthesis method

All carbon supported Ni_xBi_{100-x} [x= 100, 95, 90 and 50 at. %] catalysts are produced by sodium borohydride ($NaBH_4$) reduction method at room temperature. Initially, $NiCl_2.6H_2O$ (99.999%, Sigma-Aldrich) and $BiCl_3$ (99.9%) metal precursor salts are dissolved separately in 20 mL ethanol (99%), each. The homogenous $BiCl_3$ solution is added to the $NiCl_2.6H_2O$ solution. Next, XC Vulcan carbon (70wt%) is added to the metal precursor salts mixture and allowed to homogenize for 1 hour. For the reduction, 2 wt% $NaBH_4$ (≥98%, ACROS) dissolved in 10 ml ethanol is added dropwise to the homogenous metal-carbon mixture and allow precipitation/reduction to fully take place. Finally, the sample was washed three times with ethanol and centrifuged for 10 minutes per wash at 6000 rpm. The resulting samples were freeze dried overnight to remove remaining ethanol.

3.2.2 Characterizations

Morphological Characterization of $Ni_{95}Bi_5$/C nanoparticles were conducted by Transmission Electron Microscopy (TEM) using a JEOL JEM2100F instrument. EDS analysis was carried out by FEI Titan 80-300 at 300 keV. For the latter instrument, EDS spectra were analyzed with INCA software.

3.2.3 Electrochemical measurements

The detailed procedure was reported earlier.[30] Briefly, a conventional Teflon three electrode electrochemical cell connected to a potentiostat was used to conduct cyclic voltammetry (CV), linear sweep voltammetry (LSV) and chronoamperometry (CA) to electrochemically characterize the anode surface and analyze the activity of different catalysts. A schematic diagram of the setup is shown in the figure 3.1. All experiments were repeated more than three times and reproduced.

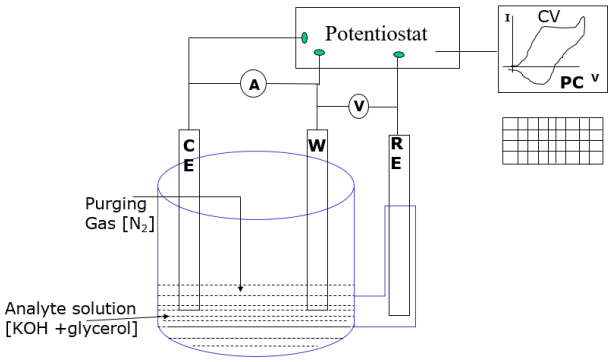

Figure 3.1: Schematic diagram of the Teflon three electrode electrochemical cell

3.2.4 Continuous electrolysis accompanied by HPLC

The exact technique, product selectivity formula and calibration curves were previously reported by houache at al.[31] In short, the electrolysis cell is composed of flow plates, carbon diffusion layers, catalysts and filter paper as shown in Figure 3.2. The electrolysis cell is a 25 cm^2 membraneless cell with $Ni_{95}Bi_5$/C and Ni/C anodes and a Pt/C cathode with metal loading of 2 $mg.cm^{-2}$. The anode and cathodes were separated by a filter paper and a Teflon gasket as shown in the schematic below. Finally, the cell was mechanically compressed. Different applied potentials (1.35 and 1.55 V), electrolyte pump rates (1.4 and 0.4 ml/s) and temperatures (R.T, 50C, and 75C) were tested.

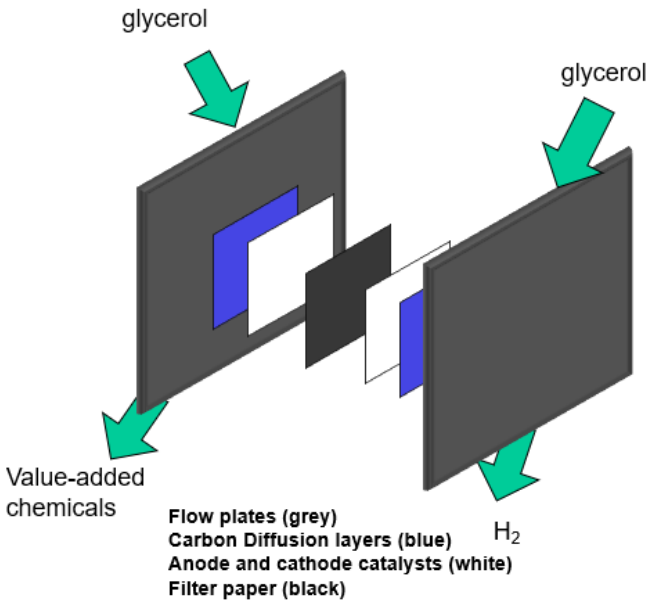

Figure 3.2: Components of the electrolysis cell

3.3 TEM images and EDS analysis

According to the TEM micrographs, there appears to be agglomerations of nickel nanoparticles on carbon support as shown in Figure 3.3a. It is very hard to accurately measure the particle grain size due to low distinction between the nickel nanoparticles and the carbon support. However, based on a few clear grains the particles vary in size from 6-13 nm which is much larger than the NiBi/C reported in literature.[29] In the study by Houache et al., carbon supported Ni_xBi_{1-x} catalysts were prepared using a different metal precursor salt which resulted in small nanoparticles size ≤3nm.[29]

Furthermore, EDS spectra agreed with the elemental composition of $Ni_{95}Bi_5/C$ and the characteristic peaks showed presence of nickel, bismuth and oxygen (Figure 3.3b). The EDS spectra on two different region showed similar characteristic peaks indicating uniform distribution of both nickel and bismuth nanoparticles.

Figure 3.3 c, depicts the STEM-energy dispersive Figure 3.3 c depicts the STEM-energy dispersive spectroscopy (EDS) mapping images for $Ni_{95}Bi_5/C$ to provide a visual representation of its elemental distribution. The Ni (shown in red) and O (shown in yellow) elements are well distributed in the selected area of $Ni_{95}Bi_5/C$ catalysts. However, the element Bi (green) is only present in more specific area of the catalyst, signifying the presence of large clusters in the sample, probably due to the synthesis methodology.

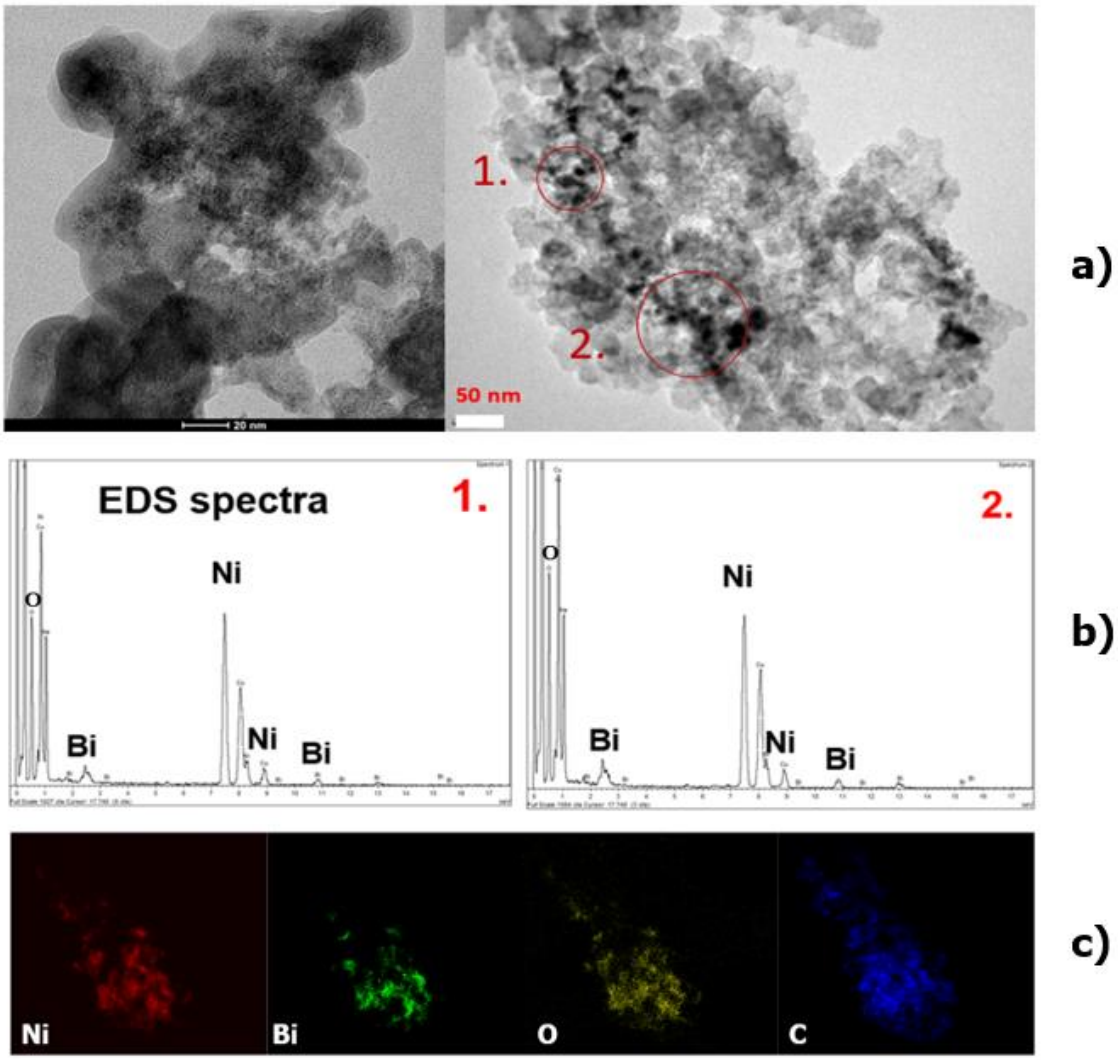

Figure 3.3: a) TEM images b) EDS spectra and c) EDS mapping of $Ni_{95}Bi_5/C$

3.4 Electrochemical measurements

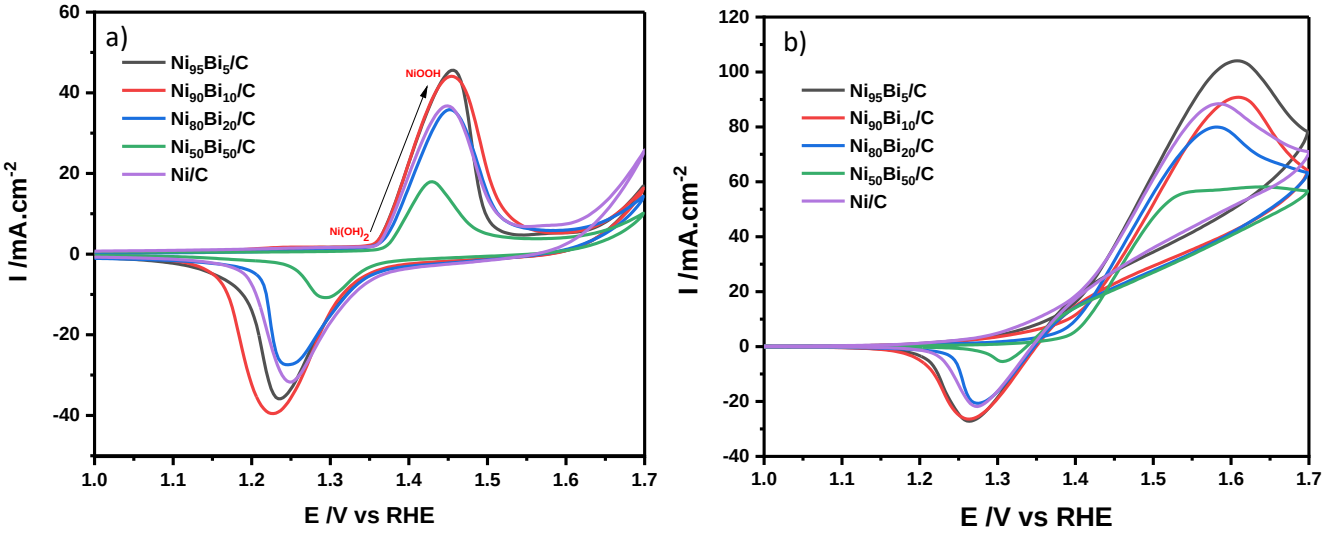

Figure 3.4: Cyclic Voltammograms (CV's) of Ni_xBi_{100-x}/C [x=100, 95, 90, 80 and 50 at. %] catalysts in N_2 purged (a) 1.0 M KOH and (b) 1.0 M KOH + 0.1 M glycerol electrolyte at 50 mV.s^{-1} scan rate and R.T

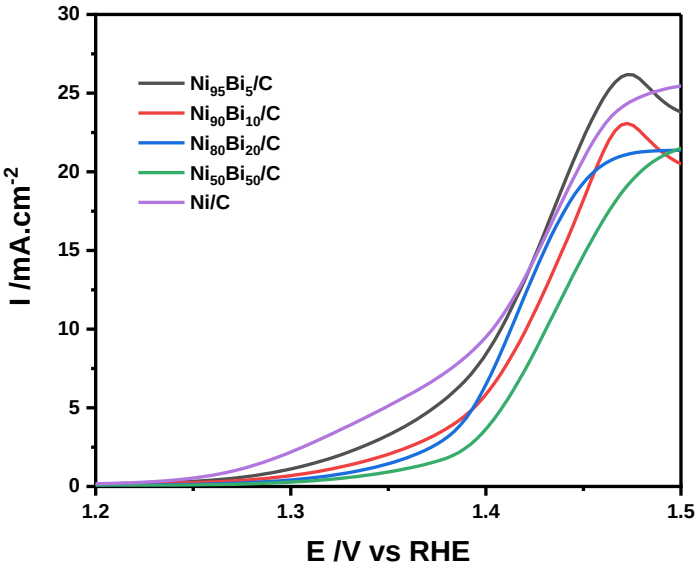

Figure 3.5: linear sweep voltammetry (LSV) of Ni_xBi_{100-x}/C catalysts in 1.0 M KOH + 0.1 M glycerol electrolyte at 1.0 mV. s^{-1} scan rate and R.T

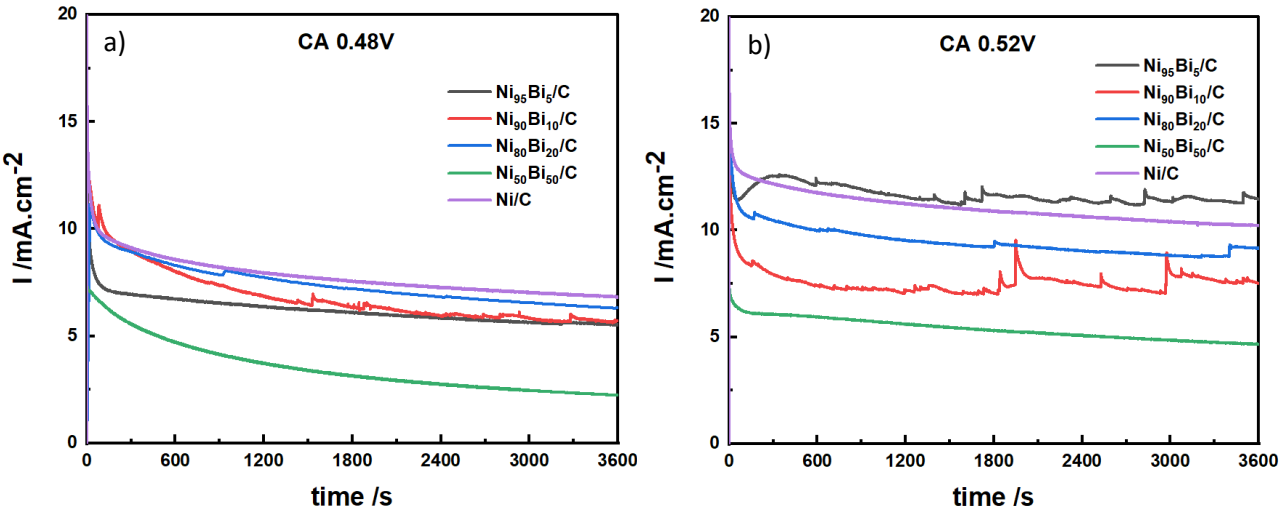

Figure 3.6: Chronoamperometry of Ni_xBi_{100-x}/C at a) 0.48 V and b) 0.52V

In order to gather understanding of the working electrode surface oxidation reactions and analyze the activity of various catalysts, cyclic voltammetry (CV), linear sweep voltammetry (LSV), and chronoamperometry (CA) were tested in a conventional three electrode electrochemical cell made of teflon. Ultimately, current collected must be normalized with the electrochemical active surface area (ECSA). However, there still lies some uncertainties with calculating the ECSA of bimetallic catalysts.[32] Therefore, in this study the current collected is normalized by the geometric area of the glassy carbon electrode (0.196 cm^2) and mass of nickel as shown in Figures 3.4-3.6 and A1, respectively.

At room temperature, cyclic voltammograms of carbon supported Ni_xBi_{100-x} [x=100, 95, 90, 80 and 50 at. %] in 1.0 M KOH aqueous solution were demonstrated in Figure 3.4a and A1a. The Ni^{2+}/Ni^{3+} redox process peaks are clearly established on all catalysts. In the forward scan, the oxidation from β-$Ni(OH)_2$ to β-NiOOH occurs at ~1.35-1.37V and reduction at ~1.35-1.37V in the reverse scan. At potentials higher than 1.5V, a peak for oxygen evolution reaction (OER) is observed. In terms of geometric area shown in Figure 3.4a, the addition of small amounts of bismuth (≤10%) resulted in more intense Ni^{2+}/Ni^{3+} redox peaks which is attributed to synergistic effects between nickel and bismuth. On the other hand, the catalyst with larger amounts of bismuth had lower current density of the redox peaks. It is most prominent on the $Ni_{50}Bi_{50}$/C catalyst which had the lowest current density for the redox peak in the forward and reverse scan. For $Ni_{50}Bi_{50}$/C, it is predicted that

$Bi(OH)_3$ species block nickel active sites making the catalyst less active or simply there are less available nickel active sites on the surface due to lower nickel loading. It has been proved by Houache et al. that bismuth on its own is not active toward glycerol electrooxidation.[28] However, CV with current normalized by mass of nickel, showed a different behavior. $Ni_{50}Bi_{50}$/C which has the least mass loading of nickel exhibited a more intense Ni^{2+}/Ni^{3+} redox peak (as shown in Figure A1a) compared to when normalized by geometric area (as shown in Figure 3.4a).

CVs of Ni_xBi_{100-x}/C catalysts in glycerol containing solutions (1.0 M KOH + 0.1 M glycerol) are demonstrated in Figure 3.4b and A1b. The glycerol electro-oxidation reaction (GEOR) occurs in the β-NiOOH formation region, as observed with other Ni-based catalysts.[33] In terms of geometric area in Figure 3.4b, $Ni_{95}Bi_5$ catalysts achieved the highest current density with the peak value of 104 $mA.cm^{-2}$ which is higher than that of Ni/C (88 $mA.cm^{-2}$). On the other hand, $Ni_{50}Bi_{50}$/C had the lowest activity with a current density of 58 $mA.cm^{-2}$. The order of activity of the catalysts from highest to lowest is $Ni_{95}Bi_5$ > $Ni_{90}Bi_{10}$ and Ni > $Ni_{80}Bi_{20}$ > $Ni_{50}Bi_{50}$. However, Ni exhibited the lowest onset potential of 1.3V compared to $Ni_{95}Bi_5$ (1.31V), $Ni_{90}Bi_{10}$ (1.35V), $Ni_{80}Bi_{20}$ (1.37V) and $Ni_{50}Bi_{50}$ (1.39V). The order of activity is altered when current is normalized with mass of nickel as shown in Figure A1b, $Ni_{50}Bi_{50}$/C (494 $A.g_{Ni}^{-1}$) > $Ni_{95}Bi_5$/C (465 $A.g_{Ni}^{-1}$) > $Ni_{90}Bi_{10}$/C and $Ni_{80}Bi_{20}$/C (~425 $A.g_{Ni}^{-1}$) > Ni/C (375 $A.g_{Ni}^{-1}$). When comparing between CVs in the absence and presence of glycerol, it is quite clear that GEOR takes place after the formation of β-NiOOH on the electrode surface which was expected as it is well known that NiOOH are the active species of nickel for organic molecules oxidation.[34]

The behavior observed in CVs were further shown in the LSVs in Figure 3.5 and A1c. According to LSV with current normalized by geometric area, $Ni_{95}Bi_5$ exhibited the highest current density at higher potentials as shown in Figure 3.5. However, Ni/C has the lowest onset potential and higher current density ($mA.cm^{-2}$) at lower potentials. On the other hand, $Ni_{50}Bi_{50}$ showed the highest mass activity ($A.g_{Ni}^{-1}$) as shown in Figure A1C. Chronoamperometry (CA) at 0.48V and 0.52V vs Hg/HgO for 3600s are shown in Figure 3.6a,b and A1d,e. According to the results the current initially increases then drops sharply and finally stabilizes. At 0.48V, Ni/C stabilizes at the highest current density of ~ 7 $mA.cm^{-}$

^{2}, as illustrated in Figure 3.6a. This behavior was also observed in the LSV as it was shown that at lower potentials Ni/C exhibited higher current density than NiBi catalysts. In terms of mass activity shown in Figure A1d, $Ni_{50}Bi_{50}$/C initially showed the highest current ($A.g_{Ni}^{-1}$) which sharply drops with time proving to be unstable compared to other Ni:Bi ratio's. In this regard, $Ni_{80}Bi_{20}$/C stabilized at the highest current (~ 40 $A.g_{Ni}^{-1}$) at 0.48V (Figure A1d). At higher potential 0.52V, $Ni_{95}Bi_{5}$ stabilized at the highest current of ~ 11 $mA.cm^{2}$ and ~58 $A.g_{Ni}^{-1}$ (Figure 3.6b and A1e).

In conclusion, bismuth in small amounts slightly enhanced the current density of the Nickel catalyst at higher overpotentials and $Ni_{95}Bi_{5}$ showed higher stability than $Ni_{50}Bi_{50}$/C. The smaller Ni_xBi_{1-x}/C nanoparticles prepared by Houache et al. showed higher current density (200 $mA.cm^{-2}$) and lower overpotential this could be explained by smaller nanoparticles of higher surface area with more active sites available for glycerol oxidation. [35] In the next section we conduct continuous electrolysis accompanied by high performance liquid chromatography (HPLC) tests to investigate particle size effect on product distributions. In addition, the effect of experimental conditions on product selectivity will be extensively studied.

3.5 Continuous glycerol electrolysis accompanied by HPLC analysis

The effect of adding bismuth on product selectivity and distributions were studied by running continuous electrolysis experiments of Ni/C and the best performing catalyst $Ni_{95}Bi_{5}$/C in 1M KOH + 0.1M glycerol for 6 hours. To compare between NiBi and Ni/C, the product distributions at fixed conditions 1.35V, R.T and 1.4 ml/s were studied and are shown in Figure 3.7a,b. Furthermore, the effect of applied potential (1.35 and 1.55 V), residence time (0.4 and 1.4 ml/s), and temperature (R.T, 50C, and 75C) were studied and shown in Figures 3.8-3.10. According to the results, the most prominent products are formic acid (FA) and glyceric acid (GA) and the secondary products are tartronic acid (TA), glycolic acid (GLA), oxalic acid (OA) and lactic acid (LA). Furthermore, the CA profiles in the $5cm^{2}$ electrolysis cell for $Ni_{95}Bi_{5}$/C and Ni/C are shown in Figure A2. Both $Ni_{95}Bi_{5}$/C and Ni/C were stable for 6 hours in the electrolysis cell.

3.5.1 Comparison between $Ni_{95}Bi_5$/C vs Ni/C at constant experimental conditions

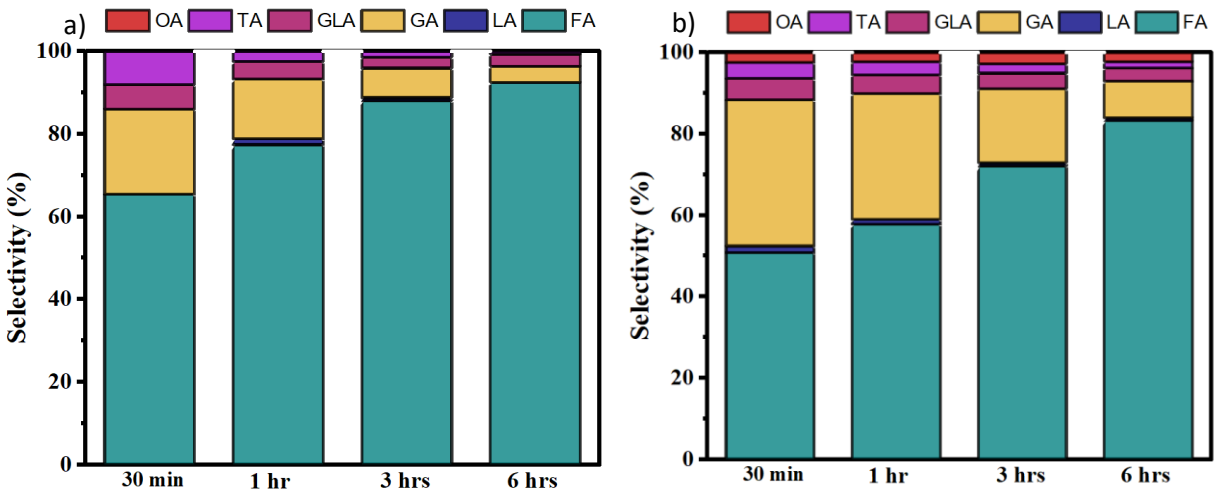

Figure 3.7: Product distributions of a) Ni/C and b) $Ni_{95}Bi_5$/C with time at fixed applied potential, temperature and electrolyte flowrate of 1.35V, R.T and 1.4ml/s. red: oxalate, purple: tartronate, pink: glycolate, yellow: glycerate, blue: lactate and green: formate.

On both catalysts, the two primary products are GA and FA (≤85-87%) and the secondary products TA, GLA, OA, and LA (≤13-15%) as shown in the figure 3.7a,b. However, NiBi catalyst exhibited higher selectivity to GA and consequently, less selectivity to FA. For instance, at 30 min, NiBi exhibited ~2 times higher selectivity to GA and the selectivity to FA is ~15% less than that of Ni/C. As time is given for the reaction to take place, the C-C-C bonds are broken to form higher selectivity to C_1 product FA and lower selectivity to GA, TA, GLA, and LA for both Ni and NiBi catalysts. Even after 6 hours of electrolysis, the selectivity to GA on NiBi catalyst is ~ 2 times higher than that of Ni/C and the selectivity to FA is ~ 10% less. Thus, the production of C_3 product GA is enhanced over bimetallic catalyst NiBi/C. This enhancement to C_3 product can be explained by bimetallic catalyst NiBi having less nickel electropositive sites and thus less capable of C-C bonds cleavage.[36]

Compared to the smaller Ni_xBi_{1-x}/C nanoparticles which resulted in 100% selectivity to FA [29], the larger nanoparticles form a variety of products (FA, GA, GLA, TA, OA, LA). The primary products are FA (50-80%) and GA (35-10%) while, the secondary products are GLA, TA, OA and LA (≤15%). Interestingly, free standing Ni_xBi_{1-x} catalysts (~9 nm particle

size) had similar product distributions to Ni_xBi_{100-x}/C (~6-13 nm particle size).[28] This could indicate that the particle size has a large effect on product selectivity in GEOR.

3.5.2 Effect of Applied potential

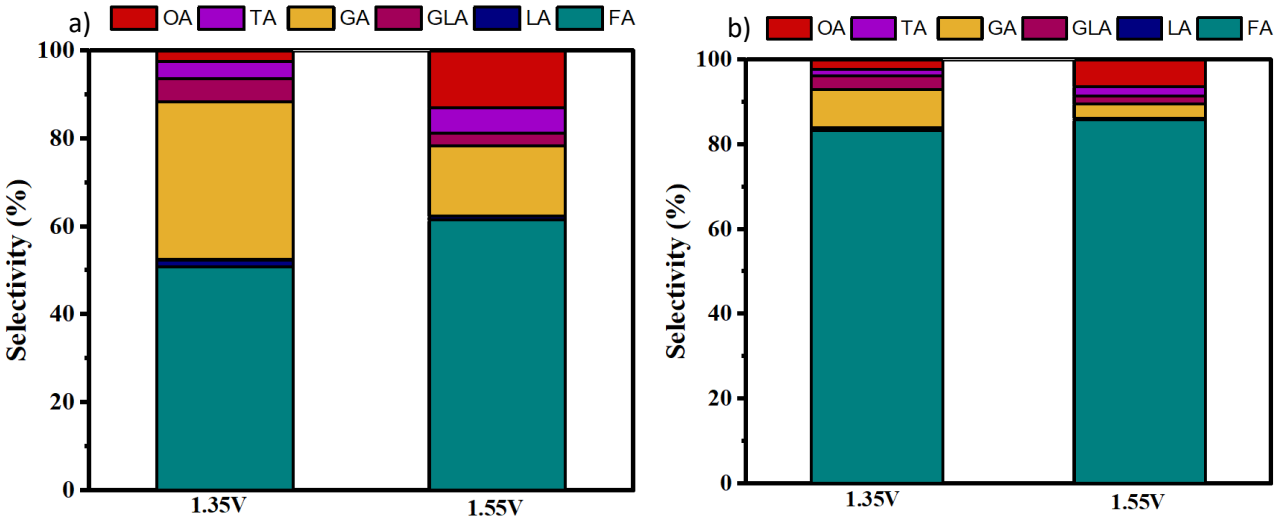

Figure 3.8: The effect of applied potential on product distributions of $Ni_{95}Bi_5/C$ with time a) 30 min and b) 6 hrs at fixed temperature and electrolyte flowrate of R.T and 1.4ml/s. red: oxalate, purple: tartronate, pink: glycolate, yellow: glycerate, blue: lactate and green: formate.

The effect of applied potential (1.35 and 1.55 V) on product distributions of NiBi catalyst was studied at R.T and 1.4 $ml.s^{-1}$ electrolyte flowrate as shown in figure 3.8a,b. After 30 minutes of electrolysis (Figure 3.8a), the selectivity to GA was ~36% at 1.35V compared to ~ 16% at 1.55V. This trend was also observed after 6 hours of electrolysis. Noticeably, at higher applied potential of 1.55V the reaction of C-C bonds cleavage is promoted to form more C_2 and C_1 products such as OA and FA and less of C_3 product GA. Compared to 1.35V, the selectivity to OA was ~6 times higher at 1.55V and 30 minutes of electrolysis while the selectivity of FA increased by 10% as shown in Figure 3.8a. Less noticeably, the same behavior was observed after 6 hours of electrolysis as illustrated in Figure 3.8b. At higher potential 1.55V, the selectivity to TA is ~1.5x higher than at 1.35V and 30 minutes of electrolysis.

3.5.3 Effect of Residence time

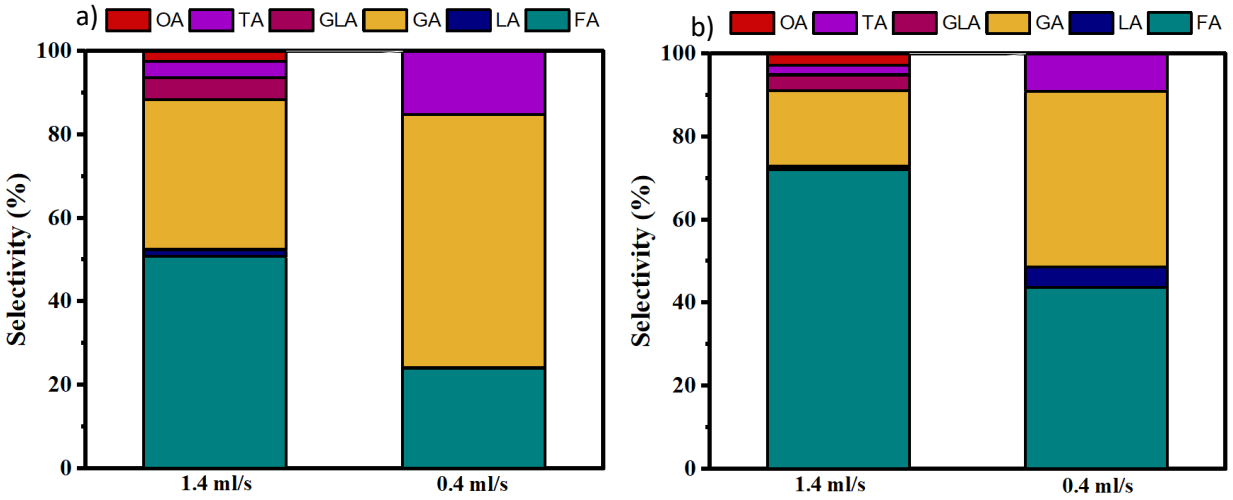

Figure 3.9: The effect of different electrolyte flowrates on product distributions of $Ni_{95}Bi_5$/C with time a) 30min and b) 3 hrs at fixed applied potential and temperature of 1.35V and R.T. red: oxalate, purple: tartronate, pink: glycolate, yellow: glycerate, blue: lactate and green: formate.

Continuous electrolysis with different pump rate of electrolyte (1.4 and 0.4 ml/s) were studied to investigate their effect on product selectivity of NiBi catalyst at 1.35V and R.T as shown in Figure 3.9a,b. Reducing the flowrate to 0.4ml/s greatly lowers the residence time of glycerol in the cell. It was observed that at lower electrolyte flowrate of 0.4 ml/s, the selectivity to GA valuable product was greatly enhanced by ~2x after 30 minutes and 3 hours of electrolysis while selectivity to FA was greatly reduced as shown in Figure 3.9a,b. In addition, a noticeable increase in TA selectivity was observed at 30 minutes and 3 hours at lower glycerol residence time. For instance, the selectivity to TA was ~15% at 0.4 ml/s compared to ~3% at 1.4 ml/s and 30 minutes of electrolysis. Prominently, C_2 products OA and GLA are not formed at lower electrolyte flowrate 0.4 ml/s as demonstrated in Figure 3.9a,b. One must note a slight increase in selectivity to LA at 0.4 ml/s after 3 hours of electrolysis as shown in Figure 3.9b. In conclusion, lowering residence time changed the product distributions significantly.

3.5.4 Effect of Temperature

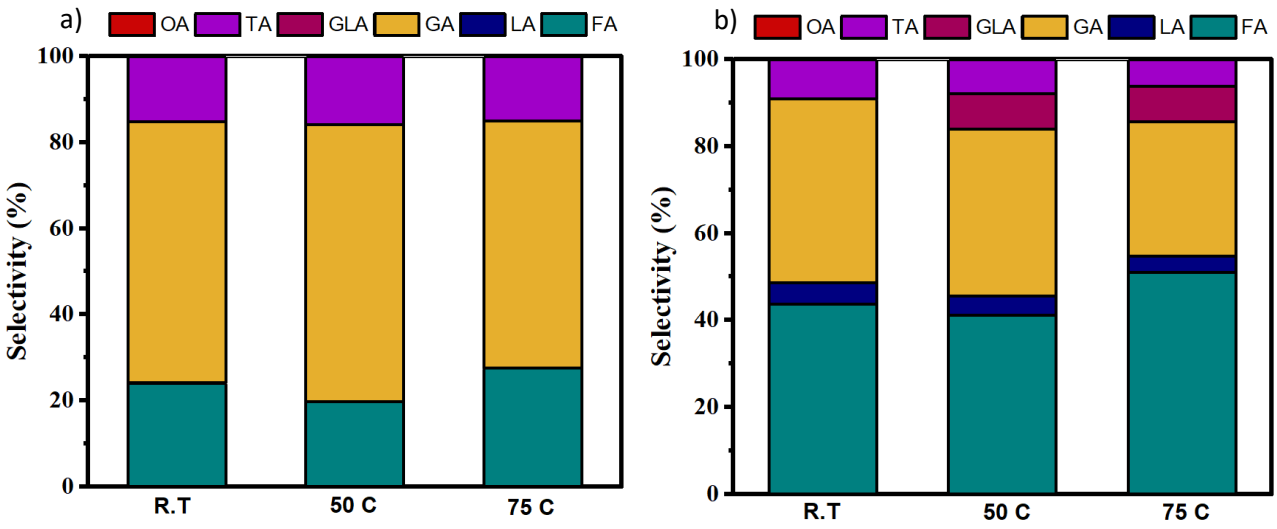

Figure 3.10: The effect of temperatures (R.T, 50C and 75C) on product distributions of $Ni_{95}Bi_5/C$ at a) 30min and b) 3 hrs with fixed applied potential and electrolyte flowrate of 1.35V and 0.4 ml/s. red: oxalate, purple: tartronate, pink: glycolate, yellow: glycerate, blue: lactate and green: formate.

As shown in Figure 3.10a,b, the temperature effect was very minimal on product distributions. The main difference is the formation of C_2 product GLA after 3 hours of electrolysis at higher temperatures (50 and 75°C).

3.6 Conclusion

In summary, the bimetallic catalyst NiBi/C with different Ni to Bi ratios were studied for GEOR. It was found that the addition of Bi enhanced selectivity of Ni to C_3 products compared to monometallic Ni/C. Particularly, selectivity to GA increased by 2x for $Ni_{95}Bi_5/C$ compared to pure Ni nanoparticles. On $Ni_{95}Bi_5/C$, GA and FA were the primary products with selectivity ≥85% and the secondary products are GLA, TA, OA and LA ≤15%.

Moreover, as the applied potential increases to 1.55V, the C-C bond cleavage rate is enhanced leading to lower selectivity to GA and higher TA, OA, FA selectivity compared to 1.35V. At 30 minutes, selectivity to GA is reduced from 36% to 16% as potential increases to 1.55V. While, selectivity to OA, TA and FA were enhanced by 6x, 1.5x and 1.2x, respectively. Additionally, reducing the residence time of glycerol in the electrolysis cell

resulted in higher selectivity to C_3 products (GA and TA) and consequently lower selectivity to FA proving slower rate of reaction. Finally, increasing the temperature to 50 and 75 °C had minimal to no effect on product distributions. Thus, running the experiments with bimetallic catalyst NiBi at lower applied potential (1.35V), residence time (0.4 $ml.s^{-1}$) and temperature (room temperature) results in highest selectivity to C_3 desired products.

Additionally, the particle size of NiBi/C has a dominant role in catalytic performance and product distributions. Larger NiBi/C nanoparticles showed lower current density of 104 $mA.cm^{-2}$ and 465 $A.g_{Ni}^{-1}$ at 1.6V vs. RHE and higher overpotential of 1.31V vs. RHE compared to smaller nanoparticles (200 $mA.cm^{-2}$ and 1.15V vs RHE) that was reported in literature, as shown in S.I Figure A3.[29] However, smaller NiBi/C nanoparticles showed to be 100% selective to FA compared to larger nanoparticles which had 35% selectivity to GA C_3 product at mild conditions (Table 3.1 and Figure A3 in SI).

Table 3.1: Comparison of NiBi/C with different particle size

Catalyst	**particle size**	**Peak current density ($mA.cm^{-2}$)**	**Onset potential (V vs RHE)**	**Selectivity**
$Ni_{95}Bi_5/C$	6-13 nm	104	1.31	FA: 50.87%, GA: 35.7%, GLA: 5.25%, TA: 3.94%, OA: 2.45%, LA: 1.59% (HPLC)
$Ni_{90}Bi_{10}/C$	≤3nm	200	1.15	FA: 100% (HPLC)

References

[1] A.G. Olabi, T. Wilberforce, M.A. Abdelkareem, Fuel cell application in the automotive industry and future perspective, Energy. 214 (2021) 118955. https://doi.org/10.1016/j.energy.2020.118955.

[2] Biodiesel, Gov. Canada. (n.d.). https://www.nrcan.gc.ca/energy-efficiency/energy-efficiency-transportation/alternative-fuels/biofuels/biodiesel/3509.

[3] A.A. Abdul Raman, H.W. Tan, A. Buthiyappan, Two-Step Purification of Glycerol as a Value Added by Product From the Biodiesel Production Process, Front. Chem. 7 (2019) 1–9. https://doi.org/10.3389/fchem.2019.00774.

[4] H.W. Tan, A.R. Abdul Aziz, M.K. Aroua, Glycerol production and its applications as a raw material: A review, Renew. Sustain. Energy Rev. 27 (2013) 118–127. https://doi.org/10.1016/j.rser.2013.06.035.

[5] A. Rusu, L. Mitrea, F. Fetea, F.V. Dulf, M. Trif, D.C. Vodnar, Biodiesel-Derived Glycerol Obtained from Renewable Biomass — A Suitable Substrate for the Growth of Candida zeylanoides Yeast Strain ATCC 20367, Microorganisms. 7 (2019) 265.

[6] N.M. Saifuddin, R. Hussein, Integration of Biodiesel and Bioethanol Processes : Convertion of Low Cost Waste Glycerol to Bioethanol 1, Adv. Nat. Appl. Sci. 6 (2012) 802–818.

[7] C. Coutanceau, S. Baranton, R.S.B. Kouamé, Selective electrooxidation of glycerol into value-added chemicals: A short overview, Front. Chem. 7 (2019) 1–15. https://doi.org/10.3389/fchem.2019.00100.

[8] M.E.G. Lyons, R.L. Doyle, I. Godwin, M.O. Brien, L. Russell, Hydrous Nickel Oxide : Redox Switching and the Oxygen Evolution Reaction in Aqueous Alkaline Solution, Electrochem. Soc. 159 (2012) 932–944. https://doi.org/10.1149/2.078212jes.

[9] L. Ren, K.S. Hui, K.N. Hui, Self-assembled free-standing three-dimensional nickel nanoparticle/graphene aerogel for direct ethanol fuel cells, J. Mater. Chem. A. 1 (2013) 5689–5694. https://doi.org/10.1039/c3ta10657h.

[10] C. Bock, H. Halvorsen, B. Macdougall, Catalyst Synthesis Techniques, in: PEM Fuel Cell Electrocatal. Catal. Layers, 2009: pp. 447–485.

[11] O.C. Nwamba, E. Echeverria, Q. Yu, K.S. Raja, materials Increased electron transfer kinetics and thermally treated graphite stability through improved tunneling paths, J. Mater. Sci. 55 (2020) 11411–11430. https://doi.org/10.1007/s10853-020-04846-6.

[12] M.S.E. Houache, K. Hughes, R. Safari, G.A. Botton, E.A. Baranova, Modification of Nickel Surfaces by Bismuth: Effect on Electrochemical Activity and Selectivity toward Glycerol, ACS Appl. Mater. Interfaces. (2020). https://doi.org/10.1021/acsami.9b22378.

[13] Y. Li, F. Zaera, Sensitivity of the glycerol oxidation reaction to the size and shape of

the platinum nanoparticles in Pt / SiO 2 catalysts, J. Catal. 326 (2015) 116–126. https://doi.org/10.1016/j.jcat.2015.04.009.

[14] S.M.S. Kumar, J.S. Herrero, S. Irusta, K. Scott, The effect of pretreatment of Vulcan XC-72R carbon on morphology and electrochemical oxygen reduction kinetics of supported Pd nano-particle in acidic electrolyte, J. Electroanal. Chem. 647 (2010) 211–221. https://doi.org/10.1016/j.jelechem.2010.05.021.

[15] N. Ć, P. Spasojevi, L. Ribi, P. Maškovi, M. Spasojevi, Synthesis , Structure and Properties of Nickel-Iron-Tungsten Alloy Electrodeposits PART I : Effect of Synthesis Parameters on Chemical Composition , Microstructure and Morphology, Sci. Sinter. 47 (2015) 347–365. https://doi.org/10.2298/SOS1503347C.

[16] M. Kazazi, F. Ghadami, M. Reza, Effect of synthesis method on the morphological and electrochemical characteristics of sulfur / MWCNT composite cathode, Solid State Ionics. 290 (2016) 40–46. https://doi.org/10.1016/j.ssi.2016.04.007.

[17] N. Truong, X. Minh, B. Thi, M. Thu, L.T. Cuc, N.H. Linh, P.N. Y, H. Ky, P. Ha, N.T. Son, effects of synthrsis conditions on structure of nickel nanowired prepared by reduction method, Vietnam J. Sci. Technol. 57 (2019) 21–28. https://doi.org/10.15625/2525-2518/57/3A/13945.

[18] J. Tientong, S. Garcia, C.R. Thurber, T.D. Golden, Synthesis of Nickel and Nickel Hydroxide Nanopowders by Simplified Chemical Reduction, Hindawi. (2014).

[19] K. Xu, R. Zou, W. Li, Q. Liu, X. Liu, J. Hu, Design and synthesis of 3D interconnected nanosheet arrays with large areal capacitance and high rate performance for supercapacitors †, J. Mater. Chem. A. 2 (2014) 10090–10097. https://doi.org/10.1039/c4ta01489h.

[20] J. Wu, P. Guo, R. Mi, X. Liu, H. Zhuang, M. Jun, H. Liu, W.-M. Lau, L.-M. Liu, Ultrathin NiCo2O4 nanosheets grown on three-dimensional interwoven nitrogen-doped carbon nanotubes as binder-free electrodes for high-performance supercapacitors, J. Mater. Chem. A. 3 (2015) 15331–15338. https://doi.org/10.1039/C5TA02719E.

[21] M.H. Tahmasebi, A. Vicenzo, M. Hashempour, M. Bestetti, M.A. Golozar, K. Raeissi, Nanosized Mn-Ni oxide thin fi lms via anodic electrodeposition : a study of the correlations between morphology , structure and capacitive behaviour, Electrochim. Acta. 206 (2016) 143–154. https://doi.org/10.1016/j.electacta.2016.04.087.

[22] J. Leicester, M.J. Redman, THERMAL DECOMPOSITION OF THE NICKEL AND COBALT, J. Appl. Chem. 12 (2007) 357–366.

[23] Q. Song, Z. Tang, H. Guo, S.L.I. Chan, Structural characteristics of nickel hydroxide synthesized by a chemical precipitation route under different pH values, J. Power Sources. 112 (2002) 428–434.

[24] M. Wu, H. Hsieh, Nickel oxide / hydroxide nanoplatelets synthesized by chemical precipitation for electrochemical capacitors, 53 (2008) 3427–3435. https://doi.org/10.1016/j.electacta.2007.12.005.

[25] S. Chang, Z. Zainal, K. Tan, N.A. Yusof, W. Mohamad, D. Wan, S.R.S. Prabaharan, Synthesis and electrochemical properties of nanostructured nickel – cobalt oxides as supercapacitor electrodes in aqueous media, Int. J. Energy Res. 39 (2015) 1366–1377. https://doi.org/10.1002/er.

[26] D.S. Hall, D.J. Lockwood, C. Bock, B.R. Macdougall, D.J. Lockwood, Nickel hydroxides and related materials : a review of their structures , synthesis and properties, Proceeding R. Soc. 471 (2015).

[27] E. Kowalewski, I.I. Kamin, Effect of metal precursor and pretreatment conditions on the catalytic activity of Ni / C in the aqueous phase, React. Kinet. Mech. Catal. 12 (2017) 3–16. https://doi.org/10.1007/s11144-017-1148-4.

[28] M.S.E. Houache, K. Hughes, R. Safari, G.A. Botton, E.A. Baranova, Modification of Nickel Surfaces by Bismuth: Effect on Electrochemical Activity and Selectivity Towards Glycerol Modification of Nickel Surfaces by Bismuth : Effect on Electrochemical Activity and Selectivity Towards Glycerol, ACS Appl. Mater. Interfaces. 12 (2020) 15095–15107. https://doi.org/10.1021/acsami.9b22378.

[29] M.S.E. Houache, R. Safari, U.O. Nwabara, T. Rafa, G.A. Botton, C. Coutanceau, E.A. Baranova, P.J.A. Kenis, Selective Electrooxidation of Glycerol to Formic Acid over Carbon Supported Ni1−xMx (M = Bi , Pd , and Au) Nanocatalysts and Coelectrolysis of CO2, ACS Appl. Energy Mater. 3 (2020) 8725–8738. https://doi.org/10.1021/acsaem.0c01282.

[30] M. Houache, K. Hughes, Electrochemical Valorization of Glycerol on Ni-rich Bimetallic NiPd Nanoparticles: Insight into product selectivity using in-situ PM-IRRAS, ACS Sustain. Chem. Eng. 17 (2019) 14425–14434. https://doi.org/10.1021/acssuschemeng.9b01070.

[31] M. Seif, E. Houache, Efficient Nanostructured Ni-based Catalysts for Electrochemical Valorization of Glycerol, 2020.

[32] E. Cossar, M.S.E. Houache, Z. Zhang, E.A. Baranova, Comparison of electrochemical active surface area methods for various nickel nanostructures, J. Electroanal. Chem. 20 (2020) 114246. https://doi.org/10.1016/j.jelechem.2020.114246.

[33] M.S.E. Houache, K. Hughes, A. Ahmed, R. Safari, H. Liu, G.A. Botton, E.A. Baranova, Electrochemical Valorization of Glycerol on Ni-Rich Bimetallic NiPd Nanoparticles: Insight into Product Selectivity Using in Situ Polarization Modulation Infrared-Re fl ection Absorption Spectroscopy, ACS Sustain. Chem. Eng. 7 (2019) 14425–14434. https://doi.org/10.1021/acssuschemeng.9b01070.

[34] L. Xu, Z. Wang, X. Chen, Z. Qu, F. Li, W. Yang, Ultrathin layered double hydroxide nanosheets with Ni(III) active species obtained by exfoliation for highly efficient ethanol electrooxidation, Electrochim. Acta. 260 (2018) 898–904. https://doi.org/10.1016/j.electacta.2017.12.065.

[35] P. Song, H. Xu, B. Yan, J. Wang, F. Gao, Y. Zhang, Y. Shiraishi, Y. Du, Particle size effects in the catalytic electrooxidation of liquid fuel on PtAg nanoparticles, Inorg. Chem. Front. 5 (2018) 1174–1179. https://doi.org/10.1039/C8QI00032H.

[36] B. Katryniok, H. Kimura, E. Skrzynska, J.-S. Girardon, P. Fongarland, M. Capron, R. Ducoulombier, N. Mimura, S. Paul, Dumeignil. Franck, Selective catalytic oxidation of glycerol: perspectives for high value chemicals, Green Chem. 13 (2011) 1960–1979. https://doi.org/10.1039/c1gc15320j.

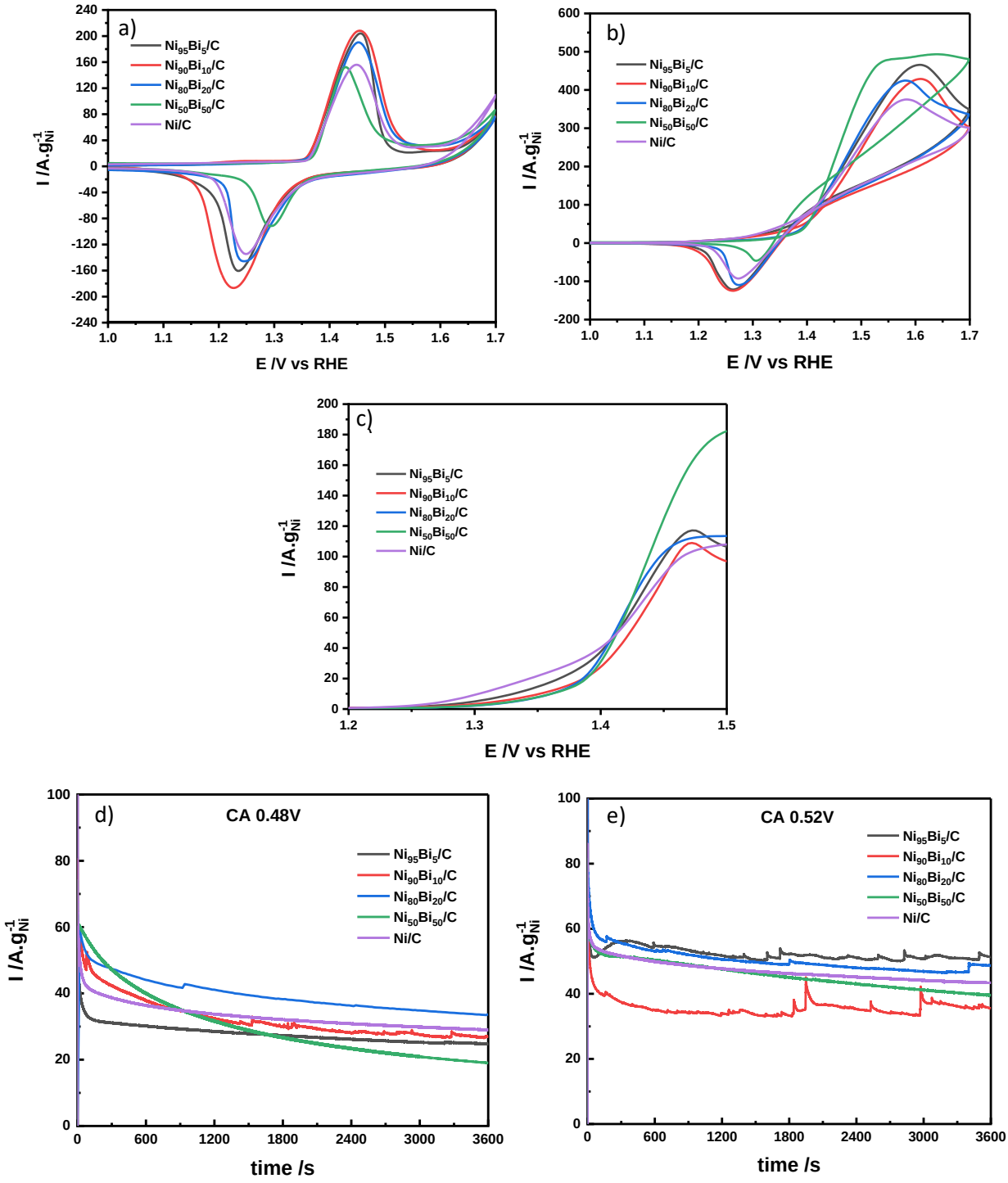

Figure A1: Cyclic voltammograms of Ni_xBi_{100-x}/C performed in a) 1M KOH and b) 1M KOH + 0.1 M glycerol aqueous solution at scan rate of 50 $mV.s^{-1}$. c) linear sweep voltammetry (LSV) at 1 $mV.s^{-1}$. (d,e) Chronoamperometry (CA) tests at potentials 0.48 V and 0.52 V vs. Hg/HgO for 60 min. [Current normalized with mass of nickel]

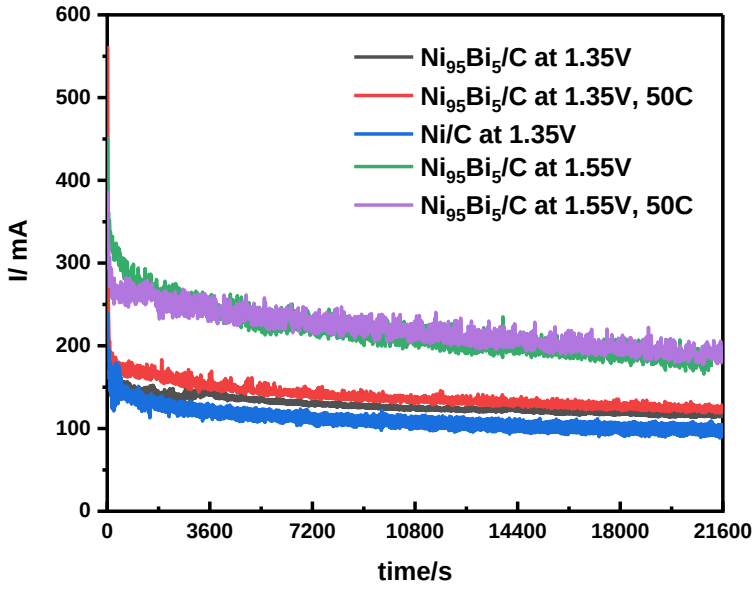

Figure A2: CA in 25cm^2 electrolysis cell at 1.35 V and 1.55V for GEOR on $Ni_{95}Bi_5$/C and Ni/C catalysts in 1.0 M KOH + 0.1 M glycerol electrolyte at room temperature and 50 °C for 6 hours.

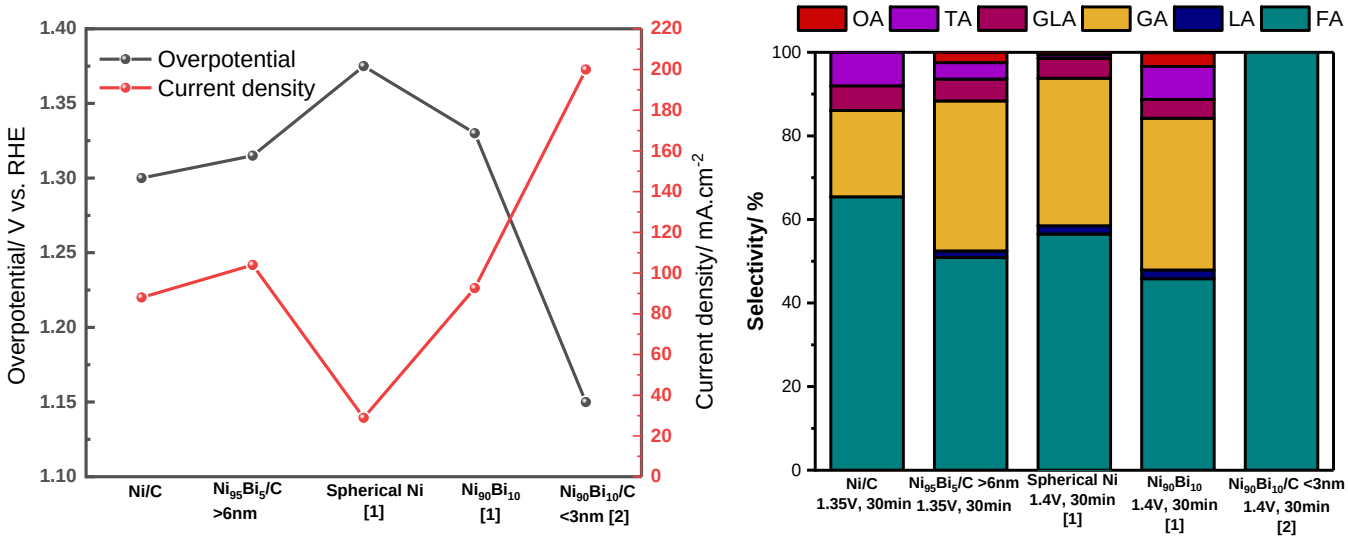

Figure A3: Comparison of electrochemical performance and product distributions of catalysts $Ni_{95}Bi_5$/C (>6nm) and Ni/C with other catalysts reported in literature. [1,2]

[1] M.S.E. Houache, K. Hughes, R. Safari, G.A. Botton, E.A. Baranova, Modification of Nickel Surfaces by Bismuth: Effect on Electrochemical Activity and Selectivity Towards Glycerol Modification of Nickel Surfaces by Bismuth : Effect on Electrochemical Activity and Selectivity Towards Glycerol, ACS Appl. Mater. Interfaces. 12 (2020) 15095–15107. https://doi.org/10.1021/acsami.9b22378.

[2] M.S.E. Houache, R. Safari, U.O. Nwabara, T. Rafa, G.A. Botton, C. Coutanceau, E.A. Baranova, P.J.A. Kenis, Selective Electrooxidation of Glycerol to Formic Acid over Carbon Supported Ni1−xMx (M = Bi , Pd , and Au) Nanocatalysts and Coelectrolysis of CO2, ACS Appl. Energy Mater. 3 (2020) 8725–8738. https://doi.org/10.1021/acsaem.0c01282.

Chapter 4: The Role of Metal Oxides (CeO_2, SnO_2, and Sb_2O_3:SnO_2) on the Selectivity of NiBi Nanoparticles to C_3 Products of Glycerol Electrooxidation

Asma Shubair, Pratik Parwani, Mohamed S. E. Houache, and Elena A. Baranova

To be submitted to Journal of Power Sources

Abstract

Fine tuning Ni-based catalysts to achieve higher catalytic activity and selectivity to C_3 products for glycerol electrooxidation reaction (GEOR) is still under research. This can be done by changing nanoparticles morphology (size and shape), adding an adatom/promoter, or depositing metals on different supports. Up to date, carbon is the main support used as it has large surface area and may be easily tuned. However, metal oxides have gained interest due to their interesting physical characteristics such as oxygen vacancies that may impact the reaction kinetics and pathway.

Herein, the effect of metal oxides (CeO_2, SnO_2 and ATO) on the electrochemical performance and product selectivity of bimetallic NiBi/C catalysts for glycerol electrooxidation reaction (GEOR) is investigated. The NiBi/C-X (X= CeO_2, SnO_2 and ATO) catalysts were synthesized by sodium borohydride reduction method at room temperature and tested by electrochemical techniques. CVs, LSVs and CAs of all catalysts were conducted in a three-electrode electrochemical cell made of Teflon material. Among the composite support catalysts, Ni/C-ATO exhibited the highest peak current density of 96 $mA.cm^{-2}$ at 1.50 V vs. RHE. Furthermore, continuous electrolysis accompanied by HPLC technique was conducted to determine product selectivity. Results show that glyceric acid (GA) and lactic acid (LA) were the primary products (≤90%) and the secondary products are tartronic acid (TA), glycolic acid (GLA), and formic acid (FA) on NiBi/C-X catalysts.

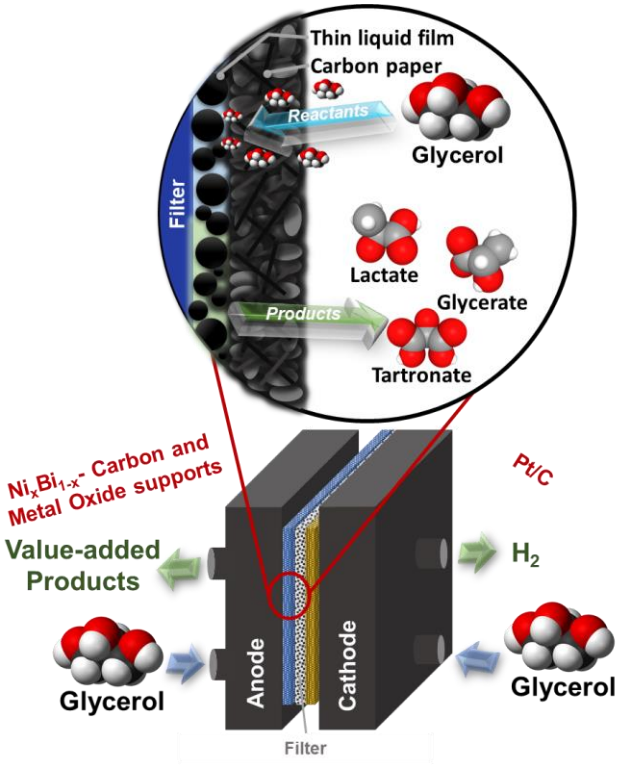
Thin liquid film
Carbon paper
Reactants
Glycerol
Filter
Lactate
Glycerate
Products
Tartronate
Ni_xBi_{1-x}- Carbon and Metal Oxide supports
Pt/C
Value-added Products
H_2
Anode
Cathode
Glycerol
Glycerol
Filter

4.1 Introduction

The movement towards more sustainable sources of energy led to the growth of the biodiesel industry.[1] The demand for biodiesel is increasing at an average rate of 7% annually until 2021.[2] In the process of biodiesel synthesis, glycerol is formed as a by-product at 10wt%.[3] The supply of glycerol exceeds its demand and this has been the trend since 2003.[2,4] The over-supply of glycerol has been a key issue in the development of the biodiesel industry as it must be either disposed or stored which causes environmental concerns or adds extra storage costs.[5] Much efforts have been made on converting this highly functionalized molecule into products of higher economical value.[5–9] By means of electrocatalytic oxidation processes, the activity and selectivity may be fine-tuned by varying the electrocatalyst type and electrode applied potential. Some of the highly valuable products such as, glyceric acid (GA), lactic acid (LA) and tartronic acid (TA) are of main interest in alkaline medium. GA is used in the treatment of skin disorders and is an intermediate in the production of amino acids.[9] TA is used as a drug-delivery agent and is a known oxygen scavenger.[10] LA is a raw material in the pharmaceutical industry and is an in important intermediate in various organic synthesis and biochemical industries.[9] These products are favorable however, tuning the selectivity is one of the main challenges in Glycerol electro-oxidation process.

Noble metals platinum, palladium and gold-based electrocatalysts have been widely studied in acidic and alkaline medium for GEOR.[11–19] There are numerous efforts in improving the activity and selectivity of these catalysts. Promoters such as, Bi [20–23], Sn [24], Pb [25], Sb [24,26] and Ag [27–29] had a considerable influence on both the activity and selectivity of noble metals in alcohol electro-oxidation reactions. For instance, incorporating bismuth to platinum increased the selectivity to the C_3 valuable product dihydroxyacetone (DHA) from 10% to 80%.[30] Additionally, the selectivity of platinum to DHA was substantially increased for platinum electrocatalyst by dissolving bismuth or antimony in the reaction solution.[26] Thus, adding bismuth or antimony in small amounts acted in enhancing the production of value-added product DHA for the platinum catalyst.

Although noble metals were highly optimized in terms of activity and selectivity, these metals are expensive which may limit their practical application in industry. For this

reason, interest to cheaper and more abundant catalysts such as; Nickel (Ni) and Cobalt (Co) have increased.[31–37] Particularly, nickel showed high electrochemical activity and long-term durability in alkaline medium for GEOR.[38] The majority of research with nickel-based catalysts showed that the C-C bonds of glycerol tend to completely break forming formic acid (FA) which is a lower value product. [33] For application in direct alcohol fuel cells (DAFC's), this result would be interesting as higher degree of C-C bond cleavage means that more electrons are being generated. However, for the motive of electro-synthesis, it is not ideal. Significant research has been made to optimize the activity and modify the selectivity of Ni-based catalysts.[4,35,38–41] A recent research by Houache et al. showed that modifying nickel with bismuth (Bi) improved the overall catalytic performance and suppressed C-C bond cleavage which resulted in higher selectivity to GA and TA.[4] The maximum GA and TA selectivity achieved on NiBi catalyst was 60.2% and 23.5%, respectively at 1.3V and 50 °C. [4] This result shows that just as bismuth enhanced the selectivity to C_3 products for platinum catalyst, it did the same for nickel-rich catalyst.

Moreover, there has been great attention to ceria (CeO_2) and stannic oxide (SnO_2) as anode catalysts or supports for alcohol electrooxidation reactions.[10,42–44] Ceria has the ability of storing and releasing oxygen without altering the lattice structure, owing to its reversible oxidation/reduction processes from Ce^{4+} /Ce^{3+}.[45] SnO_2 facilitates the formation of OH adsorbed species by promoting the dissociative adsorption of water, which are oxidizing agents in alcohol electrooxidation processes.[46] In addition, tin-based oxides are known to improve the catalyst stability and activity due to strong metal-support interactions (SMSI).[46] Furthermore, doping tin-oxides with antimony[47,48], indium [49,50] and fluorine [51,52] have been widely explored as they promote the electrical conductivity of the support. Specifically, ATO has the highest electrical conductivity compared to ITO and FTO.[53] A study by Xu. and Shen., showed the modifying Pt electrodes with CeO_2 exhibited promotion in catalytic performance for ethanol, methanol and glycerol electro-oxidation reaction.[54] Another study comparing between ATO and SnO_2 modified platinum electrodes for ethanol electrooxidation reaction showed that Pt-ATO/MWCNT has higher catalytic performance than Pt-SnO_2/MWCNT.[47] To the best of our knowledge, modifying nickel- based materials with metallic oxides CeO_2, SnO_2 and ATO has not yet been explored for GEOR.

Herein, carbon supported Ni and $Ni_{95}Bi_5$ catalysts are modified with ceria, stannic oxide and ATO for GEOR. The catalytic performance of all catalysts [Ni/C-CeO_2, Ni/C-SnO_2, Ni/C-ATO, $Ni_{95}Bi_5$/C-CeO_2, $Ni_{95}Bi_5$/C-SnO_2, and $Ni_{95}Bi_5$/C-ATO] were studied in the conventional three-electrode electrochemical cells for CV's, LSV's and CA's. Furthermore, selectivity of the catalysts was observed via continuous electrolysis accompanied by HPLC.

4.2 Experimental procedures

4.2.1 Materials:

Nickel (II) chloride hexahydrate (Sigma Aldrich 99.999%), Bismuth Chloride anhydrous (Fischer Scientific 99.9%), sodium borohydride (ACROS organics ≥98%), Vulcan carbon black (XC 72, cabot, >99%), cerium oxide (Alfa Aesar 99.5%), tin oxide (Nanoarc 99.5%), antimony tin oxide (Nanoarc 99.5%) and ethanol (Fischer scientific 99%)

4.2.2 Synthesis of $Ni_{95}Bi_5$ nanoparticles:

At room temperature, $Ni_{95}Bi_5$/C-X [X=ceria, SnO_2 or ATO] with 50 wt% supports (40wt% Carbon + 10 wt% X) were prepared by $NaBH_4$ reduction method with ethanol as a solvent. First, the metal precursor salts [$NiCl_2$ and $BiCl_3$] and supports [Carbon and X] were each solvated in 50 ml ethanol for 45 min until homogenous. Next, the metal precursor solutions and supports solution were mixed together for 30 min. $NaBH_4$ (2wt%) is dissolved in <5ml ethanol and sonicated until homogenous and is added to the combined metal + supports solution drop by drop to avoid agglomerations. The resulting mixture was kept to mix for 45 minutes to ensure complete reduction reaction took place. Then the samples were washed three

times with ethanol and centrifuged for 10 minutes per washing at 6000 rpm. Finally, all catalysts were dried in a freeze dryer overnight.

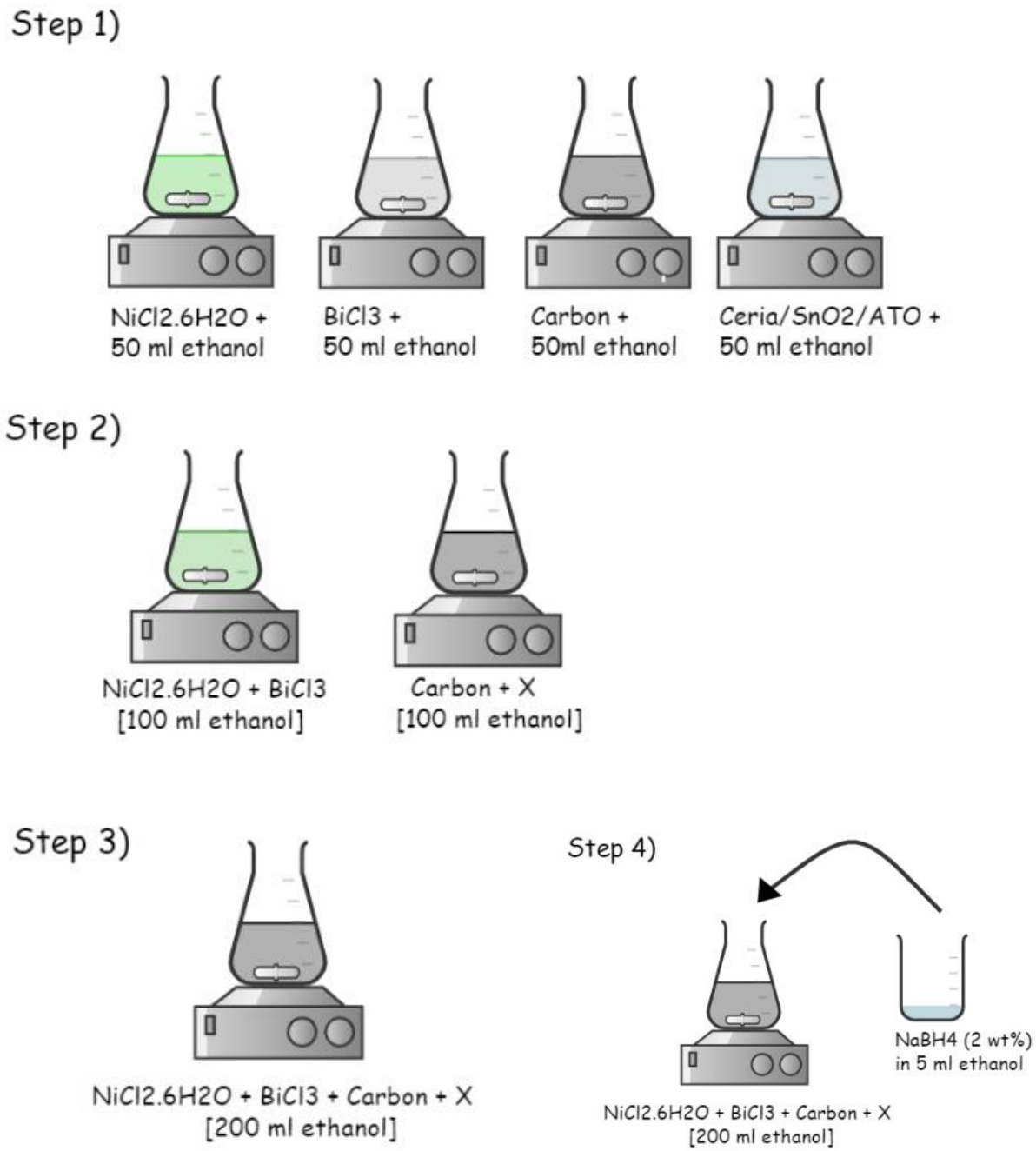

4.2.3 Electrochemical measurements:

The detailed procedure is reported in details elsewhere.[55] All tests were repeated more than three times and reproduced.

4.2.4 Continuous electrolysis measurements accompanied by HPLC:

The detailed technique was previously reported by Houache et al..[4]

4.3 Results and discussion

4.3.1 Electrochemical Characterizations of Ni/C-X and NiBi/C-X

Figures 4.1-4.6 show the CV, LSV and CA of various Ni-based catalysts Ni/C-X and NiBi/C-X [X= ceria, SnO_2 and ATO] used for GEOR. The current is normalized by the geometric area of the glassy carbon (GC) electrode (0.196 cm^2) resulting in current density (mA/cm^2). It would have been more ideal to normalize with the electrochemical active surface area (ECSA) as it gives a more accurate comparison between various metal electrodes of different sizes and surface areas. However, for nickel bimetallic electrodes the calculation of ECSA comes with so many uncertainties.[56]

Figures 4.1a and 4.2a show the cyclic voltammetry of Ni and bimetallic NiBi catalysts on different supports, Ni/C-X and NiBi/C-X [X= ceria, SnO_2 and ATO] in 1M KOH at a scan rate of 50mV/s. The higher intensity of the anode peak could indicate the presence of more active β-NiOOH species resulting in higher catalytic activity. As the first peak in the forward scan represents the anodic peak where β-$Ni(OH)_2$ is reversibly oxidized into β-NiOOH.[57,58] Among the Ni/C-X catalysts shown in Figure 4.1a, the highest anodic peak was observed by Ni/C-ATO at 1.40V whereas the lowest was observed by Ni/C-SnO2 at 1.44V. As bismuth is added to Ni/C-X catalysts, the Ni^{2+}/Ni^{3+} redox peak was intensified for all catalysts except NiBi/C-ATO. Additionally, NiBi/C-ceria exhibited the highest redox peak as illustrated in Figures 4.1 a and 4.2a. At potentials higher than 1.55V, oxygen evolution reaction (OER) is observed for all the catalysts. The onset potential of the redox peak Ni^{2+}/Ni^{3+} on Ni/C was the most negative at 1.35V followed by Ni/C-ATO<Ni/C-Ceria<Ni/C-SnO2 [Figure 4.1a]. Similarly, in the presence of bismuth NiBi/C exhibited the most negative onset potential of 1.34V as shown in Figure 4.2a.

The activity analysis of these catalysts in the presence of glycerol can be observed in Figures 4.1b and 4.2b. We can observe that GEOR takes place in the anodic region with the formation of β-NiOOH. The highest current density of 96$mA.cm^{-2}$ at 1.50V can be noticed with Ni/C-ATO > Ni/C (86$mA.cm^{-2}$ at 1.47V) > Ni/C-Ceria (77mA/cm^{-2} at 1.42V) > Ni/C-SnO_2 (52$mA.cm^{-2}$ at 1.46V), as shown in Figure 4.1b. However, as bismuth is added to these catalysts the order of the activity changes in the following order NiBi/C (104 $mA.cm^{-2}$ at 1.48V) > NiBi/C-Ceria (87.6 $mA.cm^{-2}$ at 1.40V) > NiBi/C-ATO (64.9 $mA.cm^{-2}$ at 1.51V) > NiBi/C-SnO_2 (60.2 $mA.cm^{-2}$ at 1.43V) as shown in Figure 4.2b.

Although Ni/C-ATO had the highest peak current density, its onset potential and anodic peak potential were relatively higher than other catalysts. The onset potential is the lowest with Ni/C catalyst at 1.28V and the highest at 1.38V in the presence of ATO as shown in Figure 4.1b. In the presence of bismuth, NiBi/C had the lowest onset potential of 1.29V and NiBi/C-ATO had the highest onset potential of 1.39V as demonstrated in Figure 4.2b.

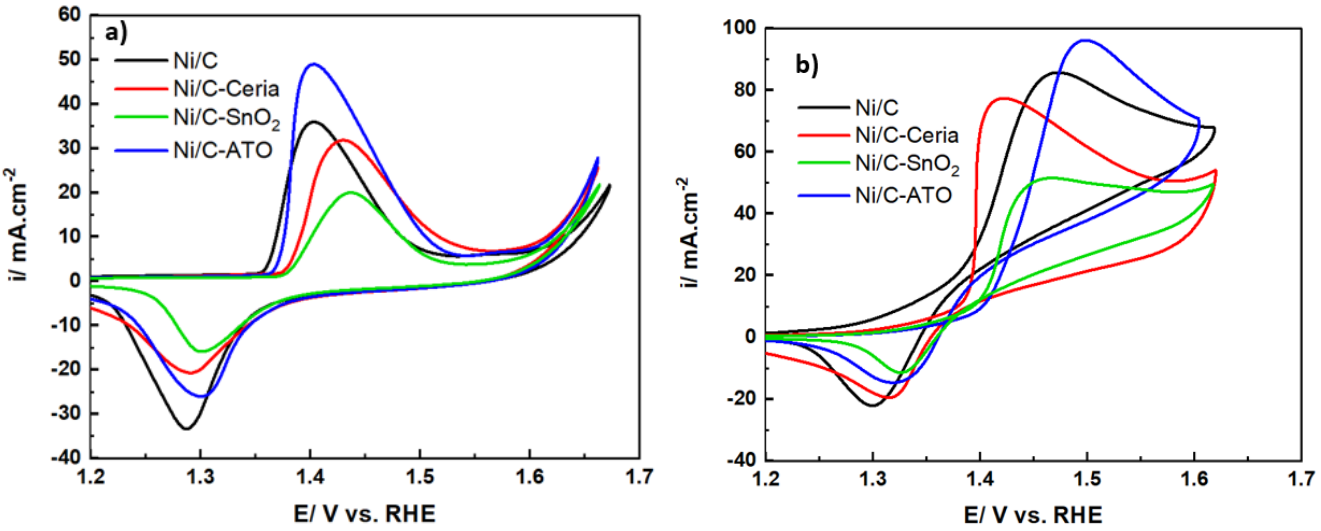

Figure 4.1. Cyclic Voltammograms of Ni/C-X [X=carbon, ceria, SnO_2 and ATO] performed in a) 1M KOH solution and b) 1M KOH + 0.1M glycerol solution at a scan rate of 50 $mV.s^{-1}$. [IR corrected]

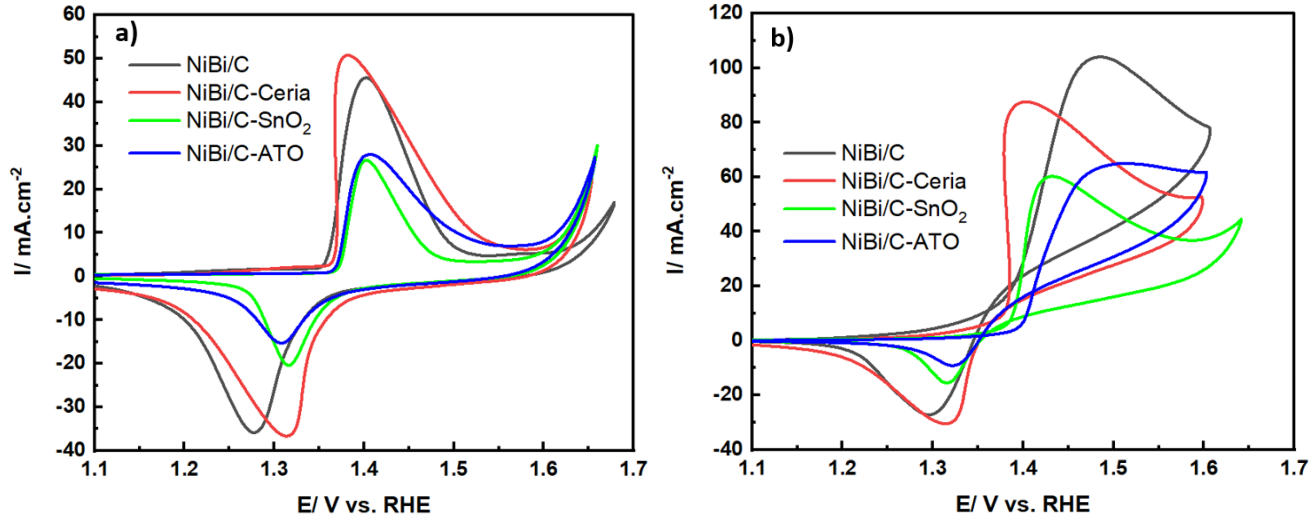

Figure 4.2. Cyclic Voltammograms of $Ni_{95}Bi_5$/C-X [X=carbon, ceria, SnO_2 and ATO] performed in a) 1M KOH solution and b) 1M KOH + 0.1M glycerol solution at a scan rate of 50 $mV.s^{-1}$. [IR corrected]

Figures 4.3 and 4.4 show the Linear sweep voltammetry (LSV) of these catalysts performed at a scan rate of 1mV/s. This method further proves that Ni/C and NiBi/C had the lowest onset potentials while Ni/C-ATO and NiBi/C-ATO had the highest. Figures

4.5a,b and 4.6a,b represent the chronoamperometry measurements carried out for 3600s at 1.40V and 1.44V. Initially, there is an increase in the current density followed by a rapid decline and stability after the first few 100 secs. When compared to LSVs (Figures 4.3 and 4.4) we observe a similar trend for each potential of 1.40V and 1.44V, where, the highest current density is observed with Ni/C and NiBi/C and lowest with Ni/C-ATO and NiBi/C-ATO. This further proves that Ni/C performs better than Ni/C-ATO at lower potentials of 1.40 and 1.44V.

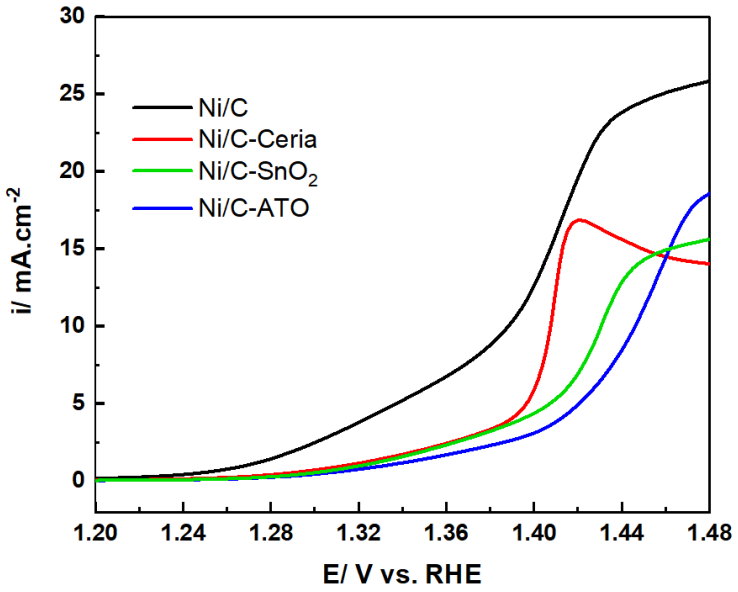

Figure 4.3. Linear sweep voltammetry (LSV) of Ni/C-X [X=carbon, ceria, SnO_2 and ATO] at $1mV.s^{-1}$. [IR corrected]

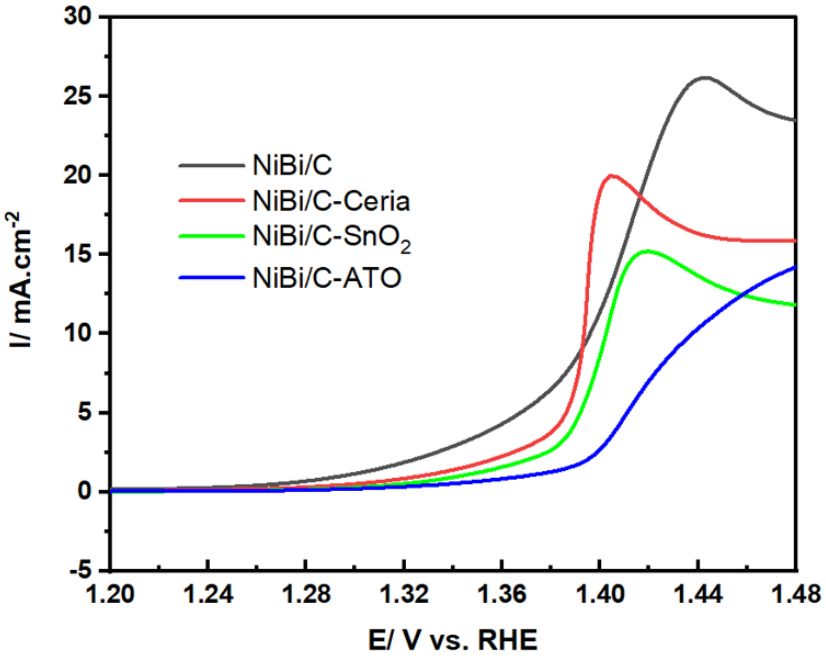

Figure 4.4. Linear sweep voltammetry (LSV) of $Ni_{95}Bi_5$/C-X [X=carbon, ceria, SnO_2 and ATO] at 1mV.s^{-1}. [IR corrected]

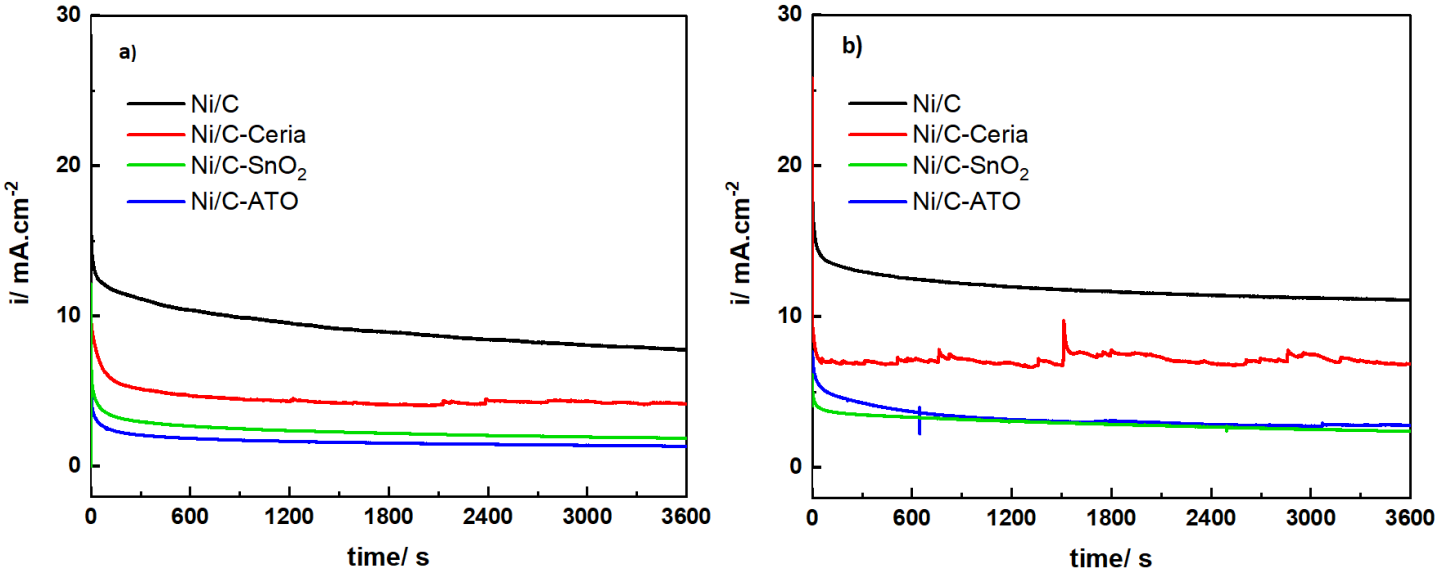

Figure 4.5. Chronoamperometry (CA) tests of Ni/C-X [X=carbon, ceria, SnO_2 and ATO] at potentials a) 1.40 and b) 1.44V vs RHE for 60 minutes.

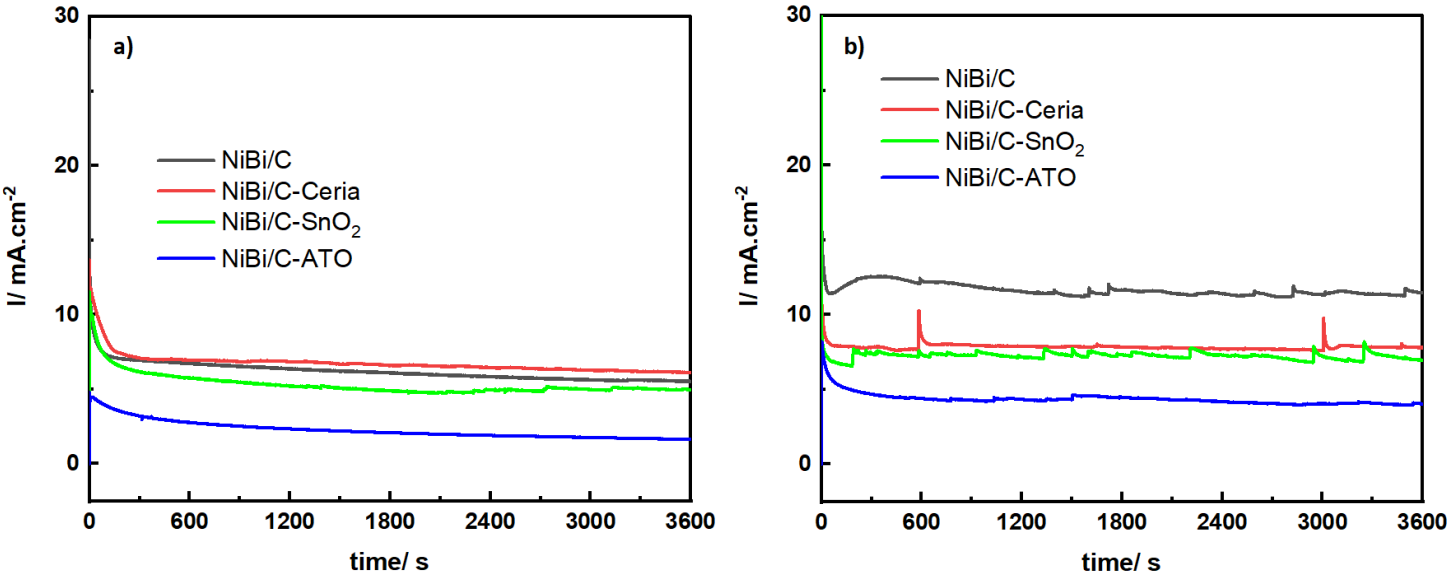

Figure 4.6. Chronoamperometry (CA) tests of $Ni_{95}Bi_5$/C-X [X=carbon, ceria, SnO_2 and ATO] at potentials a)1.40 and b)1.44V vs RHE for 60 minutes.

In conclusion, Ni- based catalysts on composites supports with metal oxides influenced the catalytic performance of the metal nanoparticles by altering the chemical properties of the metal nanoparticles.[59] Among the changes, the metal support interactions (MSI) exhibited between Ni and the reducible substrates CeO_2, SnO_2 and ATO could have blocked the reactivity by reducing the number of active sites.[59] There are two mechanisms proposed for this process of chemical alteration; i) nanoparticles are encapsulated by the substrate atoms and deactivated due to decoration of the NP structure with substrate atoms or ii) charge transfer from the substrate atoms to the metal NP's thus changing the NP electronic structure.[60–63] It can be assumed that the SnO_2 had the strongest metal support interactions with Ni thus the NP activity of nickel was largely hindered by the encapsulation of nickel into the SnO_2 substrate covering the active sites. However, doping SnO_2 with antimony resulted in an enhancement in electrical conductivity which resulted in the higher current density. [48] Additionally, bismuth enhanced the activity of all Ni- based catalysts except Ni/C-ATO as shown in the CVs demonstrated in Figure B1.

4.3.2 Continuous electrolysis in 25 cm^2 electrolysis cell accompanied by HPLC analysis

The catalysts Ni/C, NiBi/C, Ni/C-X and NiBi/C-X [X=ceria and ATO] were further studied in a 25 cm^2 membraneless electrolysis cell. Electrolytic tests are conducted at different applied potentials of 1.35 and 1.55 V and temperatures R.T and 50°C. Additionally, quantitative analysis of products in 1M KOH + 0.1M Glycerol are determined by HPLC analysis by collecting 0.6 ml of the electrolyte solution every hour. The calibration curves for C_3 (glycerate, tartronate and lactate), C_2 (glycolate and oxalate) and C_1 (formate) products are shown in supplementary information Figures B2-B4. Results indicate that the primary products on Ni/C-X and NiBi/C-X catalysts are glycerate and lactate while, for Ni/C and NiBi/C the primary products are glycerate and formate.

Figures 4.7 and 4.8 show the product distributions under different applied potentials (1.35V & 1.55V), temperatures (RT & 50°C) and times (30 min & 6 h) using HPLC technique for Ni and $Ni_{95}Bi_5$ supported on composite carbon-metal oxides mixture. Figure 4.9 shows the product distributions of carbon supported Ni and $Ni_{95}Bi_5$ with time at 1.35V and RT. The calibration curves of all products are shown in Figures B2-B4.

The selectivity of Ni/C compared to Ni/C-Ceria and Ni/C-ATO at 30 min were shown in Figure 4.7a, 4.8a and 4.9a. The different applied potentials and temperatures had minimal effects on selectivity changes of Ni/C-ceria and Ni/C-ATO. Evidently, the addition of Ceria and ATO to Ni/C immensely suppressed FA selectivity to <8% which remained constant at all conditions (Figures 4.7a and 4.8a). In addition, the selectivity towards GA and LA increased significantly in the presence of Ceria and ATO compared to Ni/C. As demonstrated in Figure 4.7a, with Ni/C-ceria the peak selectivity of GA and LA were 64% (1.35V, 50°C) and 31% (1.55V, RT), respectively. However, after 6 hours of electrolysis (Figure 4.7b), the selectivity towards LA decreases to ~12-17% and a consequent increase in GA selectivity to ~70%. Similarly, for Ni/C-ATO (Figures 4.8a and 4.9a), the selectivity to GA was 3x higher than that of Ni/C at 1.35V, R.T in 30 minutes and that of LA was ~30% more. However, after 6 hours of electrolysis, the selectivity to LA on Ni/C-ATO reduces to ~16-23% with a consequent increase in GA selectivity to ~65-72% as shown in Figure 4.8a. It is important to note that the selectivity towards GA and TA increases slightly with time for Ni/C-ceria and Ni/C-ATO in contrary to Ni/C, as shown in Figures 4.7b, 4.8b and 4.9a. It was observed that Ceria and ATO eliminated the

production of C_2 product GLA with an exception for Ni/C-ceria at 1.35V RT (Figures 4.7a,b, 4.8a,b and 4.9a).

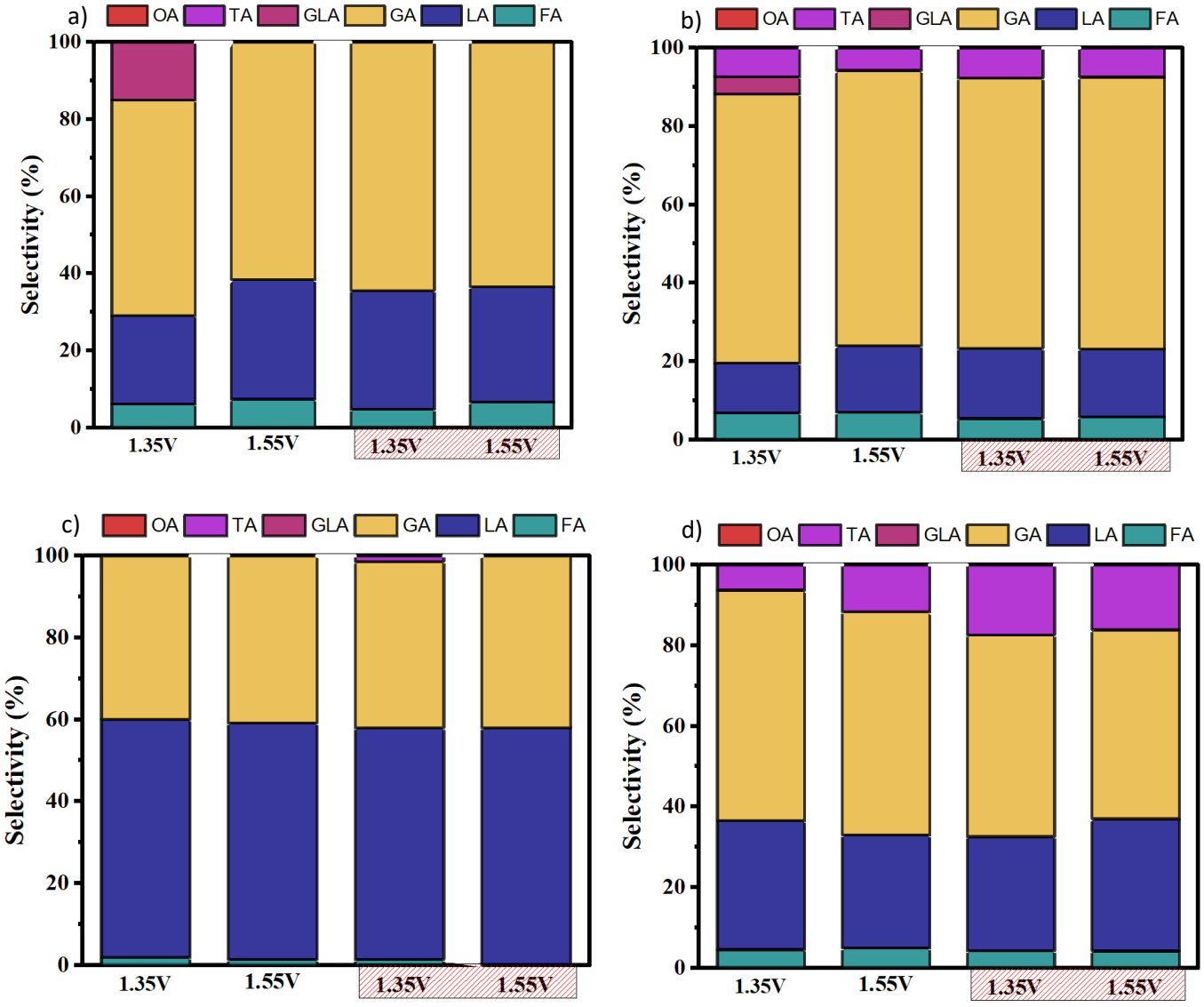

Figure 4.7: Product distributions at different applied potentials (1.35 and 1.55V) and temperatures (R.T and 50 °C) over (a,b) Ni/C-CeO_2 and (c,d) NiBi/C-CeO_2 in 1M KOH and 0.1M glycerol. The figures on the left-hand side are product distributions after 30 minutes of electrolysis, while the right-hand side are after 6 hours. red: oxalate, purple: tartronate, pink: glycolate, yellow: glycerate, blue: lactate and green: formate. The red-shaded region represents a temperature of 50 °C

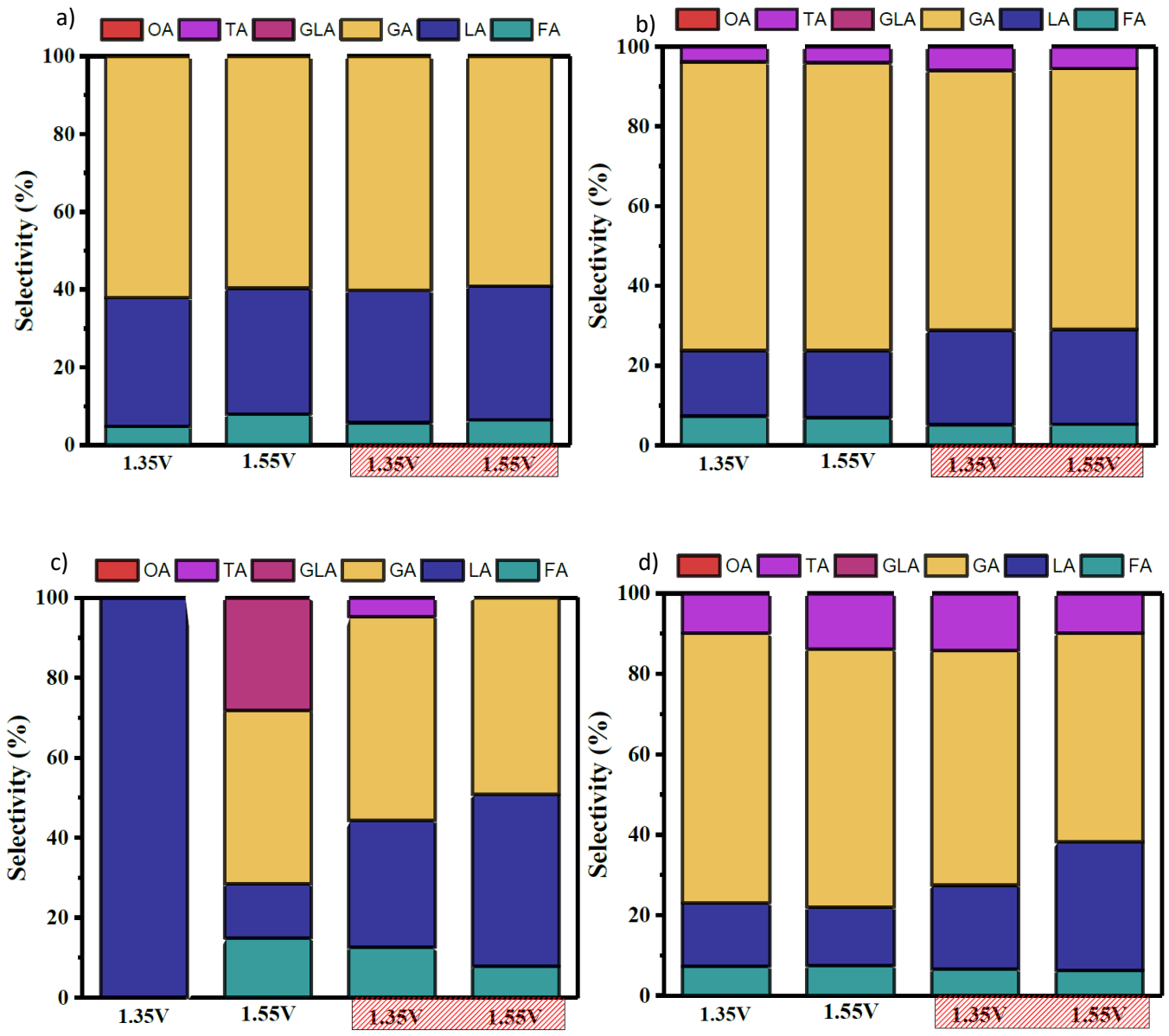

Figure 4.8: Product distributions at different applied potentials (1.35 and 1.55V) and temperatures (R.T and 50 °C) over (a,b) Ni/C-ATO and (c,d) NiBi/C-ATO in 1M KOH and 0.1M glycerol. The figures on the left-hand side are product distributions after 30 minutes of electrolysis, while the right-hand side are after 6 hours. red: oxalate, purple: tartronate, pink: glycolate, yellow: glycerate, blue: lactate and green: formate. The red-shaded region represents a temperature of 50 °C

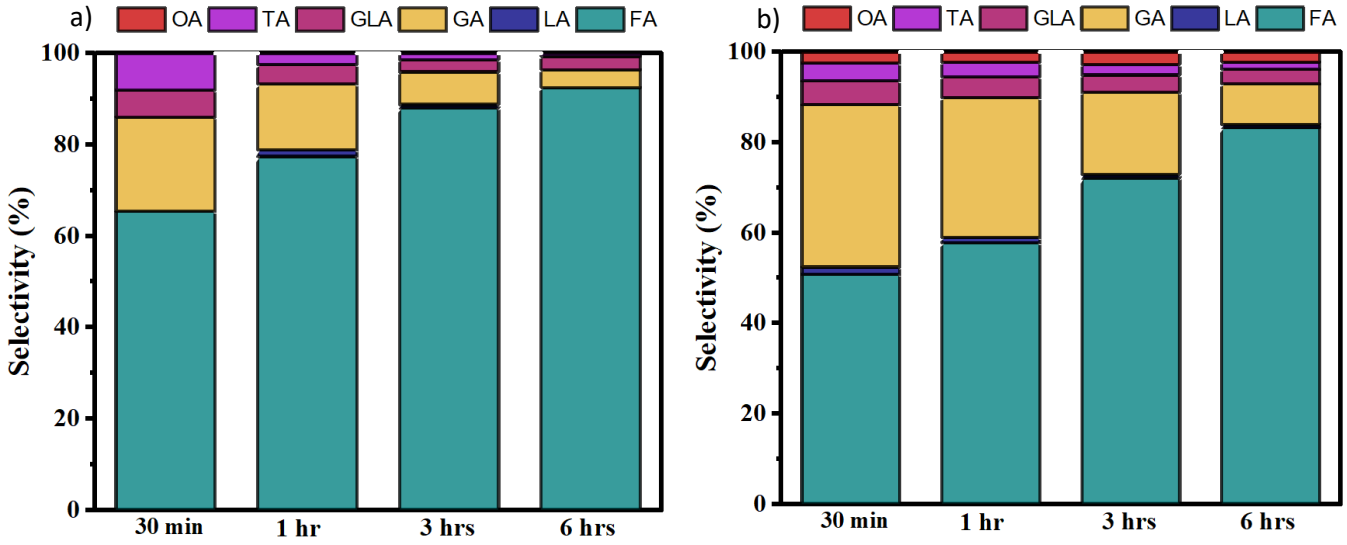

Figure 4.9: Product distributions of a) Ni/C and b) NiBi/C with time at fixed applied potential and temperature of 1.35V and R.T. red: oxalate, purple: tartronate, pink: glycolate, yellow: glycerate, blue: lactate and green: formate.

As seen in Figure 4.9a,b, addition of Bi to Ni/C decreased the overall FA selectivity by 10%-15%, however its GA selectivity increases 2x following a similar trend with time. Further reduction of FA selectivity is observed with the addition of Ceria and ATO to NiBi/C by 45-50% at 30 mins and 75% at 6hrs, as shown in Figures 4.7c,d, 4.8c,d & 4.9b.

The selectivity comparison of NiBi/C-Ceria and Ni/C-Ceria are shown in Figure 4.7. At 30 mins, a high selectivity of LA approximately 60% was observed with NiBi/C-ceria at all conditions, which is approximately 2x that of Ni/C-Ceria. At 6hrs the production of GA increased, while the selectivity of LA reduced to almost half, compared to that at 30mins for NiBi/C-Ceria as shown in Figures 4.7 c,d. We also observe a significant increase in the selectivity towards TA as the electrolysis proceeds with the peak at 17.32% at 1.35V 50C for NiBi/C-Ceria. These observations confirm that time plays a crucial role in the product distributions of TA, GA & LA. The selectivity of GA is much higher for Ni/C-Ceria> NiBi/C-Ceria at all conditions, whereas for LA it's the opposite. Based on the above HPLC results and observation we can see that the addition of Bi to just Ni/C favors the formation of C_3 products. Additionally, the presence of Ceria in both the catalysts hinders the breakage of C-C bond in glycerol resulting in a better selectivity towards C_3 products.

The addition of Bismuth to Ni/C-ATO altered the product distributions of Ni/C-ATO as shown in Figure 4.8. Similar to Ni/C-ATO, NiBi/C-ATO shows highest selectivity

to GA and LA. Initially, GA and LA are the primary products observed and with time the selectivity to GA increases consequently, LA selectivity reduces. However, a special observation with NiBi/C-ATO is observed at 1.35V, R.T and 30 minutes of electrolysis, the selectivity to LA is largely enhanced to 100% in the presence of bismuth (Figure 4.8c). However, at other conditions the selectivity of LA is comparable to that of Ni/C-ATO (Figure 4.8). Additionally, the presence of bismuth to Ni/C-ATO resulted in an initial 2x enhancement to FA selectivity at higher potential 1.55V and temperature 50C at 30 minutes as shown in Figure 4.8c. However, the selectivity of FA reduces with time to <7% as shown in Figure 4.8d. Observably, the selectivity to TA is highly enhanced at 6 hours by 2x in the presence of bismuth as shown in Figure 4.8b,d. The highest TA selectivity (10-14%) is observed with NiBi/C-ATO after 6 hours of electrolysis as shown in Figure 4.8d. However, the selectivity to GA after 6 hours of electrolysis is ~ 8% less in the presence of bismuth NiBi/C-ATO as demonstrated in Figure 4.8b,d.

The proposed reaction mechanism of NiBi/C-X [X=ceria, SnO_2 and ATO] is shown in Figure 4.10. Initially, glycerol is oxidized into glyceraldehyde which is an unstable molecule in alkaline medium. Next, the reactions are either metal-catalyzed forming C_3 (glycerate and tartronate), C_2 (glycolate) and C_1 (formate) products or it goes through base catalyzed dehydration forming lactate. In summary, as ceria and ATO are added to Ni/C and NiBi/C, the pathway that leads to formate and glycolate is significantly hindered resulting in higher selectivity to C_3 products [glycerate, lactate and tartronate] at all applied potentials and temperatures. Compared to other platinum and non-platinum group metals reported in literature, our catalysts had the highest selectivity to C_3 products glycerate and lactate as shown in Table 4.1.

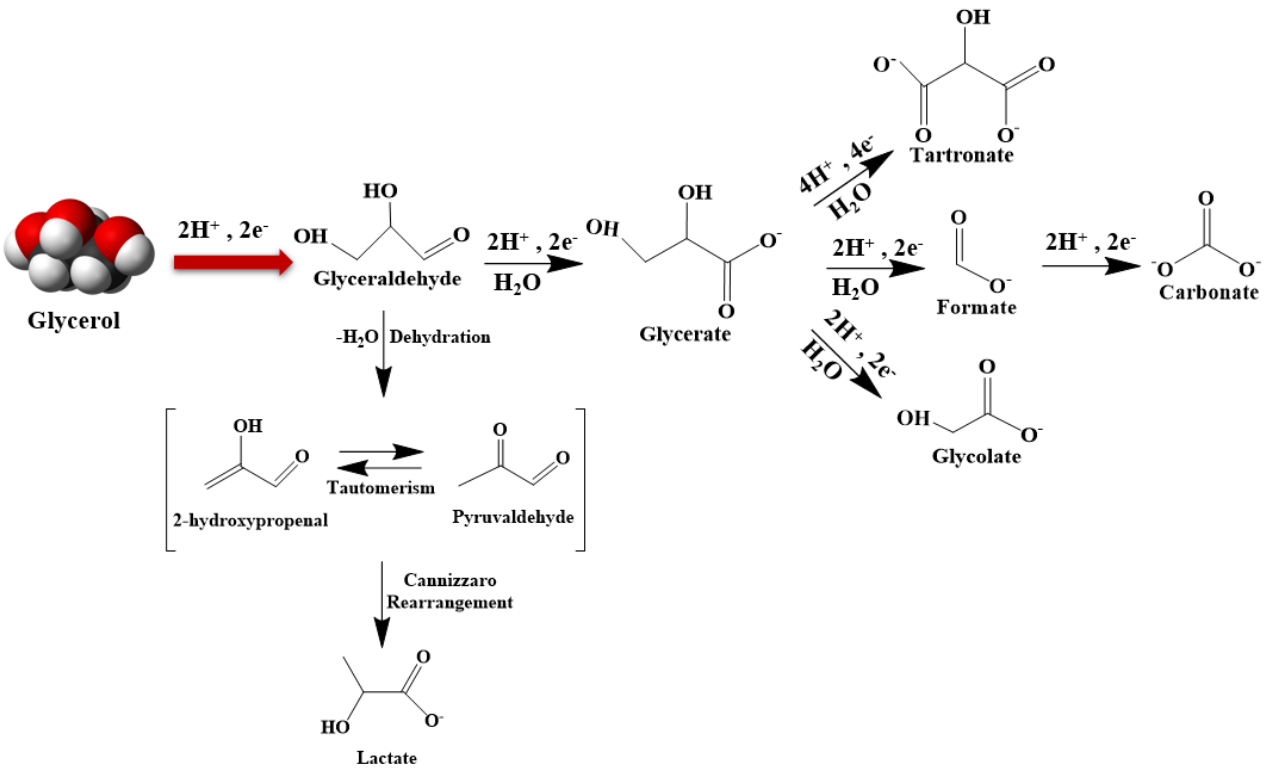

Figure 4.10: The proposed reaction mechanism of Nickel catalyst on carbon supports mixed with metal oxides

Conclusion

In this work, Ni/C-X and $Ni_{95}Bi_5$/C-X [X= CeO_2, ATO and SnO_2] were synthesized for glycerol electrooxidation reaction (GEOR) in 1.0M KOH and 0.1M glycerol electrolyte. Based on electrochemical tests, Ni/C and $Ni_{95}Bi_5$/C exhibited the lowest onset potentials of ~1.30 V vs. RHE. However, Ni/C-ATO showed the highest peak current density of 96 $mA.cm^{-2}$ at higher potential of 1.50V vs. RHE compared to other Ni/C-X catalysts. Addition of bismuth showed an enhancement in electrochemical performance of Ni/C-X catalysts except for Ni/C-ATO. Moreover, the addition of 10 wt% CeO_2 and ATO showed an enhancement in selectivity to glyceric acid (GA) and lactic acid (LA). Particularly, 100% selectivity to LA is achieved with $Ni_{95}Bi_5$/C-ATO catalyst at 1.35V, R.T and 30 minutes of electrolysis. The peak amount of GA achieved was ~72% with Ni/C-ATO catalyst at mild conditions 1.35V, R.T and after 6 hours of electrolysis. Based on our results, the addition of metal oxides largely hindered C-C bonds cleavage leading to higher selectivity to C_3 products (GA, LA and TA) and consequently, lower formation of C_1 product formic acid (FA), Furthermore, a comparison between platinum group metal (Pt/C, Pd/CNT, and Au/C) and non-platinum group metals reported in literature showed that NiBi/C-X catalysts reported in this work achieved the highest selectivity to GA and LA.

Table 4.1: Comparison with other non-platinum and platinum catalysts reported in literature

Catalyst	Synthesis technique	Conditions	Products	Ref.
Ni/C-CeO_2	NaBH4 reduction method	CA 1.35 V, 30 min [0.1 M glycerol + 1.0 M KOH]	GA:55.84%; LA: 22.95%; GLA:15.02%; FA: 6.29%	This research paper
$Ni_{95}Bi_5$/C-CeO_2			LA: 58.15%; GA: 39.9%; FA: 1.95%	
Ni/C-ATO			GA: 66.11%; LA: 33.06%; FA: 4.82%	
$Ni_{95}Bi_5$/C-ATO			LA: ~100%	
Spherical Ni		CA 1.4 V, 30 min [0.1 M glycerol + 1.0 M KOH]	FA: 56.5% ; GA: 35.3% ; GLA: 4.75% ; LA: 2% ; TA: 0.85% ; OA: 0.6%	[4]
$Ni_{90}Bi_{10}$			FA: 45.8% ; GA: 36.3% ; TA: 7.9% ; OA: 3.3%; GLA: 4.5%; LA: 2.1% ;	
$Ni_{90}Bi_{10}$ after aging			FA : 40.97%; GA: 37.5% ; TA: 8.2% ; OA: 5.5% ; GLA: 5.4%; LA: 2.5%;	
Ni/C	Impregnation/ reduction method	CA 1.6V vs. RHE, 8hrs [0.1 M glycerol + 1.0 M NaOH]	GLA: 11.5%; FA: 32.2%; GA: 0.5mM	[34]
NiFe/C			GLA: 3.7%; FA: 4%; GA: 0.1mM	
NiCo/C			GLA: 4.5%; FA: 7.5%; GA: 0.25mM	
NiFeCo/C			GLA: 10.3%; FA: 34.1%; GA: 0.2mM	
CuO	Precipitation reaction with NaOH at 60°C	CA 1.29 V vs. RHE, 1hr [0.1 M glycerol + 0.1 M NaOH]	FA: 70%; GA: 20%; DHA: 5%	[64]

Pt/C	Modified polyol method with ethylene glycol	CA – 1.1 V vs. SHE, 7h, 60 °C [2 M glycerol + 0.5 M H2SO4]	GLAD: 42.1%; GA: 57.8%; GLA: 0.5%	[65]
Pd/CNT	Modified aqueous-phase reduction method	CA – 0.1 V vs. SHE, 2h, 50 °C [1 M glycerol + 4 M KOH]	GA: 21.7% ; GLA: 8.5% ; OA: 25.3% ; TA: 39.5% ; MESOXA: 3.8% ; LA: 1.2%	[66]
Au/C	Modified solution-Phase based nanocapsule method	CA -0.35 V vs. RHE, 1hr [1 M glycerol + 2 M KOH]	GA: 15%; TA: 80%; OA: 5%	[67]

Abbreviations: DHA: dihydroxyacetone; GLAD: glyceraldehyde; GLA: glycolic acid; GA: glyceric acid; OA: oxalic acid; TA: tartronic acid; LA: lactic acid; MESOXA: mesooxalic acid; FA: formic acid.

4.4 **References**

[1] S.S. Yazdani, R. Gonzalez, Anaerobic fermentation of glycerol: a path to economic viability for the biofuels industry, Curr. Opin. Biotechnol. 18 (2007) 213–219. https://doi.org/10.1016/j.copbio.2007.05.002.

[2] R. Ciriminna, C. della Pina, M. Rossi, M. Pagliaro, Understanding the Glycerol Market, Eur. J. Lipid Sci. Technol. 116 (2014) 1432–1439.

[3] A.A. Abdul Raman, H.W. Tan, A. Buthiyappan, Two-Step Purification of Glycerol as a Value Added by Product From the Biodiesel Production Process, Front. Chem. 7 (2019) 1–9. https://doi.org/10.3389/fchem.2019.00774.

[4] M.S.E. Houache, K. Hughes, R. Safari, G.A. Botton, E.A. Baranova, Modification of Nickel Surfaces by Bismuth: Effect on Electrochemical Activity and Selectivity Towards Glycerol Modification of Nickel Surfaces by Bismuth : Effect on Electrochemical Activity and Selectivity Towards Glycerol, ACS Appl. Mater. Interfaces. 12 (2020) 15095–15107. https://doi.org/10.1021/acsami.9b22378.

[5] M.S.E. Houache, K. Hughes, E.A. Baranova, Study on catalyst selection for electrochemical valorization of glycerol, Sustain. Energy Fuels. 3 (2019) 1892–1915. https://doi.org/10.1039/c9se00108e.

[6] Y.C. Lin, Catalytic valorization of glycerol to hydrogen and syngas, Int. J. Hydrogen Energy. 38 (2013) 2678–2700. https://doi.org/10.1016/j.ijhydene.2012.12.079.

[7] V.R. Ruiz, A. Velty, L.L. Santos, A. Leyva-Pérez, M.J. Sabater, S. Iborra, A. Corma, Gold catalysts and solid catalysts for biomass transformations: Valorization of glycerol and glycerol-water mixtures through formation of cyclic acetals, J. Catal. 271 (2010) 351–357. https://doi.org/10.1016/j.jcat.2010.02.023.

[8] P.F.F. Amaral, T.F. Ferreira, G.C. Fontes, M.A.Z. Coelho, Glycerol valorization: New biotechnological routes, Food Bioprod. Process. 87 (2009) 179–186. https://doi.org/10.1016/j.fbp.2009.03.008.

[9] P.A. Alaba, C.S. Lee, F. Abnisa, M.K. Aroua, A review of recent progress on electrocatalysts toward efficient glycerol electrooxidation, Rev Chem Eng. (2020).

[10] W. Chen, Y. Zhou, Y. Shen, Product Distribution of Glycerol Electro-oxidation over Platinum-Ceria/Graphene Nanosheet, Electrochemistry. 87 (2018) 30–34.

[11] S. Carrettin, P. Mcmorn, P. Johnston, K. Griffin, J. Kiely, G.J. Hutchings, Oxidation of glycerol using supported Pt , Pd and Au catalysts, Phys. Chem. Chem. Phys. 5 (2003) 1329–1336. https://doi.org/10.1039/b212047j.

[12] S. Lee, H. Ju, S. Mook, M. Ho, W. Bae, Applied Catalysis A : General The promotional effect of Ni on bimetallic PtNi / C catalysts for glycerol electrooxidation, "Applied Catal. A, Gen. 429–430 (2012) 39–47. https://doi.org/10.1016/j.apcata.2012.04.002.

[13] Y. Kwon, K.J.P. Schouten, M.T.M. Koper, Mechanism of the Catalytic Oxidation

of Glycerol on Polycrystalline Gold and Platinum Electrodes, ChemCatChem. 3 (2011) 1176–1185. https://doi.org/10.1002/cctc.201100023.

[14] J.H. Zhang, Y.J. Liang, N. Li, Z.Y. Li, C.W. Xu, S.P. Jiang, A remarkable activity of glycerol electrooxidation on gold in alkaline medium, Electrochim. Acta. 59 (2012) 156–159. https://doi.org/10.1016/j.electacta.2011.10.048.

[15] C. Xu, S. Xie, S. Chen, Z. Liu, Comparison of Alcohol Electrooxidation on Pt and Pd Electrodes in Alkaline Medium, Int. J. Electrochem. Sci. 6 (2011) 882.

[16] Y. Holade, C. Morais, S. Arrii-Clacens, K. Servat, T.W. Napporn, K.B. Kokoh, New Preparation of PdNi/C and PdAg/C Nanocatalysts for Glycerol Electrooxidation in Alkaline Medium, Electrocatalysis. 4 (2013) 167–178. https://doi.org/10.1007/s12678-013-0138-1.

[17] G.A.B. Mello, C. Busó-Rogero, E. Herrero, J.M. Feliu, Glycerol electrooxidation on Pd modified Au surfaces in alkaline media: Effect of the deposition method, J. Chem. Phys. 150 (2019). https://doi.org/10.1063/1.5048489.

[18] L. Xin, Z. Zhang, Z. Wang, W. Li, Simultaneous Generation of Mesoxalic Acid and Electricity from Glycerol on a Gold Anode Catalyst in Anion-Exchange Membrane Fuel Cells, ChemCatChem. 4 (2012) 1105–1114. https://doi.org/10.1002/cctc.201200017.

[19] E. Habibi, H. Razmi, Glycerol electrooxidation on Pd, Pt and Au nanoparticles supported on carbon ceramic electrode in alkaline media, Int. J. Hydrogen Energy. 37 (2012) 16800–16809. https://doi.org/10.1016/j.ijhydene.2012.08.127.

[20] M.S.E. Houache, K. Hughes, E.A. Baranova, Study on catalyst selection for electrochemical valorization of glycerol, Sustain. Energy Fuels. 3 (2019) 1892–1915. https://doi.org/10.1039/c9se00108e.

[21] M.D. Bohon, B.A. Metzger, W.P. Linak, C.J. King, W.L. Roberts, Glycerol combustion and emissions, Proc. Combust. Inst. 33 (2011) 2717–2724. https://doi.org/10.1016/j.proci.2010.06.154.

[22] M.C. Figueiredo, R.M. Arán-ais, J.M. Feliu, K. Kontturi, T. Kallio, Pt catalysts modified with Bi : Enhancement of the catalytic activity for alcohol oxidation in alkaline media, J. Catal. 312 (2014) 78–86. https://doi.org/10.1016/j.jcat.2014.01.010.

[23] A. Zalineeva, A. Serov, M. Padilla, U. Martinez, K. Artyushkova, S. Baranton, C. Coutanceau, P. Atanassov, Self-Supported PdxBi Catalysts for the Electrooxidation of Glycerol in Alkaline Media, J. Am. Chem. Soc. 136 (2014) 3937–3945. https://doi.org/10.1021/ja412429f.

[24] Y. Kwon, T.J.P. Hersbach, M.T.M. Koper, Electro-Oxidation of Glycerol on Platinum Modified by Adatoms: Activity and Selectivity Effects, Top. Catal. 57 (2014) 1272–1276. https://doi.org/10.1007/s11244-014-0292-6.

[25] T. Gunji, T. Tanabe, A.J. Jeevagan, S. Usui, T. Tsuda, S. Kaneko, G. Saravanan, H. Abe, F. Matsumoto, Facile route for the preparation of ordered intermetallic Pt3Pb-PtPb core-shell nanoparticles and its enhanced activity for alkaline methanol and

ethanol oxidation, J. Power Sources. 273 (2015) 990–998. https://doi.org/10.1016/j.jpowsour.2014.09.182.

[26] X. Ning, Y. Li, H. Yu, F. Peng, H. Wang, Y. Yang, Promoting role of bismuth and antimony on Pt catalysts for the selective oxidation of glycerol to dihydroxyacetone, J. Catal. 335 (2016) 95–104. https://doi.org/10.1016/j.jcat.2015.12.020.

[27] J.F. Gomes, A.C. Garcia, L.H.S. Gasparotto, N.E. De Souza, E.B. Ferreira, C. Pires, G. Tremiliosi-Filho, Influence of silver on the glycerol electro-oxidation over AuAg/C catalysts in alkaline medium: A cyclic voltammetry and in situ FTIR spectroscopy study, Electrochim. Acta. 144 (2014) 361–368. https://doi.org/10.1016/j.electacta.2014.08.035.

[28] Y. Holade, C. Morais, K. Servat, T.W. Napporn, K.B. Kokoh, Toward the electrochemical valorization of glycerol: Fourier transform infrared spectroscopic and chromatographic studies, ACS Catal. 3 (2013) 2403–2411. https://doi.org/10.1021/cs400559d.

[29] Y. Zhou, Y. Shen, J. Xi, X. Luo, Selective Electro-Oxidation of Glycerol to Dihydroxyacetone by PtAg Skeletons, ACS Appl. Mater. Interfaces. 11 (2019) 28953–28959. https://doi.org/10.1021/acsami.9b09431.

[30] H. Kimura, K. Tsuto, T. Wakisaka, Y. Kazumi, Y. Inaya, Selective oxidation of glycerol on a platinum-bismuth catalyst, Appl. Catal. A, Gen. 96 (1993) 217–228. https://doi.org/10.1016/0926-860X(90)80011-3.

[31] B. Habibi, N. Delnavaz, Electrooxidation of glycerol on nickel and nickel alloy (Ni-Cu and Ni-Co) nanoparticles in alkaline media, RSC Adv. 6 (2016) 31797–31806. https://doi.org/10.1039/c5ra26006j.

[32] L.L. Carvalho, F. Colmati, A.A. Tanaka, Nickel–palladium electrocatalysts for methanol, ethanol, and glycerol oxidation reactions, Int. J. Hydrogen Energy. 42 (2017) 16118–16126. https://doi.org/10.1016/j.ijhydene.2017.05.124.

[33] V.L. Oliveira, C. Morais, K. Servat, T.W. Napporn, G. Tremiliosi-Filho, K.B. Kokoh, Glycerol oxidation on nickel based nanocatalysts in alkaline medium - Identification of the reaction products, J. Electroanal. Chem. 703 (2013) 56–62. https://doi.org/10.1016/j.jelechem.2013.05.021.

[34] V.L. Oliveira, C. Morais, K. Servat, T.W. Napporn, G. Tremiliosi-Filho, K.B. Kokoh, Studies of the reaction products resulted from glycerol electrooxidation on Ni-based materials in alkaline medium, Electrochim. Acta. 117 (2014) 255–262. https://doi.org/10.1016/j.electacta.2013.11.127.

[35] L. Shabnam, S.N. Faisal, A.K. Roy, V.G. Gomes, Nickel-Nanoparticles on Doped Graphene: A Highly Active Electrocatalyst for Alcohol and Carbohydrate Electrooxidation for Energy Production, ChemElectroChem. 5 (2018) 3799–3808. https://doi.org/10.1002/celc.201800818.

[36] F. Bidault, D.J.L. Brett, P.H. Middleton, N. Abson, N.P. Brandon, A new application for nickel foam in alkaline fuel cells, Int. J. Hydrogen Energy. (2009). https://doi.org/10.1016/j.ijhydene.2009.06.035.

[37] X. Jin, M. Zhao, C. Zeng, W. Yan, Z. Song, P.S. Thapa, B. Subramaniam, R. V Chaudhari, Oxidation of Glycerol to Dicarboxylic Acids Using Cobalt Catalysts, ACS Catal. 6 (2016) 4576–4583. https://doi.org/10.1021/acscatal.6b00961.

[38] M.S.E. Houache, E. Cossar, S. Ntais, E.A. Baranova, Electrochemical modification of nickel surfaces for efficient glycerol electrooxidation, J. Power Sources. 375 (2018) 310–319. https://doi.org/10.1016/j.jpowsour.2017.08.089.

[39] B. Habibi, N. Delnavaz, Electrooxidation of glycerol on nickel and nickel alloy (Ni-Cu and Ni-Co) nanoparticles in alkaline media, RSC Adv. 6 (2016) 31797–31806. https://doi.org/10.1039/c5ra26006j.

[40] L.L. Carvalho, F. Colmati, A.A. Tanaka, Nickel-palladium electrocatalysts for methanol , ethanol , and glycerol oxidation reactions, Int. J. Hydrogen Energy. 42 (2017) 16118–16126. https://doi.org/10.1016/j.ijhydene.2017.05.124.

[41] M.S.E. Houache, K. Hughes, A. Ahmed, R. Safari, H. Liu, G.A. Botton, E.A. Baranova, Electrochemical Valorization of Glycerol on Ni-Rich Bimetallic NiPd Nanoparticles: Insight into Product Selectivity Using in Situ Polarization Modulation Infrared-Re fl ection Absorption Spectroscopy, ACS Sustain. Chem. Eng. 7 (2019) 14425–14434. https://doi.org/10.1021/acssuschemeng.9b01070.

[42] N.A. Tapan, U.B. Cacan, D. Varisli, Ceria based nano-composite synthesis for direct alcohol fuel cells, Int. J. Electrochem. Sci. 9 (2014) 4440–4464.

[43] R.R. Adzic, Electrooxidation of Methanol at SnO, Mater. Sci. 24 (2012) 291–297.

[44] A.S. Pushkarev, I. V. Pushkareva, N.A. Ivanova, S.P. Du Preez, D. Bessarabov, R.G. Chumakov, V.G. Stankevich, V.N. Fateev, A.A. Evdokimov, S.A. Grigoriev, Pt/c and pt/snox/c catalysts for ethanol electrooxidation: Rotating disk electrode study, Catalysts. 9 (2019). https://doi.org/10.3390/catal9030271.

[45] J.M. Anderson, J. Patel, A.S. Karakoti, N. Greeneltch, D.J. Díaz, S. Seal, Aging effects of nanoscale ceria in ceria-platinum composite electrodes for direct alcohol electro-oxidation, Electrochim. Acta. 56 (2011) 2541–2545. https://doi.org/10.1016/j.electacta.2010.11.061.

[46] S. Geiger, O. Kasian, A.M. Mingers, K.J.J. Mayrhofer, S. Cherevko, Stability limits of tin-based electrocatalyst supports, Sci. Rep. 7 (2017) 3–9. https://doi.org/10.1038/s41598-017-04079-9.

[47] D.J. Guo, Electrooxidation of ethanol on novel multi-walled carbon nanotube supported platinum-antimony tin oxide nanoparticle catalysts, J. Power Sources. 196 (2011) 679–682. https://doi.org/10.1016/j.jpowsour.2010.07.075.

[48] E. Fabbri, A. Rabis, R. Kötz, T.J. Schmidt, Pt nanoparticles supported on Sb-doped SnO2 porous structures: Developments and issues, Phys. Chem. Chem. Phys. 16 (2014) 13672–13681. https://doi.org/10.1039/c4cp00238e.

[49] F. Liang, H. Tian, M. Jia, J. Hu, Pt nanoparticles ion-implanted onto indium tin oxide electrodes and their electrocatalytic activity towards methanol, J. Power Sources. 225 (2013) 9–12. https://doi.org/10.1016/j.jpowsour.2012.09.093.

[50] I.-S. Park, E. Lee, A. Manthiram, Electrocatalytic Properties of Indium Tin Oxide-Supported Pt Nanoparticles for Methanol Electro-oxidation, J. Electrochem. Soc. 157 (2010) B251–B255. https://doi.org/10.1149/1.3268126.

[51] H. Chen, Z. Sun, X. Liu, A. Han, P. Du, Cobalt-Salen Complexes as Catalyst Precursors for Electrocatalytic Water Oxidation at Low Overpotential, J. Phys. Chem. C. 119 (2015) 8998–9004. https://doi.org/10.1021/jp511584z.

[52] C.K.T. Chew, C. Salcianu, P. Bishop, C.J. Carmalt, I.P. Parkin, Functional thin film coatings incorporating gold nanoparticles in a transparent conducting fluorine doped tin oxide matrix, J. Mater. Chem. C. 3 (2015) 1118–1125. https://doi.org/10.1039/c4tc02275k.

[53] H.S. Oh, H.N. Nong, P. Strasser, Preparation of mesoporous Sb-, F-, and in-doped SnO2 bulk powder with high surface area for use as catalyst supports in electrolytic cells, Adv. Funct. Mater. 25 (2015) 1074–1081. https://doi.org/10.1002/adfm.201401919.

[54] C. Xu, K.S. Pei, Novel Pt/CeO2/C catalysts for electrooxidation of alcohols in alkaline media, Chem. Commun. (2004) 2238–2239. https://doi.org/10.1039/b408589b.

[55] M. Houache, K. Hughes, Electrochemical Valorization of Glycerol on Ni-rich Bimetallic NiPd Nanoparticles: Insight into product selectivity using in-situ PM-IRRAS, ACS Sustain. Chem. Eng. 17 (2019) 14425–14434. https://doi.org/10.1021/acssuschemeng.9b01070.

[56] E. Cossar, M.S.E. Houache, Z. Zhang, E.A. Baranova, Comparison of electrochemical active surface area methods for various nickel nanostructures, J. Electroanal. Chem. 20 (2020) 114246. https://doi.org/10.1016/j.jelechem.2020.114246.

[57] M. Alsabet, M. Grdeń, G. Jerkiewicz, Electrochemical Growth of Surface Oxides on Nickel. Part 3: Formation of β-NiOOH in Relation to the Polarization Potential, Polarization Time, and Temperature, Electrocatalysis. 6 (2014) 60–71. https://doi.org/10.1007/s12678-014-0214-1.

[58] S.L. Medway, C.A. Lucas, A. Kowal, R.J. Nichols, D. Johnson, In situ studies of the oxidation of nickel electrodes in alkaline solution, J. Electroanal. Chem. 587 (2006) 172–181. https://doi.org/10.1016/j.jelechem.2005.11.013.

[59] M. Ahmadi, H. Mistry, B. Roldan Cuenya, Tailoring the Catalytic Properties of Metal Nanoparticles via Support Interactions, J. Phys. Chem. Lett. 7 (2016) 3519–3533. https://doi.org/10.1021/acs.jpclett.6b01198.

[60] A. Bruix, J.A. Rodriguez, P.J. Ramírez, S.D. Senanayake, J. Evans, J.B. Park, D. Stacchiola, P. Liu, J. Hrbek, F. Illas, A new type of strong metal-support interaction and the production of H 2 through the transformation of water on Pt/CeO 2(111) and Pt/CeO x/TiO 2(110) catalysts, J. Am. Chem. Soc. 134 (2012) 8968–8974. https://doi.org/10.1021/ja302070k.

[61] W. Jochum, D. Eder, G. Kaltenhauser, R. Kramer, Impedance measurements in

catalysis: Charge transfer in titania supported noble metal catalysts, Top. Catal. 46 (2007) 49–55. https://doi.org/10.1007/s11244-007-0314-8.

[62] O. Dulub, W. Hebenstreit, U. Diebold, Imaging cluster surfaces with atomic resolution: The strong metal-support interaction state of pt supported on TiO2(110), Phys. Rev. Lett. 84 (2000) 3646–3649. https://doi.org/10.1103/PhysRevLett.84.3646.

[63] Q. Fu, T. Wagner, Interaction of nanostructured metal overlayers with oxide surfaces, Surf. Sci. Rep. 62 (2007) 431–498. https://doi.org/10.1016/j.surfrep.2007.07.001.

[64] C. Liu, M. Hirohara, T. Maekawa, R. Chang, T. Hayashi, Selective electro-oxidation of glycerol to dihydroxyacetone by a non- precious electrocatalyst – CuO, Appl. Catal. B Environ. 265 (2020) 118543. https://doi.org/10.1016/j.apcatb.2019.118543.

[65] Y. Kim, H.W. Kim, S. Lee, J. Han, D. Lee, J.R. Kim, T.W. Kim, C.U. Kim, S.Y. Jeong, H.J. Chae, B.S. Kim, H. Chang, W.B. Kim, S.M. Choi, H.J. Kim, The Role of Ruthenium on Carbon-Supported PtRu Catalysts for Electrocatalytic Glycerol Oxidation under Acidic Conditions, ChemCatChem. 9 (2017) 1683–1690. https://doi.org/10.1002/cctc.201601325.

[66] N. Benipal, J. Qi, Q. Liu, W. Li, Carbon nanotube supported PdAg nanoparticles for electrocatalytic oxidation of glycerol in anion exchange membrane fuel cells, Appl. Catal. B, Environ. 210 (2017) 121–130. https://doi.org/10.1016/j.apcatb.2017.02.082.

[67] Z. Zhang, L. Xin, J. Qi, D.J. Chadderdon, K. Sun, K.M. Warsko, W. Li, Selective electro-oxidation of glycerol to tartronate or mesoxalate on Au nanoparticle catalyst via electrode potential tuning in anion-exchange membrane electro-catalytic flow reactor, Appl. Catal. B Environ. Environ. 147 (2014) 871–878. https://doi.org/10.1016/j.apcatb.2013.10.018.

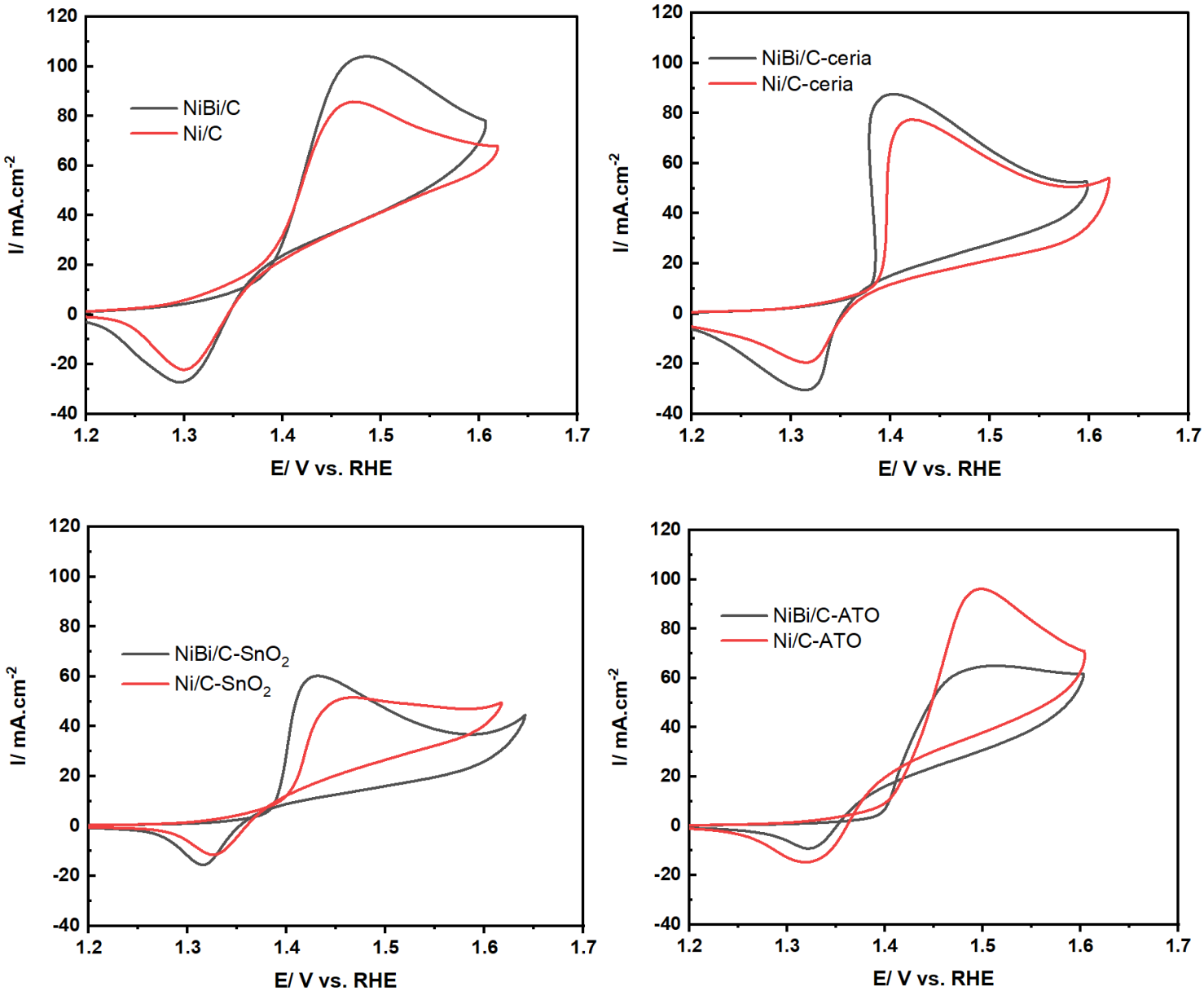

Figure B1: Cyclic voltammograms in 1.0M KOH + 0.1M glycerol electrolyte of Ni/C-X vs. NiBi/C-X [X=C, Ceria, SnO_2 and ATO] at a scan rate of 50 $mV.s^{-1}$.

Oxalic acid

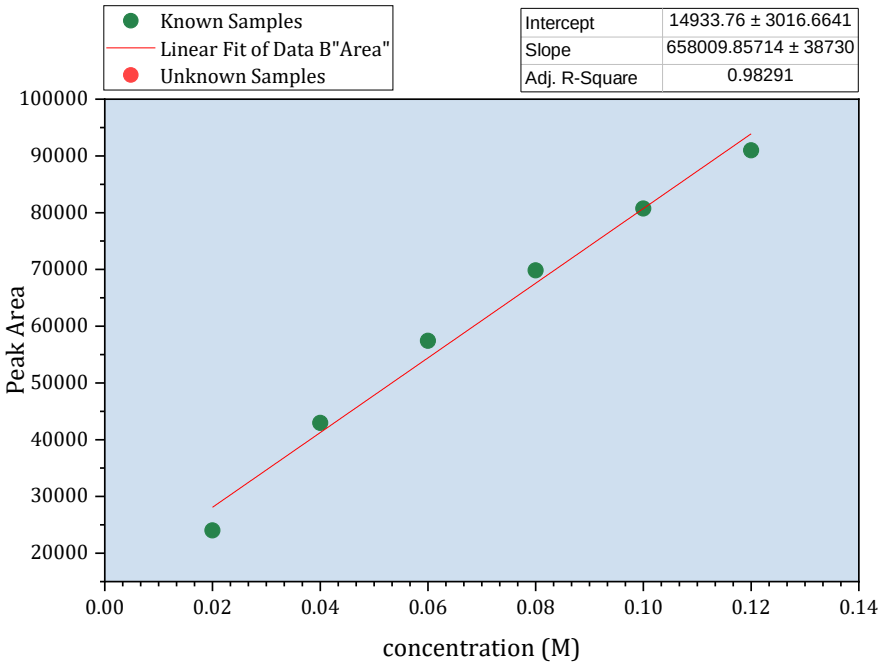

Tartronic acid

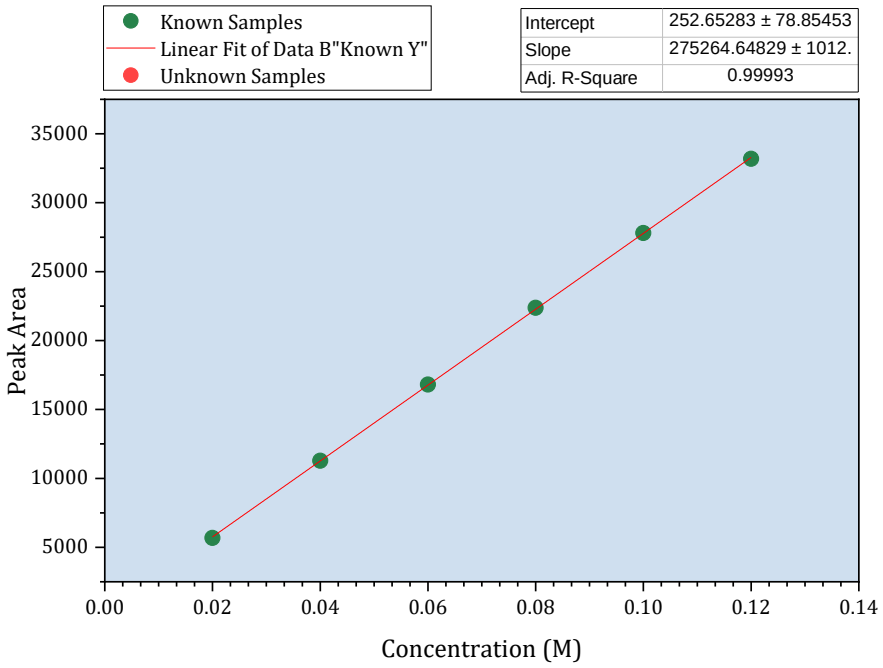

Figure B2: Calibrated curves of oxalic and tartronic acids determined from HPLC with retention time of 6.2 and 7.7 min, respectively using DAD (diode array detector) UV/Vis detector 210 nm.

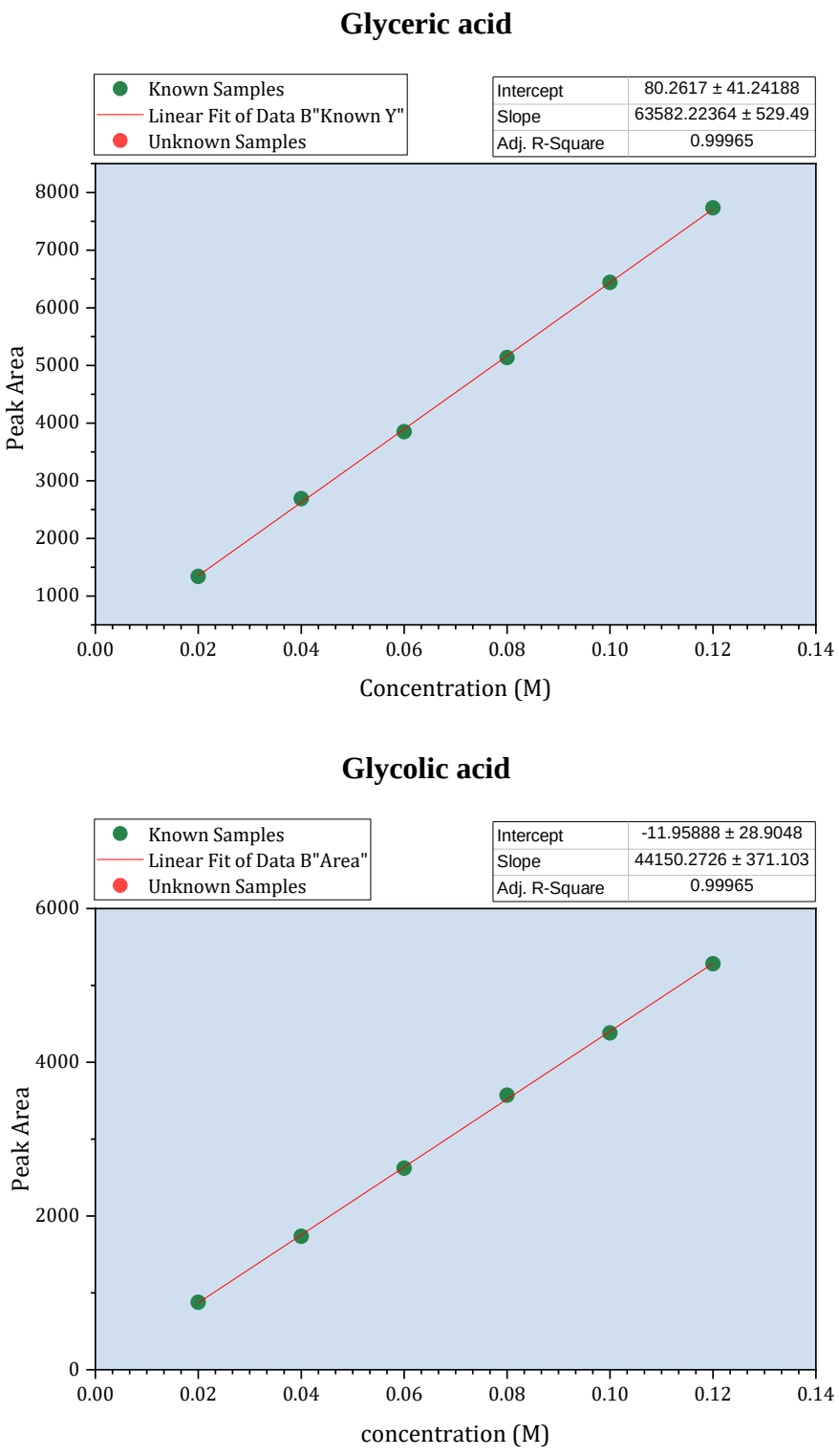

Figure B3: Calibrated curves of glyceric and glycolic acids determined from HPLC with retention time of 10.6 and 12.0 min, respectively using DAD (diode array detector) UV/Vis detector 210 nm.

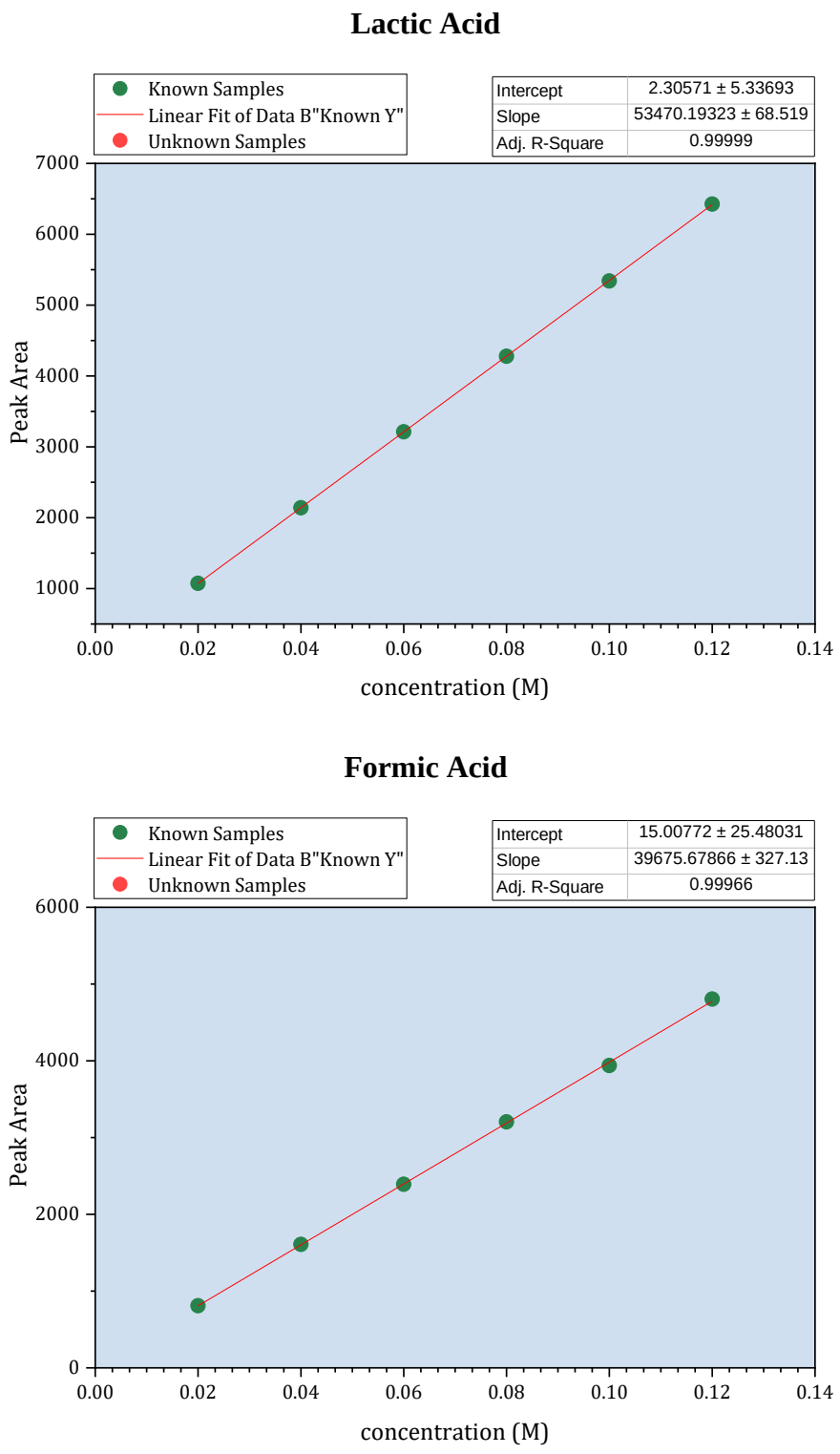

Figure B4: Calibrated curves of lactic and formic acids determined from HPLC with retention time of 12.4 and 13.5 min, respectively using DAD (diode array detector) UV/Vis detector 210 nm.

Chapter 5: Overall conclusion and future recommendations

In chapter 3, carbon supported Ni_xBi_{100-x} [x=100, 95, 90, 80 and 50 at.%] are fabricated by sodium borohydride reduction method. TEM images indicated agglomerations of nanoparticles and nanoparticle size varying between 6-13 nm. Moreover, EDS spectra and EDS mapping showed well distribution of Ni and O elements with Bi available in large clusters in specific areas. By electrochemical techniques, compared to various Ni:Bi atomic ratios, $Ni_{95}Bi_5$/C exhibited the highest current density 104 $mA.cm^2$ with onset potential of 1.31 V vs. RHE. Furthermore, $Ni_{95}Bi_5$/C showed superior selectivity to C_3 products compared to Ni/C. As shown in table 5.1, selectivity to C_3 products (GA, TA, LA) is 41.43 with $Ni_{95}Bi_5$/C (≥ 6nm NP size) compared to 34.57% with Ni/C. Furthermore, our $Ni_{95}Bi_5$/C (≥ 6nm NP size) in chapter 3 presented a clear enhancement to C_3 product selectivity when compared to 100% FA selectivity observed with $Ni_{90}Bi_{10}$/C (≤3nm NP size) presented in literature. However, the smaller $Ni_{90}Bi_{10}$/C catalyst presented in literature exhibited higher catalytic activity and lower onset potential. One can conclude, that the particle size and physical characteristics of Ni-based catalysts had an impact on electrochemical performance and product selectivity towards glycerol electrooxidation reaction. Further in-depth studies on effect of synthesis method (metal precursor salt, mixing technique and drying techniques) on the physical properties and electrochemical performance of Ni-based catalysts for GEOR must be conducted to gather better understanding of effects of particle size and morphology on the catalytic activity of Ni nanoparticles.

In chapter 4, the effect of metal oxides (CeO_2, SnO_2, and ATO) on the electrochemical performance and product selectivity of Ni/C and NiBi/C catalysts were tested. All Ni and NiBi on carbon-metal oxide composite support were synthesized by sodium borohydride reduction method. By means of electrochemical characterizations, the lowest onset potentials of ~1.30V vs. RHE were observed by Ni/C and $Ni_{95}Bi_5$/C, respectively. Among all Ni-based catalysts, Ni/C-ATO exhibited the highest current density of 96 $mA.cm^{-2}$ at potential of 1.50 V vs. RHE. Addition of bismuth to Ni/C-X catalysts showed an enhancement to current density except for NiBi/C-ATO. Furthermore, the product

selectivity to C_3 products (GA, LA, and TA) were greatly enhanced in the presence of metal oxides. As shown in Table 5.1, the selectivity to C_3 products in order of highest to lowest, $Ni_{95}Bi_5$/C-ATO (100%)> Ni/C-ATO (99.17%)> $Ni_{95}Bi_5$/C-ceria (98.05%)> Ni/C-ceria (78.29%)> $Ni_{95}Bi_5$/C (41.43%)> Ni/C (34.57%). Our catalysts presented in chapter 4 compared to other non-platinum catalysts reported in literature had higher selectivity to C_3 products. Interestingly, Ni and NiBi/C-X catalysts presented higher or comparable C_3 selectivity to precious metal Pd/CNT (62.4% C_3), Au/C (96%) and Pt/C (99.9%). However, precious metals have much lower onset potentials and higher catalytic activity compared to Ni-based catalysts which can still be further improved by developing nickel bimetallic or trimetallic catalysts. Further studies are required to gather better understanding of mechanism of glycerol electrooxidation on Ni-based catalysts with metal oxides.

Table 5.1: Summary of product selectivity of Platinum and non-platinum group metals for GEOR

Catalyst	Synthesis	Electrolyte	E (onset) V vs RHE	Conditions	Selectivity	Ref.
Ni/C	$NaBH_4$ reduction method	0.1 M Glycerol + 1 M KOH	1.29	CA 1.35V, 30min	FA: 65.43%; GA: 20.64%; TA: 8%; GLA: 5.93%	Chp 3
$Ni_{95}Bi_5$/C (≥6nm NP size)			1.31		FA: 50.87% ; GA: 35.9% ; GLA: 5.25% ; TA: 3.94% ; OA: 2.45% ; LA: 1.59%	
Ni/C-ceria			1.33		GA:55.84%; LA: 22.95%; GLA:15.02%; FA: 6.29%	Chp 4
$Ni_{95}Bi_5$/C-ceria			1.30		LA: 58.15%; GA: 39.9%; FA: 1.95%	
Ni/C-ATO			1.38		GA: 66.11%; LA: 33.06%; FA: 4.82%	
$Ni_{95}Bi_5$/C-ATO			1.39		LA: ~100%	
Spherical Ni			1.375	CA 1.4V, 30min	FA: 56.5% ; GA: 35.3% ; GLA: 4.75% ; LA: 2% ; TA: 0.85% ; OA: 0.6%	[1]
$Ni_{90}Bi_{10}$			1.33		FA: 45.8% ; GA: 36.3% ; TA: 7.9% ; OA: 3.3% ; GLA: 4.5% ; LA: 2.1%	
$Ni_{90}Bi_{10}$ after aging			1.33		FA: 40.97% ; GA: 37.5% ; TA: 8.2% ; OA: 5.5% ; GLA: 5.4% ; LA: 2.5%	
$Ni_{90}Bi_{10}$/C (≤3nm NP size)			1.15	CA 1.35V, 1h	FA: 100%	[2]
Ni/C	Impregnation/ Reduction Method	0.1 M Glycerol + 0.1 M NaOH	1.30	CA 1.6V vs RHE, 8h	GLA: 11.5%; FA: 32.2%; GA: 0.5mM	[3]
NiFe/C			1.2		GLA: 3.7%; FA: 4%; GA: 0.1mM	
NiCo/C			1.44		GLA: 4.5%; FA: 7.5%; GA: 0.25mM	
NiFeCo/C			1.25		GLA: 10.3%; FA: 34.1%; GA: 0.2mM	
CuO	Precipitation reaction with NaOH at 60°C	0.1 M Glycerol + 0.1 M NaOH	1.20	CA 1.29V vs RHE, 1h	FA: 70%; GA: 20%; DHA: 5%	[4]
Pt/C	Polyol method with ethylene glycol	2 M Glycerol + 0.5 M H_2SO_4	1.46	CA -1.1V vs SHE, 7h, 60°C	GLAD: 42.1%; GA: 57.8%; GLA: 0.5%	[5]
Pd/CNT	Modified aqueous-phase reduction method	1 M Glycerol + 4 M KOH	0.6	CA -0.1V vs SHE, 2h, 50°C	GA: 21.7% ; GLA: 8.5% ; OA: 25.3% ; TA: 39.5% ; MESOXA: 3.8% ; LA: 1.2%	[6]
Au/C	Modified solution-phase based nanocapsule method	1 M Glycerol + 2 M KOH	0.7	CA -0.35V vs RHE, 1h	GA: 15% ; TA: 80% ; OA: 5%	[7]

Abbreviations: DHA: dihydroxyacetone; GLAD: glyceraldehyde; GLA: glycolic acid; GA: glyceric acid; OA: oxalic acid; TA: tartronic acid; LA: lactic acid; MESOXA: mesooxalic acid; FA: formic acid.

Future recommendations:

- In depth study of the synthesis method effect on nanoparticles size and physical properties of Ni-based catalysts and their effect on GEOR performance/ selectivity.
- Metal oxides showed interesting results in terms of products to C_3 products however, its GEOR electrochemical performance can be further improved by synthesis of nanostructured metal oxides (ceria, SnO_2 and ATO) with larger surface area.
- Since effect of support showed a clear impact on product distributions of Ni-based catalysts for GEOR, it could be interesting to study other metal oxide supports such as; TiO_2 and Al_2O_3 or tuning the shape of carbon support such as; carbon nanotubes.

References:

[1] M.S.E. Houache, K. Hughes, R. Safari, G.A. Botton, E.A. Baranova, Modification of Nickel Surfaces by Bismuth: Effect on Electrochemical Activity and Selectivity Towards Glycerol Modification of Nickel Surfaces by Bismuth : Effect on Electrochemical Activity and Selectivity Towards Glycerol, ACS Appl. Mater. Interfaces. 12 (2020) 15095–15107. https://doi.org/10.1021/acsami.9b22378.

[2] M.S.E. Houache, R. Safari, U.O. Nwabara, T. Rafa, G.A. Botton, C. Coutanceau, E.A. Baranova, P.J.A. Kenis, Selective Electrooxidation of Glycerol to Formic Acid over Carbon Supported Ni1−xMx (M = Bi , Pd , and Au) Nanocatalysts and Coelectrolysis of CO2, ACS Appl. Energy Mater. 3 (2020) 8725–8738. https://doi.org/10.1021/acsaem.0c01282.

[3] V.L. Oliveira, C. Morais, K. Servat, T.W. Napporn, G. Tremiliosi-Filho, K.B. Kokoh, Studies of the reaction products resulted from glycerol electrooxidation on Ni-based materials in alkaline medium, Electrochim. Acta. 117 (2014) 255–262. https://doi.org/10.1016/j.electacta.2013.11.127.

[4] C. Liu, M. Hirohara, T. Maekawa, R. Chang, T. Hayashi, Selective electro-oxidation of glycerol to dihydroxyacetone by a non- precious electrocatalyst – CuO, Appl. Catal. B Environ. 265 (2020) 118543. https://doi.org/10.1016/j.apcatb.2019.118543.

[5] Y. Kim, W. Kim, S. Lee, J. Han, D. Lee, The Role of Ruthenium on Carbon-Supported PtRu Catalysts for Electrocatalytic Glycerol Oxidation under Acidic Conditions, ChemCatChem. 9 (2017) 1683–1690. https://doi.org/10.1002/cctc.201601325.

[6] N. Benipal, J. Qi, Q. Liu, W. Li, Carbon nanotube supported PdAg nanoparticles for electrocatalytic oxidation of glycerol in anion exchange membrane fuel cells, Appl. Catal. B, Environ. 210 (2017) 121–130. https://doi.org/10.1016/j.apcatb.2017.02.082.

[7] Z. Zhang, L. Xin, J. Qi, D.J. Chadderdon, K. Sun, K.M. Warsko, W. Li, Selective electro-oxidation of glycerol to tartronate or mesoxalate on Au nanoparticle catalyst via electrode potential tuning in anion-exchange membrane electro-catalytic flow reactor, Appl. Catal. B Environ. Environ. 147 (2014) 871–878. https://doi.org/10.1016/j.apcatb.2013.10.018.

Appendices:
Influence of Pd and Au on Electrochemical Valorization of Glycerol over Ni-rich Surfaces

Mohamed S. E. Houache[a], Asma Shubair[a], Mario G. Sandoval[b], Reza Safari[c], Gianluigi A. Botton[c], Paula V. Jasen[b], Estela A. González[b], Elena A. Baranova[a]*

(*Under review in Journal of Catalysis*)

[a]Department of Chemical and Biological Engineering, Centre for Catalysis Research and Innovation (CCRI), University of Ottawa, 161 Louis-Pasteur Ottawa ON, Canada, K1N 6N5
[b] Instituto de Física del Sur (IFISUR), Departamento de Física, Universidad Nacional del Sur (UNS), CONICET, Av. L. N. Alem 1253, B8000CPB-Bahía Blanca, Argentina
[c]Department of Materials Science and Engineering, McMaster University, 1280 Main St. W. Hamilton, ON, Canada, L9H 4L7

Abstract (150 words-MAX)

Herein we synthesized bi-metallic Pd@Ni and Au@Ni core-shell like nanoparticles for glycerol electrooxidation reaction (GEOR) in alkaline media. Catalytic activity and stability were evaluated via various electrochemical techniques. Among different atomic ratios, $Ni_{80}Pd_{20}$ and $Ni_{90}Au_{10}$ nanoparticles showed the highest current densities which are ~ 4.5 and 4.2 times higher than spherical Ni, respectively. The addition of Pd and Au (<20 at.%) to Ni nanoparticles led to a remarkable glycerate selectivity of ~ 73.1% and 65.7% for $Ni_{80}Pd_{20}$ and $Ni_{90}Au_{10}$ catalysts at 1.3 V and 50 ℃, respectively. Notably, after 6 hours of electrolysis Pd@Ni and Au@Ni tend to suppress the C-C bond cleavage, compared to Ni at any applied potentials and temperatures. Based on the DFT calculations, the addition of auxiliary metals to Ni reduced the work function of M@Ni NPs, which strengthened the OH adsorption onto the catalyst surface and enhanced the removal of GEOR intermediates.

KEYWORDS: Ni_xM_{1-x} catalysts; Glycerol electrooxidation; Electrolysis; Selectivity; Density Functional Theory; Work Function

*Corresponding author: Tel: 16135625800 (x 6302); fax: 16135625172;

E-mail: elena.baranova@uottawa.ca (Elena A. Baranova)

Graphical Abstract

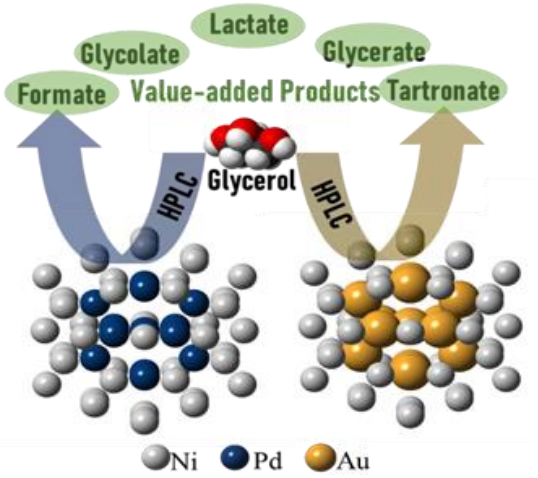

Highlights

- Bimetallic shell/core-like are synthesised via a heatless chemical reduction
- The activity and products of glycerol oxidation over the Ni-rich catalysts are studied.
- Addition of Pd and Au enhances the selectivity towards C2 and C3 products
- DFT calculations for the bimetallic systems are more stable and reactive than Ni NP

1. INTRODUCTION

Glycerol electrooxidation reaction (GEOR) is a viable and efficient way of converting an excess of glycerol, a by-product of biodiesel production [1-3], to value added chemicals [4-6]. GEOR was proposed over two decades ago, however there are still several questions that remain to be answered before this process could see practical application. The central issue is a type of electrocatalyst and the nature of the active sites that in turn dictate the catalytic activity and selectivity towards desired products [4]. There are several possible reaction pathways for the partial electro-oxidation of glycerol, which result in various products: glycerate, tartronate, hydroxypyruvate, glycolate, oxalate, dihydroxyacetone, mesoxalate and formate [7-10], therefore development of efficient and stable electrocatalysts with high selectivity to the preferred products has been a central topic of GEOR research in recent years [5].

Several noble platinum-, palladium- and gold-based catalysts have been developed [11-15]. Results showed that gold outperforms the other noble metals in alkaline media due to its relatively high anti-poisoning capabilities and large capacity to adsorb hydroxyl ions, which promote the oxidation reaction [16]. *Maumau et al.* tested Au/C which showed to have high current density and anti-poisoning ability to surface oxides compared to Pd/C [17]. Similarly, gold disk electrodes exhibited nine times higher current density than palladium disks [18]. Regarding selectivity, the main products formed on Pd, Pt and Au have been shown to be glycerate ions, mesoxalate and/or tartronate with a unique selectivity to hydroxypyruvate ion on gold [19,20]. In addition, AuPt alloy showed a selectivity to lactic acid (73%), which is a valuable product used in several industries [8].

Among the non-noble metals, nickel is the most common metal used in electrochemical technologies, e.g., rechargeable batteries, fuel cells, sensors, alkaline water electrolysis and supercapacitors, [21-23] due to its high current densities and good stability in alkaline media [24]. Several recent studies explored Ni and Ni-based electrocatalysts for GEOR [24-29]. It is proposed that the region of nickel oxy-hydroxide formation (NiOOH) at (~1.4V vs RHE) is the active phase for GEOR on Ni surfaces [24-26]. Oliveira et al. reported that main products on carbon supported Ni, NiCo and NiFe are formate with minor amounts of glycolate, glycerate, tartronate, and oxalate [26]. In our recent report, we synthesized Ni-Bi double-shell/core structure that showed a 2-fold enhanced GEOR activity when compared to monometallic Ni [28]. The addition of 10 atomic (at.) % of Bi improved the formation of C_3 products by suppressing the C-C bond cleavage. In another study, we reported that Ni-Pd double-shell/core nanoparticles (NPs) of various composition showed higher electrocatalytic activity towards GEOR than mono-metalic Ni due to a synergistic effect between the two metals, however, the reaction pathway and

selectivity were similar to that of monometallic Ni [29]. For carbon supported Ni_xM_{1-x} (M = Bi, Pd and Au) nanomaterials with different atomic ratios, generated 100% selectivity towards formate with 100% conversion at + 1.55V [27]. This work was a pioneer in combining glycerol and CO_2 valorization using Ni-rich materials.

Theoretical methods for studying properties of bimetallic NPs have become an important tool for predicting reactivity, stability and magnetic properties of nano clusters. Several authors studied the structural properties, stability, anisotropy, strain, mixing energies, magnetic properties and chemical order of NPs formed by metals of the groups 10 and 11 [30-36]. These NPs present a size-dependent evolution of their structure and properties, where the geometric shape and the energetic stability of NP could drastically change with size [30]. Also, the accumulation of strain at the atomic level and its subsequent release can be responsible for the symmetry breaking that make possible the different size- and composition-dependent transitions between the core@shell arrangements [31].

Zhu et al. investigated the structural and electronic properties of the icosahedral $Pd_{55-n}Ni_n$ (n = 0-55) clusters using DFT [37]. The authors found that the core-shell $Ni_{13}@Pd_{42}$ cluster is the most stable structure. The electronic property analysis revealed that the interaction between Pd-4d and Ni-3d orbitals makes the main contribution and a strong d–d self-interaction among the 3d orbitals of the Ni atoms. They also found that with an increasing number of Ni atoms, the d-band center of the surface Pd atoms shift away from the Fermi level, while the root mean squared d-band width broadens. This feature is also observed in the partial density of states (DOS) of the Pd surface atoms. The charges are partially transferred from Pd to Ni in the bimetallic cluster and partially from Ni atoms on the top sites to Ni atoms in the core.

In a recent publication, the impact of oxygen traces during TEM measurments on the phase transition from Ni-Au to Au-Ni core-shell clusters were investigated [38]. The combined theoretical and experimental approach showed that in the presence of trace oxygen, an Au-Ni core-shell system becomes thermodynamically preferred at elevated temperatures, even before a full oxidation of the reactive metal takes place. The diffusion of Ni to the surface is catalyzed by the presence of oxygen. Therefore, for bimetallic nanoparticles in this size regime, the gas adsorption onto the protective noble metal shell can destabilize the core-shell structure by an enhancement of intermetallic diffusion.

Herein, we synthesize bimetallic nickel rich catalysts Ni_xAu_{1-x} [x = 100, 98, 95, and 90 at.%] and Ni_xPd_{1-x} [x = 100, 95, 90 and 80 at.%] catalysts using a sodium borohydride method, which could be easily scaled up. Firstly, the fabiracted nanoparticles were characterized in detail using transmission electron

microscopy (TEM), X-ray diffraction (XRD), X-ray photoelectron microscopy (XPS), energy-dispersive X-ray spectroscopy (EDS) and electron energy loss spectroscopy (EELS). In addition, the electrochemical performance was evaluated by cyclic voltammetry (CV), chronoamperometry (CA), linear sweep voltammetry (LSV) and durability test (cycling for 300 cycles) in alkaline media. Product distributions of GEOR were also analyzed by HPLC in a memebranless continuous electrolysis cell (25 cm^2) at different applied potentials and temperatures. Finally, to shed light on the experimental observations and elucidate the interaction between Ni and the second metal (Pd or Au), a series of DFT calculations on smaller, finite model systems have been carried out. To this end, we calculated the excess energy, electronic structure, d band center, work function (WF) and strain between core-shell layers and corelated these results with the experimental findings.

2. METHODOLOGY SECTION

2.1 Material synthesis

The Ni_xAu_{1-x} (x = 100, 98, 95, and 90 at.%) and Ni_xPd_{1-x} (x= 100, 95, 90 and 80 at.%) catalysts were synthesized via wet chemical synthesis. The detailed methodology was reported in our previous work [29]. Briefly, the metal precursor salts nickel (II) chloride hexahydrate (ALDRICH Chemistry, 99.999% purity), gold (III) chloride (ACROS Organics, 99% purity) and palladium (II) chloride (ALDRICH Chemistry, ≥ 99.9% purity) were dissolved in ethanol solvent in a controlled weight percentage ratio. After complete dissolution, the sodium borohydride powder (ACROS Organics, 98+% purity), which is the reducing agent, was added to the mixture. Finally, the samples were centrifuged and freeze dried.

2.2 Physicochemical and electrochemical characterizations

Various physicochemical procedures (TEM, SAED, XRD, XPS, HAADF, EDS, EELS) were implemented. In addition, different electrochemical tests (CV, LSV, CA) were conducted. The detailed procedures were explained elsewhere [29].

2.3 Chromatographic analysis of products

The continuous electrolysis cell (25 cm^2) was used to study the catalyst performance and product distributions during GEOR [28]. The HPLC measurement and standard calibration details were previously reported along with a sample calculation [28].

2.4 Theoretical modeling and calculations

To develop several finite size models to complement experimental characterization we perform DFT calculations using the VASP code [39]. The calculations are spin polarized since most systems have magnetic properties. According to the experimental results for the NPs, we focus on icosahedral and decahedral clusters. We studied the 13- and 55-atoms icosahedral (Ih_{13} and Ih_{55}, respectively) and 54-atoms decahedral (Dh_{54}) nanoparticles. The 13 atoms systems were studied in order to validate our theoretical methodology. These results are discussed in the supporting information and compared with other experimental and theoretical findings from literature. The 55-atoms icosahedral NP serves as a model system resembling the experimental finding, with an almost spherical shape and (111) faces terminations. Also, the NPs with icosahedral structure have good stability [34,40-42]. From the point of view of surface energy, this structure is a highly strained non-crystalline one with a quasi-spherical shape and close-packed

surface, which optimizes the surface energy well. In addition, the icosahedral NPs are obtained by packing together twenty tetrahedrons sharing a common vertex. This packing causes the high internal strain of the structure and the efficient minimization of the surface energy, which favored this structure at small sizes [34,40,41]. The decahedral structure also has (111) faces termination. In both systems the composition of bimetallic NP is in the range of that synthetized experimentally. More information on the schematic models is given in Fig. S1 in SI. The Ih_{13}-, Dh_{54}- and Ih_{55}-NPs are conFig.d as $core_m@shell_n$ systems, i.e., $M_m@Ni_n$ (as mentioned before Ni_xM_{1-x}) particles (M = Au and Pd), where "m" is the number of M-atoms in the core and "n" is the number of Ni-atoms in the shell. In this work, we study the Ih_{13}-$M_1@Ni_{12}$, Ih_{55}-$M_1@Ni_{54}$, Ih_{55}-$M_{13}@Ni_{42}$ and Dh_{54}-$M_7@Ni_{47}$ systems.

3. RESULTS AND DISCUSSION

3.1 Physicochemical characterization of Ni_xM_{1-x} NPs

The morphological features of as prepared Ni_xM_{1-x} (M = Pd and Au) NPs were investigated by TEM. Fig. 1a and d shows representative micrographs of $Ni_{90}Pd_{10}$ and $Ni_{90}Au_{10}$, nanoparticles, respectively. TEM reveals almost spherical nanosized particles possessing irregular aggregate shapes, with average particles sizes in the range of 3-5 nm. For these materials, the high rates of agglomeration could be elucidated by the strong attractive magnetic force between colloids during the synthesis procedure [29]. Nevertheless, the presence of the second metal Pd or Au, have approximately halved the average catalyst size compared to our previously reported spherical Ni (9.2 ± 2.4 nm) [28].

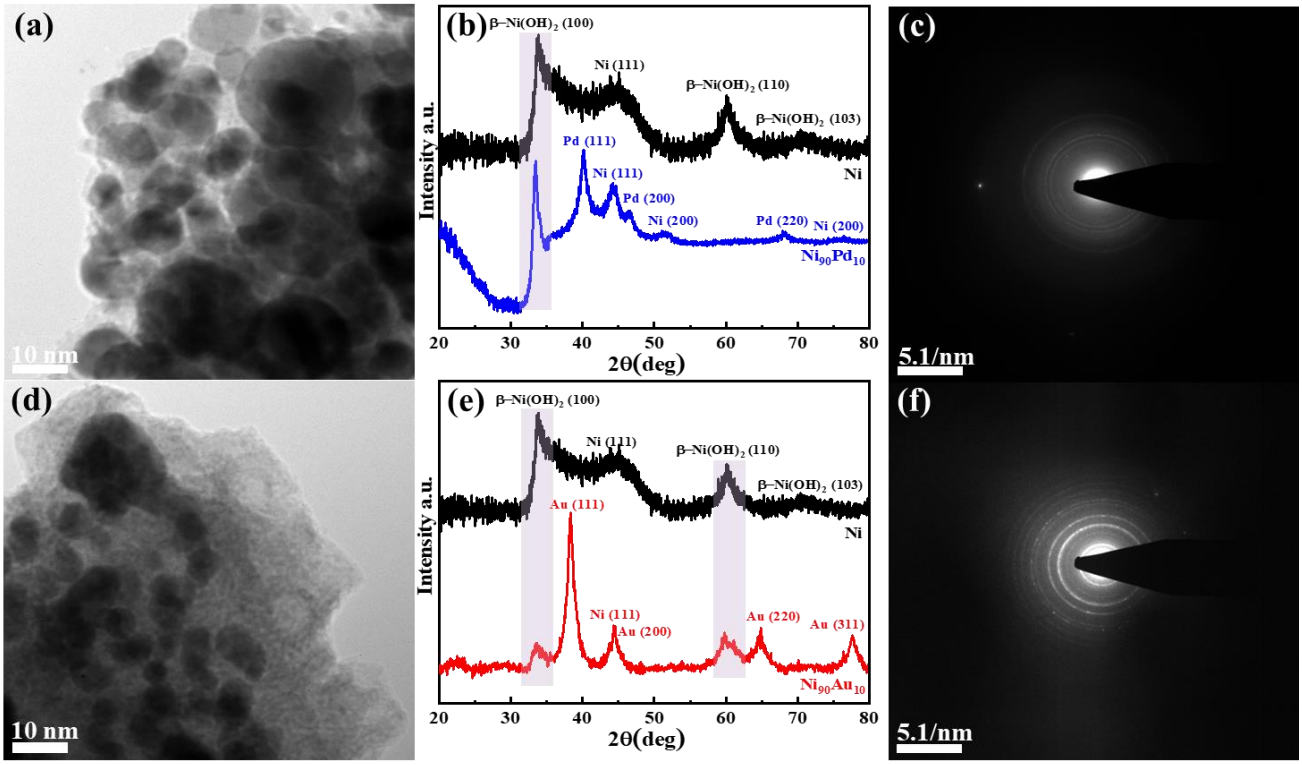

Fig. 1. Morphology and structure characterizations of $Ni_{90}Pd_{10}$ and $Ni_{90}Au_{10}$ nanostructures (a,d) TEM image, (b,e) XRD patterns and (c,f) SAED patterns, respectively.

Moreover, XRD measurements were conducted to identify the crystal structure of nanosized $Ni_{90}Pd_{10}$ and $Ni_{90}Au_{10}$ catalysts. As shown in Fig. 1b and e, the peaks showed distinct face-centered cubic (fcc) structure of Pd(111) and Au(111), respectively, with the presence of Ni(111) and β-$Ni(OH)_2$(100). The corresponding selected area electron diffraction (SAED) pattern (Fig. 1c and f) revealed asset of full

rings, indicating that the bi-metallic nanoparticles have high polycrystalline nature, which is in agreement with our XRD data. However, the diffraction rings were not indexed due to close proximity of Ni to Pd and Au.

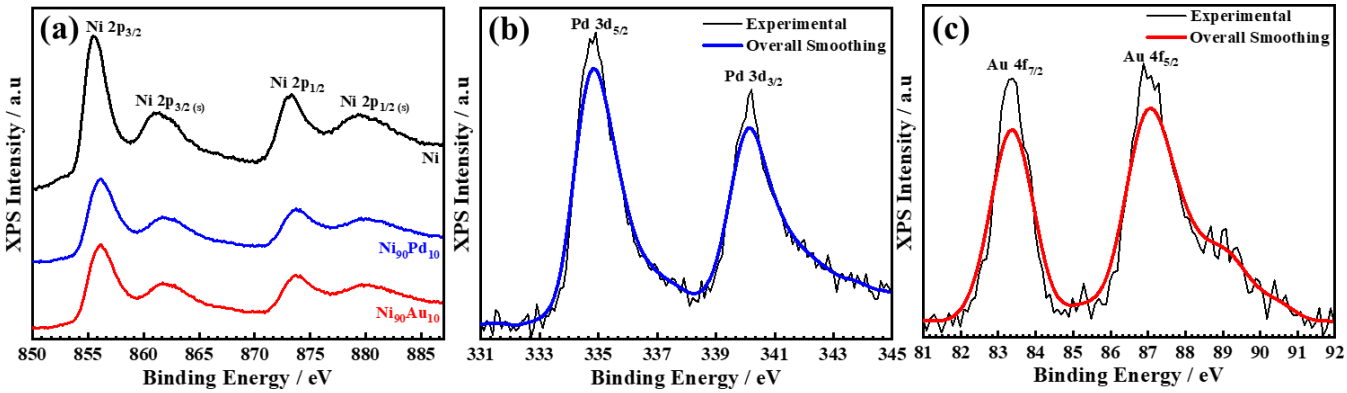

Fig. 2. High resolution XPS spectrum for (a) Ni 2p (b) Pd 3d and (c) Au 4f.

To gain additional information about the surface electronic state and chemical composition of Ni_xM_{1-x} catalysts, Fig. 2(a-c) depict the XPS spectra of Pd 3d and Au 4f core level regions, respectively, along with Ni 2p XPS spectrum. Monometallic Ni shows Ni $2p_{3/2}$ and Ni $2p_{1/2}$ peaks with binding energies at 856.1 and 873.9 eV, respectively, and two satellite peaks positioned at 861.9 and 880.0 eV. The position of the peaks corresponds to the formation of $Ni(OH)_2$ phase with the 17.8 eV binding energy distance [43,44]. For $Ni_{90}Pd_{10}$ and $Ni_{90}Au_{10}$ samples, one can observe similar peaks corresponding to Ni 2p with a higher shift of 0.5 eV compared to Ni, which indicates that the chemical environment of Ni^{2+} is affected. Fig. 2b, the Pd 3d spectrum is positioned between 331-345 eV with two doublets Pd $3d_{5/2}$ (334.8 eV) and Pd $3d_{3/2}$ (340.1eV) in Fig. 7.1e. The peaks position and the full width at half maximum (FWHM ≈1.49 ±0.04 eV) of the peaks confirm the presence of Pd atoms in the metallic state (Pd (0)) with the 5.3 eV binding energy distance [45,46]. In Fig. 2c, the two XPS peaks located at binding energies of 83.4 and 87.1 eV (spin-orbital splitting of 3.7 eV and FWHM ≈1.31 ±0.07 eV) were attributed to Au $4f_{7/2}$ and Au $4f_{5/2}$, respectively, these values are in good correlation with the reported values for pure metal gold (Au(0)) [45,47].

The spatial distributions of Pd and Au elements in Ni-rich NPs were characterized by the STEM-energy dispersive spectroscopy (EDS) mapping as depicted in Fig. 3 a and b, respectively. The Z-contrast images illustrate that Ni (red) is uniformly distributed in the selected area. However, Pd and Au (green) are present in a large cluster in more specific area of the nanosized NPs. The EDS spectra are also in good

correlation with the elemental composition of $Ni_{90}Pd_{10}$ and $Ni_{90}Au_{10}$. The physicochemical characterizations of other samples ($Ni_{80}Pd_{20}$ and $Ni_{95}Au_5$) are illustrated in the supporting information (Fig. S2 and S3).

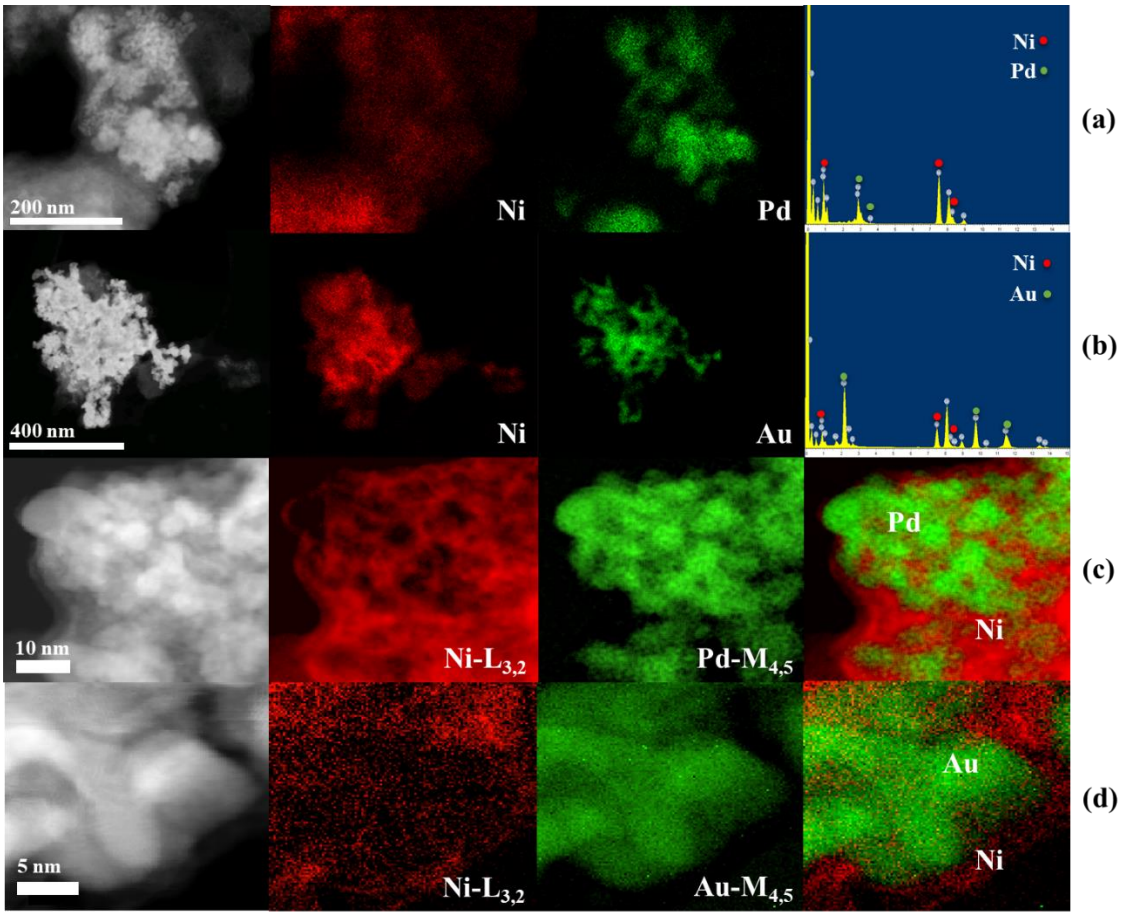

Fig. 3. Dark Field-STEM image, EDS elemental spectrum and mapping of (a) Ni and Pd elements of $Ni_{90}Pd_{10}$ and (b) Ni and Au elements of $Ni_{90}Au_{10}$. HAADF-STEM images and EELS Mapping of (c) $Ni_{90}Pd_{10}$ and (d) $Ni_{90}Au_{10}$ catalysts.

Furthermore, the chemical microstructures of $Ni_{1-x}M_x$ surfaces were also mapped using STEM-EELS analysis. Fig. 3c and d illustrate the elemental distribution of (Ni $L_{2,3}$ and Pd–$M_{4,5}$) and (Ni $L_{2,3}$ and Au–$M_{4,5}$) within the $Ni_{90}Pd_{10}$ and $Ni_{90}Au_{10}$ NPs, respectively, which were extracted from different signals centered at ~855, 400 and 2200 eV for Ni $L_{2,3}$, Pd–$M_{4,5}$ and Au–$M_{4,5}$, (Fig. S4 in ESI). The corresponding STEM–EELS map of Ni-M clearly shows that Pd and Au (green) ions are mostly located in the core region and non-uniform thin layer of Ni (red) ions are segregated on the surface forming a shell. This indicates

the formation of M-core@Ni shell-like structures, with Au and Pd mostly present in the core of NPs indicating that both Au and Pd served as seeds during the NPs synthesis [29].

3.2 Glycerol electrooxidation on Ni_xM_{1-x} NPs

Fig. 4 shows cyclic voltammograms (CVs) of Ni_xPd_{1-x} (x = 100, 95, 90 and 80 at. %) and Ni_xAu_{1-x} (x = 100, 98, 95 and 90 at. %) catalysts in a N_2-purged 1M KOH solution at 50 mV s^{-1}. The current densities of unsupported Ni_xM_{1-x} were normalized per mass of active nickel phase, to avoid uncertainties involved in calculation of the electrochemical active surface areas (ECSA) of Ni-based materials [27]. The comparison of current densities per the geometric area (0.196 cm^2) is given in Fig. S5a-b in ESI.

The CVs in the absence of glycerol were consistent with voltammogram profiles reported in the literature for Ni-rich catalysts [24-27].On monometallic Ni, the anodic peak (~0.59V) and the cathodic peak (~0.33V) correspond to the surface redox process of β-NiOOH/β-Ni(OH)$_2$ [28]. For $Ni_{80}Pd_{20}$, a peak in the cathodic region centered at ~ -0.33 V (Fig. 4a inset) represents the reduction of PdO active sites available on the surface [29], whereas for $Ni_{95}Pd_5$ and $Ni_{90}Pd_{10}$, this peak is negligible, demonstrating Pd is mostly segregate in the core. Similarly, no reduction peak of quasi-2D oxide state of Au was observed as shown in Fig. 4b. Addition of Pd and Au enhanced the current density of the Ni^{2+}/Ni^{3+} peak.

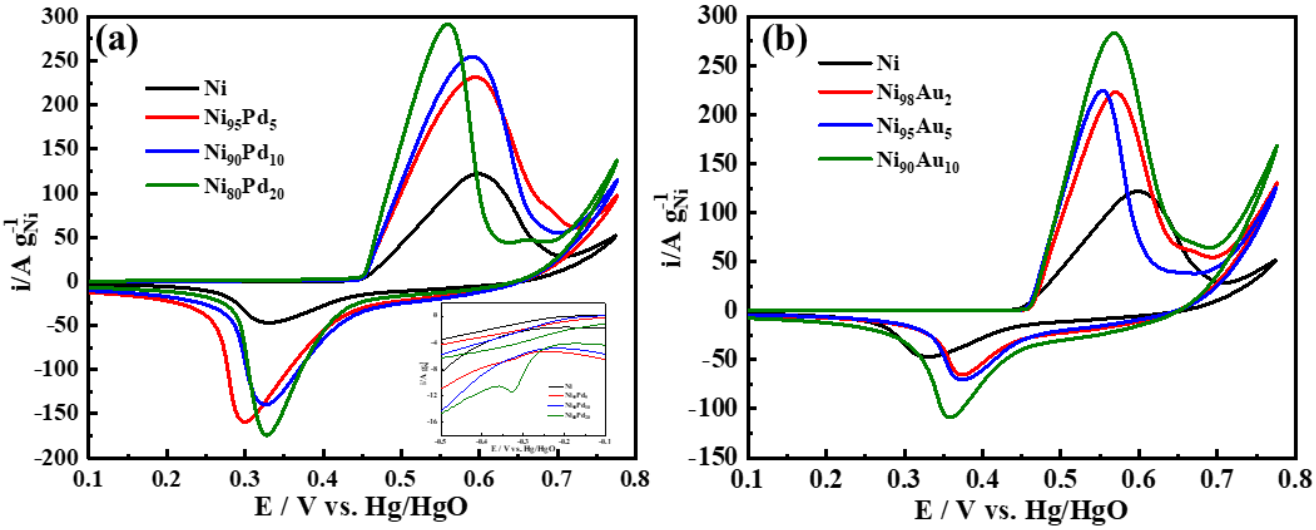

Fig. 4. Cyclic voltammograms of Ni-based catalysts (a) Ni_xPd_{1-x} and (b) Ni_xAu_{1-x} performed in 1 M KOH electrolyte at scan rate of 50 mV s^{-1} (10^{th} stable cycle).

It can be noted that the $Ni_{80}Pd_{20}$ and $Ni_{90}Au_{10}$ catalysts have higher Ni^{II}/Ni^{III} redox peak (~3 x) followed by a more reversible redox process compared to monometallic Ni as shown in Fig.4. The reason for the low current density of pure Ni is its low conductivity, as it is mostly present as Ni oxide [48]. You can clearly see how $NiOOH/Ni(OH)_2$ peaks are separated for Ni. Moreover, the presence of palladium and gold had a positive outcome in improving the conductivity as well as the oxygen evolution reaction (OER). The OER current growth was initiated at ~ 0.71 V vs. Hg/HgO for Ni compared to ~ 0.67 V for $Ni_{80}Pd_{20}$ and $Ni_{90}Au_{10}$. This is due to either the synergistic effect between Pd and Au on Ni redox electrochemistry or the $M_{1-x}Ni_x$ core-shell structure, resulting in a larger active surface area due to the smaller particle size.

Cyclic voltammograms of unsupported Ni_xM_{1-x} catalysts in the presence of glycerol is shown in Fig. 5 and Fig. S5 in ESI. The CVs demonstrate a continuous enhancement in GEOR activity and negative shift of onset potential with increase in Pd and Au content. For the set of catalysts studied, $Ni_{80}Pd_{20}$ and $Ni_{90}Au_{10}$ showed the highest mass current densities of 543 $A.g^{-1}_{Ni}$ and 504 $A.g^{-1}_{Ni}$, respectively compared to 122.4 $A.g^{-1}_{Ni}$ for Ni (Fig. 5a and b). The onset potential of GEOR is negatively shifted by ~ 100mV and 50 mV for $Ni_{80}Pd_{20}$ and $Ni_{90}Au_{10}$ compared to spherical Ni, indicating an enhancement in oxidation kinetics. Moreover, these current densities are higher than the ones reported for Ni_xPd_{1-x}[29]. For $Ni_{80}Pd_{20}$ synthesized at high temperature using hydrazine as reducing agent showed a ~2.5x lower mass activity compared to our recent $Ni_{80}Pd_{20}$ catalyst fabricated using sodium borohydride methode. Addition of Pd and Au promoted the activity of Ni much more than bismuth [28]. For NiBi electrocatalysts, the maximum current density obtained over $Ni_{90}Bi_{10}$ was 436.5 $A.g^{-1}_{Ni}$, which is lower than the data obtained in this report. For higher Pd and Au content, we observed an additional oxidation peak centered at ~ -0.1 V vs. Hg/HgO which attributed to GEOR on Pd sites for $Ni_{80}Pd_{20}$ (Fig. 5a, inset) [29]. Whereas, two additional oxidation peaks appeared at ~0.12 V vs. Hg/HgO ascribed to GEOR on Au sites, demonstrating that gold by itself has much lower overpotential compared to Ni [49]. Fig. 5b, inset illustrates more intense peaks with higher Au content.

The increase in activity with addition of Pd and Au is further observed in the linear sweep voltammetry (LSV) test in Fig. S5 c and d in ESI. Clearly, bimetallic catalysts have lower onset potentials and higher mass current densities than on monometallic Ni. The durability tests of the unsupported Ni_xM_{1-x} catalysts were attained by running 300 consecutive CV cycles in 1 M KOH + 0.1 M glycerol. After 300 cycles in (Fig. 5c and d), $Ni_{80}Pd_{20}$ and $Ni_{90}Au_{10}$ exhibited the highest activity and retained ~51% of their initial current density compared to ~22% for Ni. The drop of activity can be explained by mechanical degradation of the catalysts and/or surface blocking by intermediates. Based on the electrochemical analysis, we

conclude that the $M_{1-x}Ni_x$ core-shell-like structure displayed superior GEOR stability and activity performance than monometallic Ni. This enhancement of GEOR performance of Ni-rich catalysts is due to synergistic and electronic effects between the bi-phases of Ni-Pd and Ni-Au.

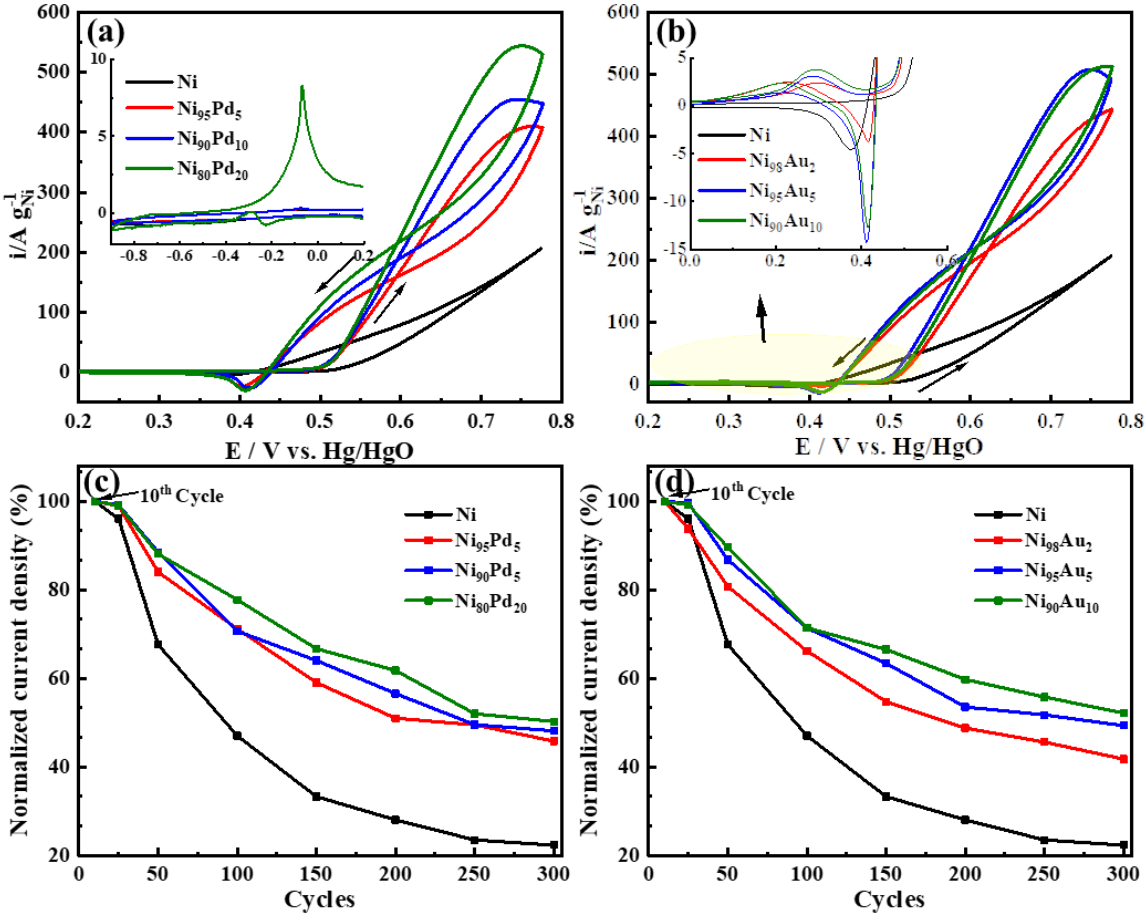

Fig. 5. Cyclic voltammograms of Ni-based catalysts (a) Ni_xPd_{1-x} and (b) Ni_xAu_{1-x} performed in 1M KOH + 0.1M glycerol solution at scan rate of 50 mV s^{-1} (10^{th} stable cycle). Normalized current density percentage vs CV cycles of (c) Ni_xPd_{1-x} and (d) Ni_xAu_{1-x} catalysts.

3.3 Electrolysis experiments and product distribution

The best performing $Ni_{80}Pd_{20}$ and $Ni_{90}Au_{10}$, as well as Ni electrocatalysts were further investigated in the 25 cm^2 membraneless continuous electrolysis cell (flow rate = 1.6 mL s^{-1}). The electrolytic tests were carried out at various applied potentials of 1.3, 1.4 and 1.55 V, temperature ((R.T) and 50°C) and two KOH concentrations of 0.1 and 1 M in 0.1 M glycerol. The resulting cell current during 6 h experiment is reported in Fig. S6 in ESI. The quantitative analysis of products was carried out using HPLC analysis by collecting 0.6 ml of the electrolyte solution every 1h. The comparison in glycerol conversions and product

distributions of the catalysts are shown in Figs. 6-7 and S7-S10 in supporting information. The calibration curves for the C_3 (glycerate, tartronate, and lactate), C_2 (glycolate and oxalate) and C_1 (formate) products were reported previously [28]. According to the HPLC results, the primary products are glyceric (GLA) and formic acid (FA) while, the secondary products are tartronic (TA), lactic (LA), glycolic (GA) and oxalic (OX) acids.

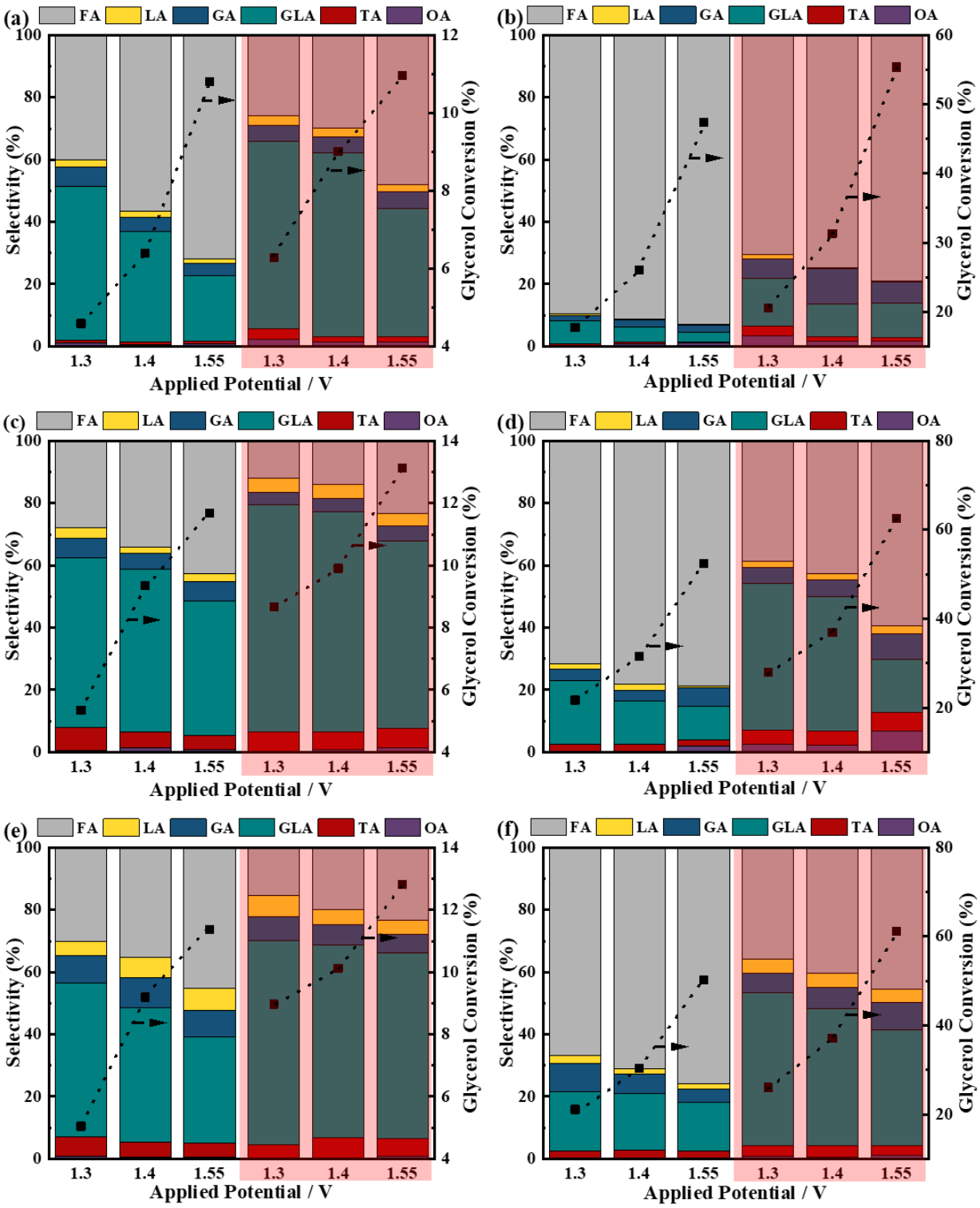

Fig. 6. Product distributions and glycerol conversion (dashed line) under different applied potentials and temperatures over the (a,b) Ni, (c,d) $Pd_{20}Ni_{80}$ and (e,f) $Au_{10}Ni_{90}$ in a 1M KOH+0.1 M glycerol. The left-hand Fig.s illustrate product distributions after 30 min, while the right-hand illustrates products after 6 hrs

Gray: formate; Yellow: lactate; Navy: glycolate; Dark Cyan: glycerate; Wine: tartronate and Violet: oxalate. The red shaded border represents temperature at 50 ^{0}C.

In Fig. 6a-f, all catalysts show the same trend where the application of the low potential (1.3 V) resulted in the highest selectivity towards GLA and the lowest glycerol conversion (< 14%). A temperature increase resulted in higher selectivity to GLA and consequently less FA production. These trends are consistent with our previous results for $Ni_{90}Bi_{10}$ [28]. Noticeably, the addition of Pd and Au reduced the extent of the decrease in GLA selectivity when applying higher potentials, the glyceric acid production in Ni, $Ni_{80}Pd_{20}$ and $Ni_{90}Au_{10}$ decreases by ~ 2.4x, 1.3x, and 1.5x, respectively (Fig. 6a, c and e). The production of C_3 products especially glycerate is enhanced over the bi-metallic catalysts. Specifically, $Ni_{80}Pd_{20}$ achieved the highest GLA selectivity (73.02%) at 1.3 V and 50°C (Fig. 6c), which represents the highest $C_3/(C_1+C_2)$ achieved with Ni-rich catalysts to date [25-29]. Tartronic acid production, a high-value added product [50], is seven times higher over bimetallic NiPd and NiAu catalysts compared to monometallic Ni at 1.3V and R.T. The selectivity change on $Ni_{80}Pd_{20}$ and $Ni_{90}Au_{10}$ could be due to the lower particle size of the bimetallic catalysts compared to monometallic Ni. [51,52]. Because the bimetallic catalysts have less of the electropositive Ni sites and thus less ability to C-C bond cleavage, this could explain the selectivity change [51]. Furthermore, $Ni_{90}Au_{10}$ has the highest tendency to produce LA (~3x) and GA (~2x) compared to Ni at 1.4 V and R.T (Fig. 6e). The fact that the addition of 10 at. % of Au to Ni-rich catalysts induced the production of lactate, indicates that Au increases the oxidative dehydration capacity of the catalyst favoring the reaction pathway leading to LA [53]. Also, the addition of gold modifies the electronic configurations of Ni resulting in different reaction pathways that led to partially oxidized intermediates such as TA and GA [51].

It was previously noticed that time has a vital role on product distributions [28]. After 6 hours of continuous electrolysis, we observed that GLA concentration dropped gradually to FA and glycerol conversion increased progressively as shown in Fig. 6 b,d,f and S7-S9 in ESI. On the other hand, $Ni_{80}Pd_{20}$ and $Ni_{90}Au_{10}$ catalysts produced less C_1 products after 6 h of electrolysis, compared to Ni. By applying a moderate potential of 1.4 V at 50°C, the selectivity to formate is much higher on monometallic Ni (74.5%) compared to Ni-Pd (42.6%) and Ni-Au (40.3%). Additionally, at higher potential of 1.55V, $Ni_{80}Pd_{20}$ had the highest selectivity of oxalic acid (6.9%) at 50°C as illustrated in Fig. 6d. This observation indicates that the addition of a ≤20 at. % of Pd and Au prompts the C_3 selectivity and hinders the further oxidation of GLA to FA.

The effect of 0.1 M KOH concentration on product distributions of $Ni_{80}Pd_{20}$ and $Ni_{90}Pd_{10}$ was investigated at 1.4 V as shown in Fig. 7a-d and S10. For comparison, with time at room temperature, the glycerate production is reduced by (3.72x and 2.4x) in 1 M KOH vs. (1.6x and 1.23x) at 0.1M KOH for $Ni_{80}Pd_{20}$ and $Ni_{90}Au_{10}$, respectively. Similar trend is observed at higher temperatures. Based on the HPLC results, the proposed reaction pathway on Ni, NiPd and NiAu catalysts for GEOR is initially oxidized by the primary alcohol electrooxidation (glyceraldehyde), which is in good agreement with our previous study [28,29]. Further oxidation is either metal-catalyzed to produce GLA, TA, GA, OX, FA and carbonate or base-catalyzed dehydration forming lactate after Cannizzaro rearrangement [53].

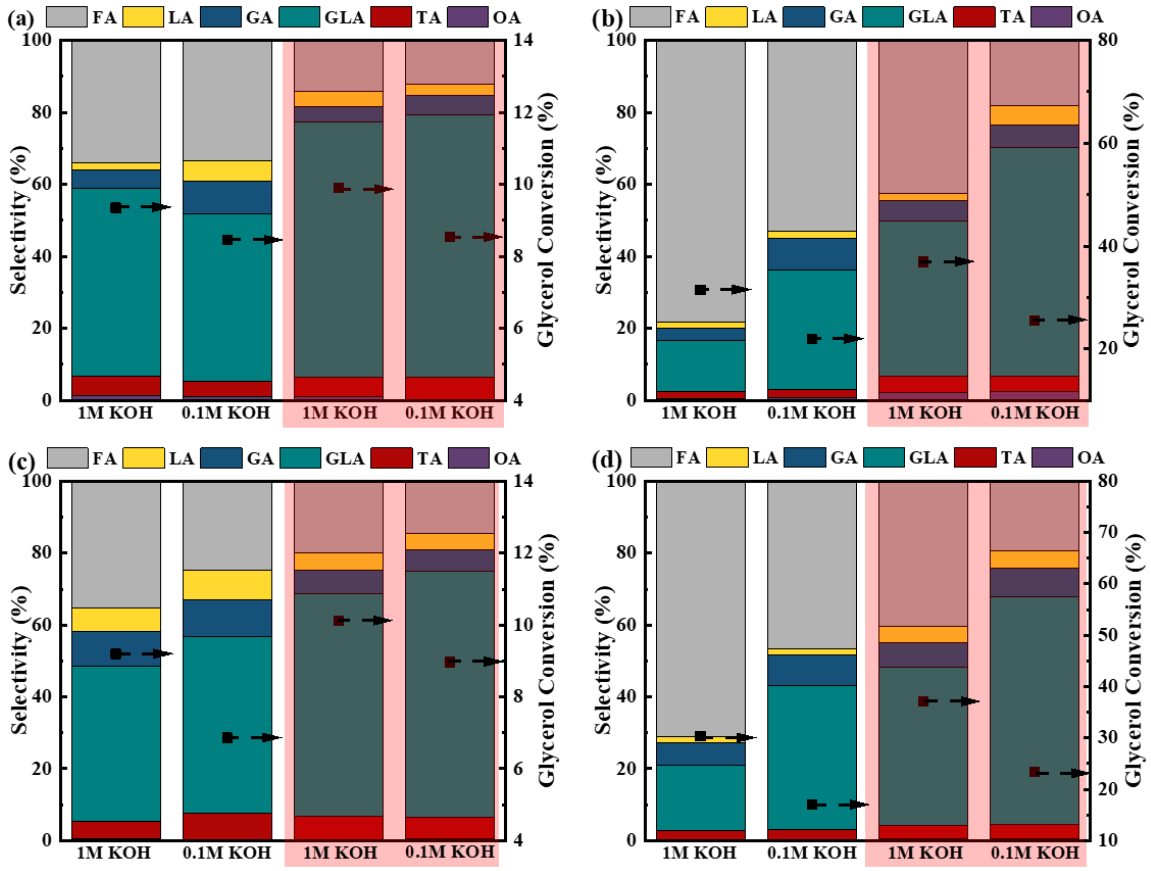

Fig. 7. Product distributions and glycerol conversion at 1.4 V over the (a,b) $Ni_{80}Pd_{20}$ and (c,d) $Ni_{90}Au_{10}$ in a 0.1/1 M KOH+0.1 M glycerol. The left-hand Fig.s illustrate product distributions after 30 min, while the right-hand illustrates products after 6 hrs. The red shaded border represents temperature at 50 ^{0}C.

In summary, addition of small amounts of Pd and Au impacts the selectivity by hindering the GLA oxidation to FA compared to the monometallic Ni, leading to higher selectivity to C_3 products at different

applied potentials and temperatures. In addition, lower KOH concentration further enhances the hindering of C-C bond cleavage, leading to higher C_3 products after 6 hours of continuous electrolysis.

To understand the exceptional GEOR performance of the core/shell-like structured Pd/Ni and Au/Ni nanocatalysts, we performed DFT studies on Ih_{13}-M_1@Ni_{12}, Ih_{55}-M_1@Ni_{54}, Ih_{55}-M_{13}@Ni_{42} and Dh_{54}-M_7@Ni_{47} systems to calculate strain between core-shell layers, excess energy, electronic structure, d band center and work function (WF).

3.4 Theoretical results

3.4.1 Stability and geometrical analysis

In order to analyze the results at varying composition, we calculate the normalized excess energy E* (equation 2 in ESI). The excess energy values for the systems shown in Fig. 8. As expected, all pure NPs have 0 eV. For the Ih_{13} systems, the more stable configurations are Au_1@Ni_1Au_{11} and Ni_1@Pd_1Ni_{11}. The configurations of Pd_1@Ni_{12}, Pd_1@Pd_1Ni_{11}, Ni_1@Pd_{12} and Pd_1@Ni_{12} present some morphological instability, although this does not mean that the cores have unstable configurations. The NPs have locally stable minima, whose energy is however much higher than the energy of the optimal configurations. These morphologies do not persist as the lowest-energy morphology when the proportion of core atoms increases in the nanoparticle, i.e., the term instability is referred to the overall core morphology and not to the local minimum corresponding to the centered core [31]. In the case of Ih_{55}- and Dh_{54}-NPs, the Ni_1@Au_1Ni_{11}@Ni_{42} (Layer1@Layer2@Layer3 - Fig. E1) and Pd_{13}@Ni_{42} systems were the more stable, respectively. The configurations Au_{13}@Ni_{42} and Au_7@Ni_{47} also present morphological instability.

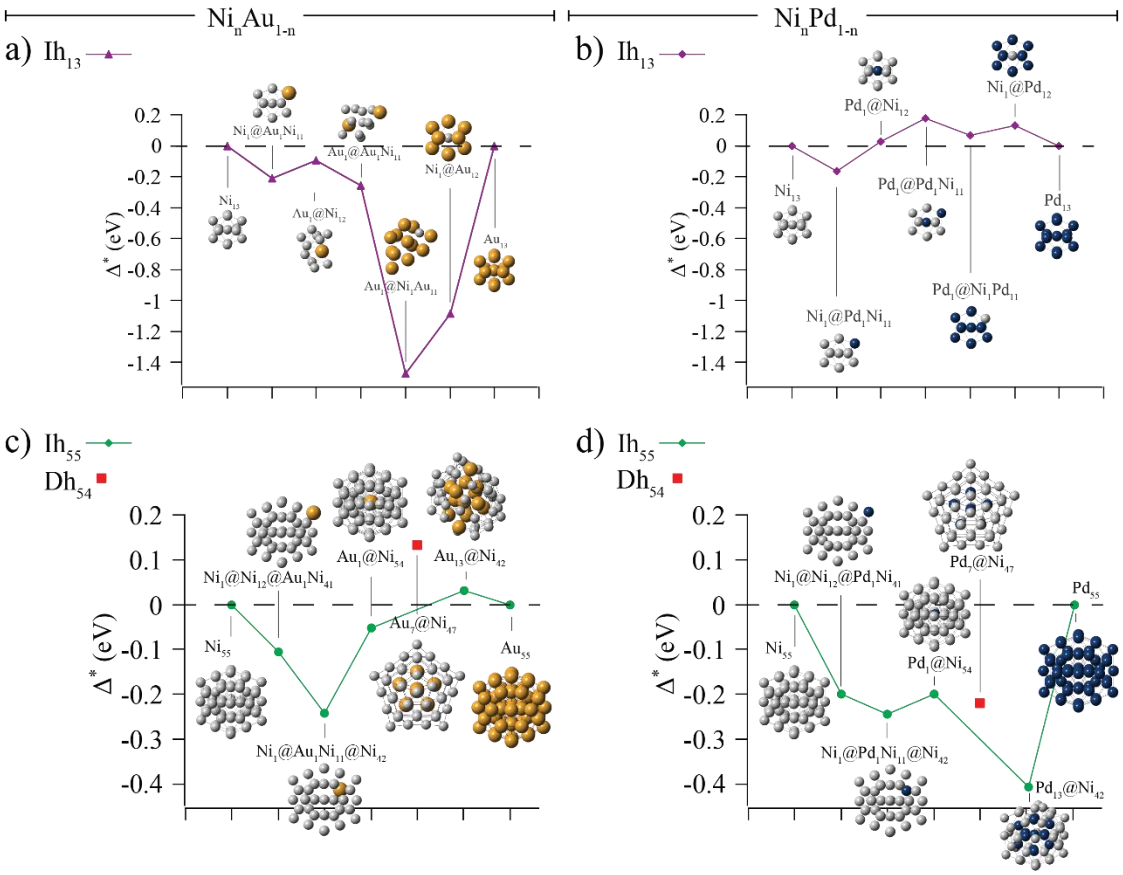

Fig. 8 Excess energy values of the N_nM_{1-n} NPs for (a,b) the 13-atoms icosahedral systems (purple) and (c,d) 55-atoms icosahedral systems (green) and 54-atoms decahedral systems (red).

The morphological instability has a physical origin that is related to strain release. In Fig. 9 optimized structures of the Ih_{13}, Dh_{54} and Ih_{55} NPs are shown. It can be seen that the Au@Ni icosahedral systems have the most important strain percentage ($e_{\text{Layer \#}}$, # = 2, 3), which is consistent with a strong structural deformation and the formation of mixed shell systems (the equation for strain (Eq. 4) is presented in ESI). This is consequence of the mismatch between the metal atomic radii. Also, in the system strain is reducing when the Ni shell diameter is higher than that of the Au core. For the Pd@Ni icosahedral NP we found less strain and therefore less structural deformation, which is consistent with a similar atomic radius of these metals. Despite this, the presence of strain and the fact of the mixed shell system have negative excess energy indicate that the Pd could segregate to the shell, but in a less amount that in the case of the NP with Au in the core. In the decahedral NPs the strain values are smaller and they have less geometrical distortion, as a consequence of more open structure. These results agree with the range of stable composition described in the STEM-EELS analysis (Fig. 3 c and d) and CVs in 1 M KOH (Fig. 4).

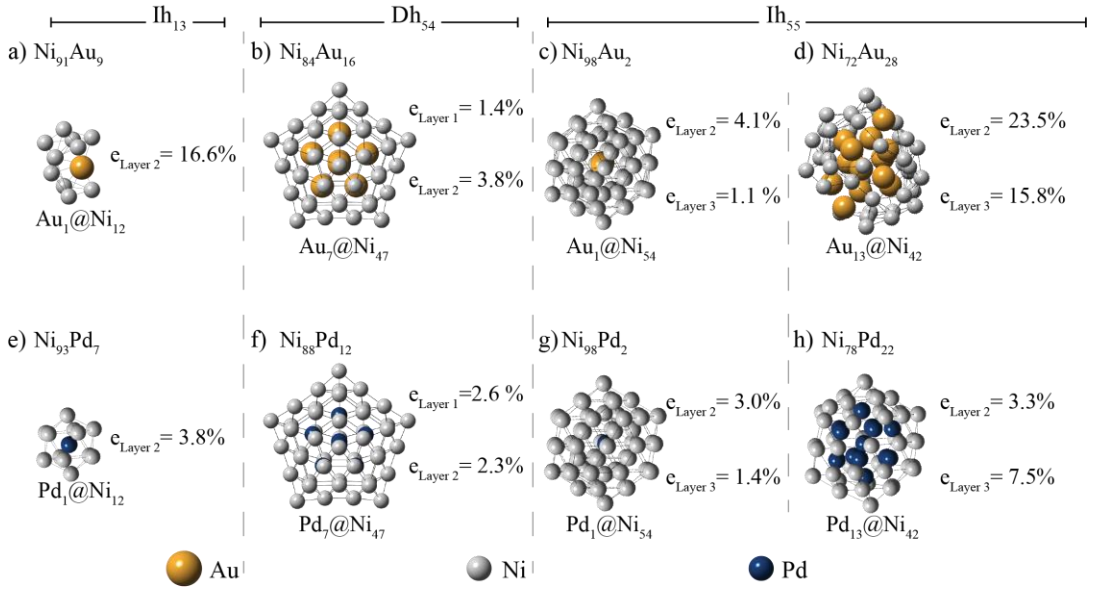

Fig. 9. Optimized structures for theoretical core@shell nanoparticles. The labels above the NP system correspond to the estimated composition percentage of each metal.

3.4.2 Electronic structure

Regarding electronic structure, the d-band PDOS curves are shown in Fig. 10. It can be seen that all systems are metallic. Also, with the exception of Au monometallic NP (see Fig. 10a, both side), the spin up and spin down contributions are shifted and are asymmetrical which is consistent with a magnetic behavior.

The large magnetic moment value in the bare Ni_{55} icosahedral system (47.7 μ_{BB}), suffer a slightly decrease when the central atom if substituted by an Au- or Pd-atom. When the all core atoms are replaced by Au or Pd atoms (i.e. the 13th central atoms in the core) the magnetic moment decreases about 5.7 μ_B or 4.3 μ_B, respectively as illustrated on the left-hand side of Fig. 10 c, e, g, i and k. In addition, the Pd_{55} NP has the smallest magnetic moment of the icosahedral systems (Fig. 10m, left-hand side) and the decahedral systems show similar behavior (Fig. 10. right-hand side). The magnetic moment values for the monometallic systems agree with those reported by *Wang et al*. [54,55] and *Yang et al*. [56]. The d-band center (ε_d) is an important factor for studying the systems reactivity, for this reason we calculate the values for the monometallic and bimetallic NP using Equation 5 in ESI.

The ε_d values show the following trend for icosahedral systems: Pd_{55} < $Pd_{13}@Ni_{42}$ < Ni_{55} < $Pd_1@Ni_{54}$ = $Au_1@Ni_{54}$ < Au_{55} < $Au_{13}@Ni_{42}$ (Fig. 10b, d, f, h, j, l and n on the left). For the decahedral NPs the order is Pd_{54} < $Pd_7@Ni_{47}$ < Au_{54} < Ni_{54} < $Au_7@Ni_{47}$ (Fig. 10b, d, f, h and j on the right). It can be

noted that these trends do not follow any linear relationship for the bimetallic systems with respect to reactivity. The d-band center value is based on the degree of filling, average energy and width of the localized d-band of the metal surface and how they interact with the adsorbate energy levels. In particular, there are two simple mechanisms for changing the chemical properties of the NP. First, the average bond length between the metal atoms in the shell surface is different from that of the monometallic particle, resulting in changes of the strain. Second, hetero-metallic bonding interactions (called the 'ligand effect') between the surface atoms and the substrate can result in a change of the surface electronic structure, thereby modify the surface chemical properties. This indicates that the chemical reactivity cannot be analyzed only with the d-band center approach, because of the complex interplay between different parameters. Then, for a better understanding of NPs reactivity, charge transfer, work function (WF) and electronegativity must also be considered.

In these metallic systems, the information about the ability of the metal to gain or lose electrons could be provided from the WF and Fermi level (E_F) values. Electrons can freely exchange at the metal−metal interface [57]. The different E_F values produce a net flow of electrons from the material with the lowest WF to that with the highest WF value, until the E_F values in both phases is equilibrated. During this process, some of transferred charge will be distributed on the surfaces, generating an electric field, although most of it will be retained at the metal contact interface, like a surface dipole. This reveals an outer potential difference between M and Ni metals that is directly proportional to the WF value difference.

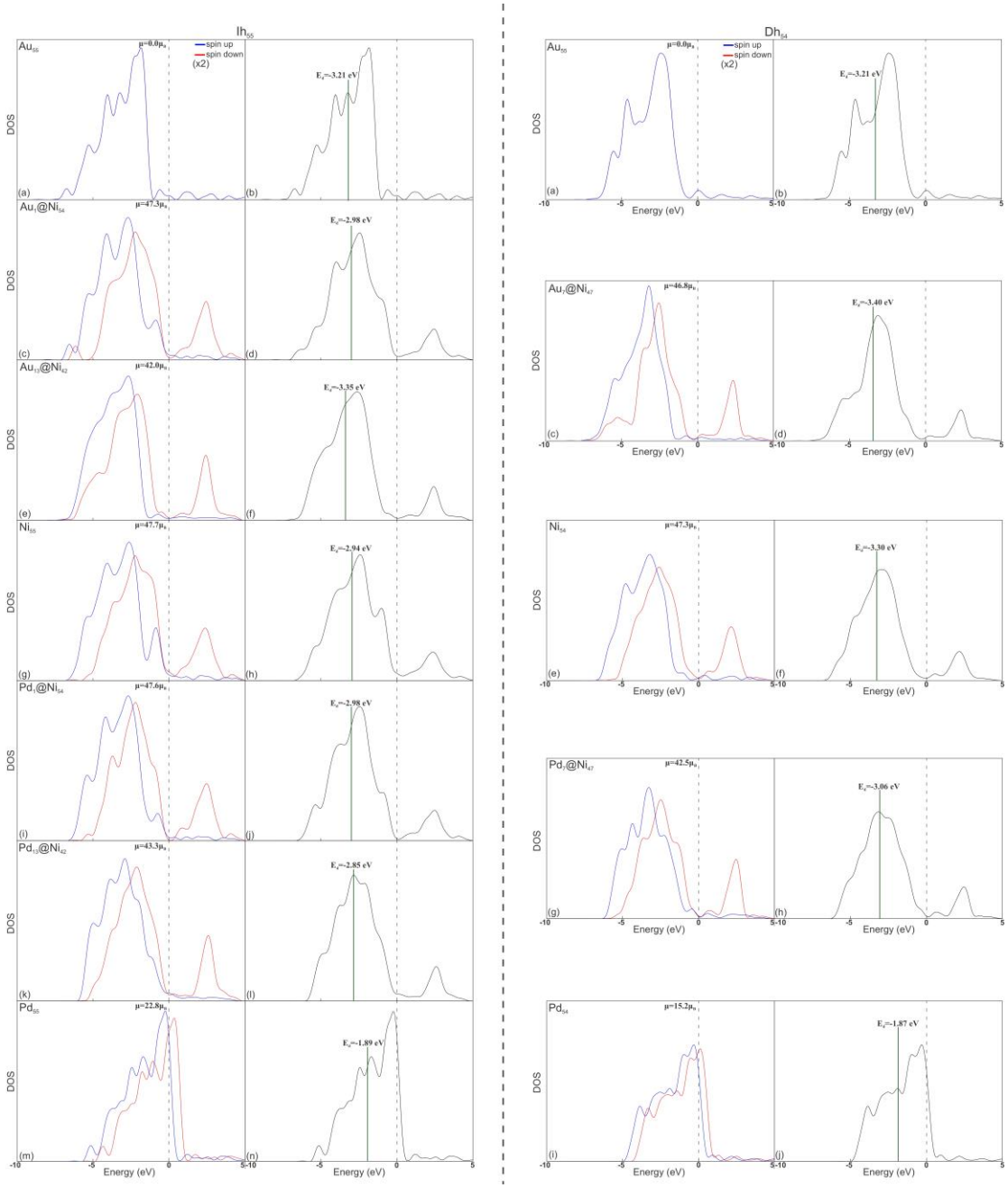

Fig. 10. Curves of d-band PDOS for the 55-atoms icosahedral systems (left) and 54-atoms decahedral systems (right). The blue and red lines indicate the spin up and spin down contributions, respectively. The black line corresponds to the total d-band curve.

The WF and E_F obtained for the studied systems is listed in Table S1. The calculated Fermi level values are following Pd (-4.338 eV) < Au (-4.307 eV) < Ni (-3.487 eV) for the Dh_{54}, and Pd (-3.835) < Au (-3.817 eV) < Ni (-3.374 eV) for the Ih_{55} structures. The WF values are ordered as follows: Pd (4.71 eV) > Au (3.97 eV) > Ni (3.75 eV) for the Ih_{13}, Pd (5.09 eV) > Au (5.06 eV) > Ni (3.98 eV) for the Dh_{54}, and

Au (5.07 eV) > Pd (4.88 eV) > Ni (4.17 eV) for the Ih_{55} structures. Also, the WF values for the Dh_{54} are Pd (5.09 eV) > Au (5.06 eV) > Ni (3.98 eV), and for the Ih_{55} clusters are Au (5.07 eV) > Pd (4.88 eV) > Ni (4.17 eV). In addition, the electronegativity order of the metallic elements is Au > Pd > Ni.

These values are consistent with the electron density transfer from Ni to other metals when they are in contact, as can be seen in Fig. 11. In all of our bimetallic systems the core and the shell develop negative and positive net charge, respectively. Then, it is clear that the charge is transferred from the shell atoms to the core atoms, leading to a surface shell being partially positive. In addition, a smaller WF value for $M_m@Ni_n$ NPs compared with mono-metallic Ni NPs, could indicate a higher reactivity [58]. Replacing the core of Dh_{54} Ni NP by Au- or Pd-atoms, increase the WF values about 0.08 or 0.09 eV. Finally, changing the central atom in Ih_{55}-Ni NP by Au- or Pd-atom induces a decrease in the WF of about 0.12 or 0.16 eV, while if the complete core is replaced by Au- or Pd-atoms the decrease is 0.13 and 0.24 eV, respectively. These results could indicate that the $Pd_{13}@Ni_{42}$ system is the most reactive, which is in agreement with our experimental data. As previously mentioned by *Logsdail et al.*, the interfacial charge transfer effects are then dependent on the inherent material WF [59].

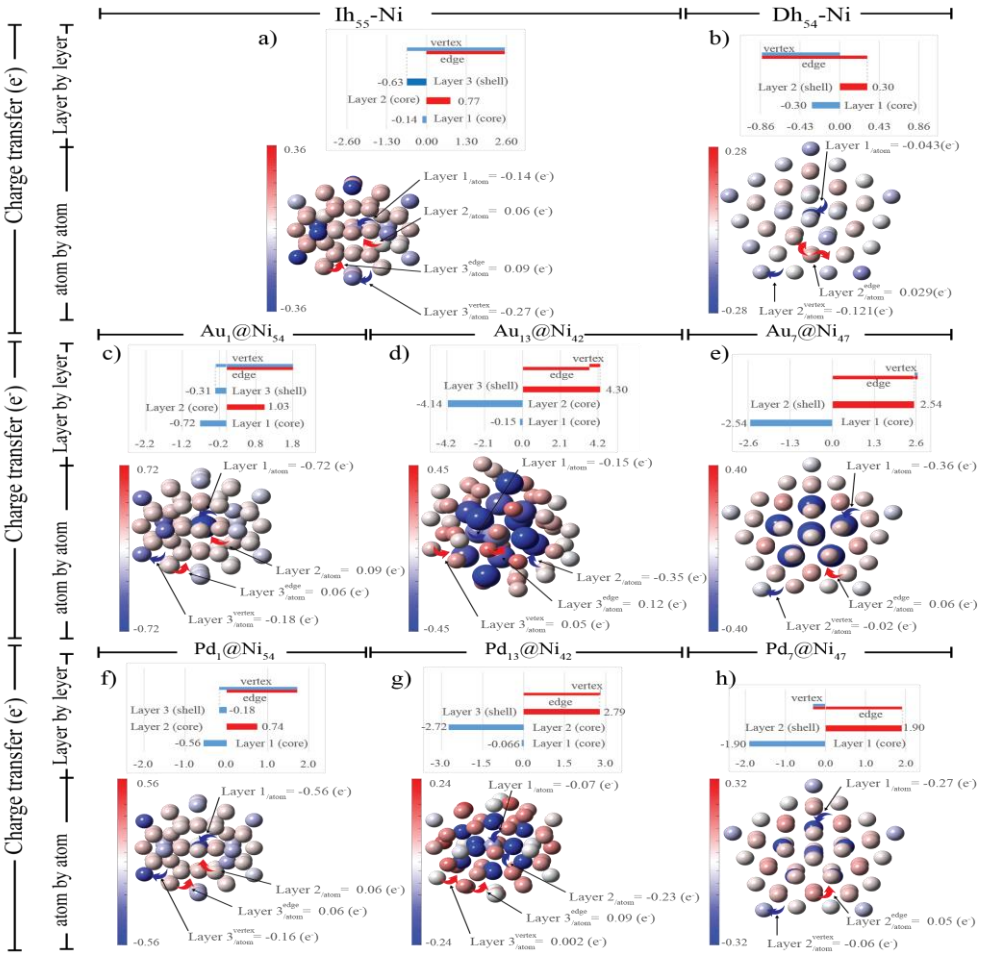

Fig. 11. Densities charge distributions for Au@Ni and Pd@Ni NPs.

The layer-by-layer net charge distribution (upper part of each subfigure) and the distribution of charge onto the individual atoms in the cross section (lower part of each subfigure) of $M_m@Ni_n$ systems (M = Au, Pd) are shown in Fig. 11. In this Figure, the charges have been normalized by the total amount of charge transferred from Ni to M of each particular system. It is clear that the charge is not equally distributed onto the atoms within the same layer, and also is different between layers. As expected, by analyzing the number of electrons carriers (e^-) for each system, the layer by layer net charge distribution between the cross sections reveals that almost all of the charge transfer occurs at the nanoparticle metal−metal interface in all systems, i.e., the charge transfer is distributed within the metal phases, where the total charge is retained directly at the contact interface [57]. As predicted by WF values, in the case of Ih_{55}-$M_1@Ni_{54}$ and Dh_{54}-$M_7@Ni_{47}$, mostly of the transferences occurs form Ni-atoms to M-atoms, but some of the charge is transferred to the Ni vertex atoms too, as a geometrical property (Fig. 11c, f, e and h, respectively). In the case of Ih_{55}-$M_{13}@Ni_{42}$ systems the transference occurs form Ni-atoms to M-atoms and there is no charge concentrated in the vertex.

Overall, our assessment is that the catalytic activity and selectivity of Au@Ni and Pd@Ni catalysts can be related to the core-shell-like structure and metal segregation withing the NPs. For these catalysts, the lattice parameter mismatch between the surrounded shell and the core, results in a strong strain in the crystal lattice over the atomic layers around the interface, thereby altering d-band center of the metals. The relative d-band center is closely associated to the molecule's adsorption, thus varying the product selectivity and catalytic activity. In contrast, the shell thickness for most of core-shell structures strongly influenced the catalytic activity via the tuned electronic effects. The M@Ni (M = Pd or Au) NPs is comprised of a Pd or Au core (-ve charge) and an outer Ni shell (+ve charge). Based on the electronic effects, the addition of Au or Pd reduced WF values for M@Ni NPs, which strengthened the OH adsorption onto the catalyst surface and then induced the GEOR intermediates removal. Ni nanoparticles adhering to the M@Ni surfaces can also employ as the catalytic active sites, and thus enhancing the active site density of these materials.

4. CONCLUSION

In this work, Ni_xPd_{1-x} (x = 100, 98, 95 and 90 at.%) and Ni_xAu_{1-x} (x = 100, 95, 90 and 80 at.%) nanoparticles were investigated for glycerol electrooxidation (GEOR) in 1 M KOH. Based on our physiochemical characterization, Ni-rich bimetallic possess a core-shell like structure, which is highly beneficial for GEOR. Among different atomic ratios, $Ni_{80}Pd_{20}$ and $Ni_{90}Au_{10}$ nanoparticles showed the highest current densities of 543 and 504 $A.g^{-1}_{Ni}$, which are ~ 4.5 and 4.2 times of spherical Ni, respectively. The addition of Au or Pd (< 20 at.%) resulted in the negative onset potential shift up to 100 mV for GEOR. 6h electrolysis at various applied potential and temperature in combination with HPLC analysis revealed that Ni@Pd and Ni@Au tend to yield more C_3 products at any given potentials and temperatures than Ni alone. For instance, a remarkable glycerate selectivity of ~ 73.1% and 65.7% was achieved on $Ni_{80}Pd_{20}$ and $Ni_{90}Au_{10}$ catalysts at 1.3 V and 50 °C, respectively. Notably, at high-applied potential (1.55 V) the monometalic Ni is mostly selective (93.1%) to formate via the C-C bonds cleavage. Overall, the core-shell like catalytic systems produced higher current density with better selectivity to C_3 products. Theoretical calculations revealed that Pd@Ni cluster is the most stable system compared to Au@Ni and monometallic Ni. In addition, on the Au@Ni clusters the atomic radii mismatch produced an important strain between its layers. The excess energy indicated that the mixed shell systems are energetically more stable. Furthermore, the higher reactivity of Pd@Ni system compared to Au@Ni and monometallic Ni systems was explained based on WF, electronegativity, Bader charges and electronic structure results thus showing an excellent correlation between our experimental and theoretical findings.

REFERENCES

[1] W. Mahmood, C. Theodoropoulos, M. Gonzalez-Miquel, Green Chem., 2017, 19, 5723-5733.
[2] L. Silva, F. Lopez-Suarez, M. Perez-Cadenas, S. Santos, L. Costa, K. Eguiluz, G. Salazar-Banda, Appl. Catal. B, Environ., 2016, 198, 38-48.
[3] Z. Li, J. Yan, J. Sun, P. Xu, C. Ma, C. Gao, Commun. Chem., 2018, 1, 1-7.
[4] M. S. E. Houache, K. Hughes, E. A. Baranova, Sustain. Energy Fuels., 2019, 3,1 892-1915.
[5] C. Coutanceau, S. Baranton, R. S. B. Kouamé, Frontiers in chemistry, 7, 100.
[6] G. Dodekatos, S. Schu, H. Tu, ACS Catal., 2018, 8, 6301-6333.
[7] H. Xu, P. Song, C. Fernandez, J. Wang, M. Zhu, Y. Shiraishi, Y. Du, ACS Appl. Mater. Interfaces., 2018, 10, 12659-12665.
[8] C. Dai, L. Sun, H. Liao, B. Khezri, R.D. Webster, A.C. Fisher, Z.J. Xu, J. Catal., 2017, 356, 14-21.
[9] Y. Zuo, L. Wu, K. Cai, T. Li, W. Yin, D. Li, N. Li, J. Liu, H. Han, ACS Appl. Mater. Interfaces., 2015, 7, 1-23.
[10] M.R. Burton, A. Selvam, J. Lawrie-ashton, A.M. Squires, N. Terrill, I. Nandhakumar, M. Burton, A. Selvam, J. Lawrie-ashton, A. Squires, N. Terrill, ACS Appl. Mater. Interfaces., 2018,10(43), 37087-37094.
[11] Y. Zhou, Y. Shen, J. Piao, ChemElectroChem., 2018, 5, 1636-1643.
[12] A. Zalineeva, S. Baranton, C. Coutanceau, Electrochim. Acta., 2015, 176, 705-717.
[13] P. K. Shen, C. Xu, Electrochem. Commun., 2006, 8, 184-188.
[14] J. L. Bott-Neto, A. C. Garcia, V. L. Oliveira, N. E. De Souza, G. Tremiliosi-Filho, J. Electroanal. Chem. 2014, 735, 57-62.
[15] J. Song, J. Yu, M. Zhang, Y. Liang, C. Xu, Int. J. Electrochem. Sci., 2012, 7, 4362-4368.
[16] D. Z. Jeffery, G. A. Camara, Electrochem. Commun., 2010, 12, 1129-1132.
[17] T. R. Maumau, R. M. Modibedi, M. K. Mathe, Mater. Today Proc., 2018, 5, 10542-10550.
[18] J. Zhang, Y. Liang, N. Li, Z. Li, C. Xu, S. Ping, Electrochim. Acta, 2012, 59, 156-159.
[19] M. Simões, S. Baranton, C. Coutanceau, Appl. Catal. B Environ., 2010, 93, 354-362.
[20] Z. Zhang, L. Xin, W. Li, Appl. Catal. B Environ., 2010, 119, 40-48.
[21] D. W. Wang, F. Li, H. M. Cheng, J. Power Sources, 2008, 118, 1563-1568.
[22] F. Bidault, D. J. L. Brett, P. H. Middleton, N. Abson, N. P. Brandon, Int. J. Hydrogen Energy, 2009, 34, 6799-6808.
[23] A.K. Shukla, S. Venugopalan, B. Hariprakash, J. Power Sources, 2001, 100, 125-148.
[24] M. S. E. Houache, E. Cossar, S. Ntais, E. A. Baranova, J. Power Sources, 2018, 375, 310-319.
[25] V.L. Oliveira, C. Morais, K. Servat, T.W. Napporn, P. Olivi, K.B. Kokoh, G. Tremiliosi-Filho, Electrocatalysis, 2015, 6, 447-454.
[26] V.L. Oliveira, C. Morais, K. Servat, T.W. Napporn, G. Tremiliosi-Filho, K.B. Kokoh, Electrochim. Acta, 2014, 117, 255-262.
[27] M. S. E. Houache, R. Safari, U. O. Nwabara, T. Rafaïdeen, G. A. Botton, P. J. Kenis, P. J., S. Baranton, C. Coutanceau, E. A. Baranova, *ACS Applied Energy Materials*, 2020, 3(9), 8725-8738.
[28] M. S. E. Houache, K. Hughes, R. Safari, G. A. Botton, E. A. Baranova, ACS Appl. Mater. Interfaces. 2020, 12, 15095-15107.
[29] M. S. E. Houache, K. Hughes, A. Ahmed, R. Safari, H. Liu, G. A. Botton, E. A. Baranova, ACS Sustain. Chem. Eng., 2019, 7, 14425-14434.
[30] R. Ferrando, J. Jellinek, R.L. Johnston, Chem. Rev., 2008, 108, 845-910
[31] R. Ferrando, J. Phys.: Condens. Matter, 2015, 27(1), 013003.
[32] D. Bochicchio, R. Ferrando, Nano Lett., 2010, 10, 4211-4216.
[33] D. Bochicchio, R. Ferrando, Phys. Rev. B, 2013, 87, 165435.

[34] F. Baletto, R. Ferrando, Rev. Modern Phys., 2005, 77, 371-423.
[35] R. Ferrando, A. Fortunelli, G. Rossi, Phys. Rev. B, 2005, 72, 085449.
[36] R. Ferrando, A. Fortunelli, R. L. Johnston, Phys. Chem. Chem. Phys., 2008, 10(5), 640-649.
[37] J. Zhu, P. Cheng, N. Wang, S. Huang, Comp. Theo. Chem., 2015, 1071, 9-17.
[38] M. Schnedlitz, M. Lasserus, R. Meyer, D. Knez, F. Hofer, W. E. Ernst, A. W. Hauser, Chem. Mater., 2018, 30, 1113-1120.
[39] https://www.vasp.at/
[40] F. Baletto, R. Ferrando, J. Chem. Phys., 2002, 116, 3856-3863.
[41] J.A. Alonso, Chem. Rev., 2000, 100, 637-678.
[42] D. Cheng, W. Wang, Nanoscale, 2012, 4, 2408-2415.
[43] Y. Z. Su, K. Xiao, N. Li, Z. Q. Liu, S. Z. Qiao, J. Mat. Chem. A, 2014, 2, 13845-13853.
[44] D. Zhu, C. Guo, J. Liu, L. Wang, Y. Du, S. Z. Qiao, Chem. Comm., 2017, 53, 10906-10909.
[45] H. U. Shin, D. Lolla, Z. Nikolov, G. G. Chase, J. Ind. Eng. Chem., 2016, 33, 91-98.
[46] S. Yang, J. Dong, Z. Yao, C. Shen, X. Shi, Y. Tian, X. Zhang, Sci. Reports, 2014, 4, 4501.
[47] Z. Ebrahimpour, N. Mansour, Appl. Surf. Sci., 2017, 394, 240-247.
[48] Oshchepkov, A. G., Braesch, G., Bonnefont, A., Savinova, E. R., & Chatenet, M. (2020). Recent advances in the understanding of Ni-based catalysts for the oxidation of hydrogen-containing fuels in alkaline media. *ACS Catalysis*.
[49] N. Pittayaporn, A. Therdthianwong, S. Therdthianwong, J. Appl. Electrochem., 2018, 48, 251-262.
[50] J. Sankar, E. N. Onyeozili, E. E. Kalu, ChemEngineering., 2017, 1, 11.
[51] B. Katryniok, H. Kimura, E. Skrzynska, J.-S. Girardon, P. Fongarland, M. Capron, R. Ducoulombier, N. Mimura, S. Paul, Dumeignil. Franck, Green Chem., 2011, 13, 1960-1979.
[52] F. Porta, L. Prati, J. Catal., 2004, 224, 397-403.
[53] C. Dai, L. Sun, H. Liao, B. Khezri, R.D. Webster, A.C. Fisher, Z.J. Xu, J. Catal., 2017, 356, 14-21.
[54] Q. Wang, K. H. Lim, Sh.-W. Yang, Y. Yang, Y. Chen, Theor. Chem. Acc., 2011, 128, 17-24.
[55] Q. Wang, X. Lu, Y. Zhen, W. Li, G. Chen, Y. Yang, J. Chem. Phys., 2018, 149, 244307.
[56] Z. Yang, Q. Wang, X. Shan, W. Li, G. Chen, H. Zhun, J. Chem. Phys. 142, (2015) 074306.
[57] N. Holmberg, K. Laasonen, P. Peljo, Phys. Chem. Chem. Phys., 2016, 18, 2924-2931.
[58] K. Tedsree, T. Li, S. Jones, A. Chan, K. K. M. Yu, P. Bagot, E. Marquis, G. Smith, S. C. E. Tsang, Nature Nanotechnology, 2011, 6, 302-307.
[59] A. J. Logsdail, L. OliverPaz-Bórbon, C. A. J. Phys. Chem. C, 2018, 122, 5721-5730.